

Originaldokument gespeichert auf dem Dokumentenserver der Universität Basel
edoc.unibas.ch



Dieses Werk ist unter dem Vertrag „Creative Commons Namensnennung-Keine kommerzielle Nutzung-Keine Bearbeitung 2.5 Schweiz“ lizenziert. Die vollständige Lizenz kann unter
creativecommons.org/licenses/by-nc-nd/2.5/ch
eingesehen werden.



Namensnennung-Keine kommerzielle Nutzung-Keine Bearbeitung 2.5 Schweiz

Sie dürfen:



das Werk vervielfältigen, verbreiten und öffentlich zugänglich machen

Zu den folgenden Bedingungen:



Namensnennung. Sie müssen den Namen des Autors/Rechteinhabers in der von ihm festgelegten Weise nennen (wodurch aber nicht der Eindruck entstehen darf, Sie oder die Nutzung des Werkes durch Sie würden entlohnt).



Keine kommerzielle Nutzung. Dieses Werk darf nicht für kommerzielle Zwecke verwendet werden.



Keine Bearbeitung. Dieses Werk darf nicht bearbeitet oder in anderer Weise verändert werden.

- Im Falle einer Verbreitung müssen Sie anderen die Lizenzbedingungen, unter welche dieses Werk fällt, mitteilen. Am Einfachsten ist es, einen Link auf diese Seite einzubinden.
- Jede der vorgenannten Bedingungen kann aufgehoben werden, sofern Sie die Einwilligung des Rechteinhabers dazu erhalten.
- Diese Lizenz lässt die Urheberpersönlichkeitsrechte unberührt.

Die gesetzlichen Schranken des Urheberrechts bleiben hiervon unberührt.

Die Commons Deed ist eine Zusammenfassung des Lizenzvertrags in allgemeinverständlicher Sprache: <http://creativecommons.org/licenses/by-nc-nd/2.5/ch/legalcode.de>

Haftungsausschluss:

Die Commons Deed ist kein Lizenzvertrag. Sie ist lediglich ein Referenztext, der den zugrundeliegenden Lizenzvertrag übersichtlich und in allgemeinverständlicher Sprache wiedergibt. Die Deed selbst entfaltet keine juristische Wirkung und erscheint im eigentlichen Lizenzvertrag nicht. Creative Commons ist keine Rechtsanwalts-gesellschaft und leistet keine Rechtsberatung. Die Weitergabe und Verlinkung des Commons Deeds führt zu keinem Mandatsverhältnis.

The role of the coactivators PGC-1 α and PGC-1 β in retina and skeletal muscle

Inauguraldissertation

zur
Erlangung der Würde eines Doktors der Philosophie
vorgelegt an der
Philosophisch-Naturwissenschaftlichen Fakultät
der Universität Basel

von

Anna Franziska Egger
aus Innsbruck, Österreich

Basel, 2011

Genehmigt von der Philosophisch-Naturwissenschaftlichen Fakultät
auf Antrag von

Prof. Dr. Christoph Handschin

Prof. Dr. Christian Grimm

Basel, den 18.10.2011

Prof. Dr. Martin Spiess

Dekan

This work has been performed under supervision of

Prof. Dr. Christoph Handschin

Prof. Dr. Christian Grimm

At the Department of Pharmacology, Biozentrum Basel, University of Basel

1. Zusammenfassung	5
2. Summary	7
3. Introduction	9
3.1. The PGC-1 family of coactivators	9
3.2. Structural features of PGC-1α	10
3.3. The discovery of PGC-1α	11
3.4. Binding partners	12
3.5. PGC-1α in skeletal muscle	12
3.5.1. Mechanisms upstream of PGC-1α	12
3.5.1.1. Transcriptional regulation	12
3.5.1.2. Posttranslational regulation	14
3.5.1.3. Splicing mediated regulation	15
3.5.2. Mechanisms downstream of PGC-1α	15
4. The role of PGC-1α in retina	18
4.1. Introduction	18
4.1.1. Retina structure	18
4.1.2. Phototransduction	19
4.1.2.1. In darkness	20
4.1.2.2. In light	20
4.1.3. PGC-1α in retina	21
4.1.4. Apoptotic pathways	21
4.1.4.1. Apoptosis in retina	23
4.1.4.2. Apoptosis and PGC-1α	24
4.2. Project aims	26
4.3. Manuscript	27
4.5. Conclusions	50
5. The role of PGC-1β in skeletal muscle	52
5.1. Introduction	52
5.1.1. PGC-1β in skeletal muscle	52
5.1.1.1. PGC-1β and angiogenesis	53
5.1.1.2. PGC-1β and fiber type determination	54
5.1.1.3. Specific role of PGC-1β in skeletal muscle	54
5.1.1.4. PGC-1β and glucose homeostasis	54
5.1.2. Skeletal muscle specific knockdown of PGC-1β	55
5.1.2.1. The construct	55
5.1.2.2. The delivery	56
5.1.2.2.1. Somatic delivery	56
5.1.2.2.2. Transgenic mouse delivery	56
5.1.2.2.3. Viral delivery	57
5.2. Project aims	60
5.3. Material & Methods	61
5.4. Results	68
5.5. Discussion	86
5.6. Conclusions	91
6. Perspectives	92
7. References	94
8. CV	109
9. Acknowledgements	111

1. Zusammenfassung

Peroxisome proliferator aktivierter Rezeptor γ Coaktivator-1 (PGC-1) bezeichnet eine Familie von Coaktivatoren, bestehend aus PGC-1 α , PGC-1 β und PRC^{1,2,3}. Diese binden an Transkriptionsfaktoren wie beispielsweise nukleäre Rezeptoren und induzieren so die Expression von Zielgenen, welche mitochondrielle Biogenese⁴, Glukose Aufnahme in die Zelle⁵ sowie Gluconeogenese⁶, oxidative Phosphorylierung (OXPHOS)^{7,8} und β -Oxidation von Fettsäuren⁹ steuern. PGC-1 wurde erstmals in braunem Fettgewebe¹ identifiziert und wurde seitdem vor allem in Geweben mit hohem Energieumsatz nachgewiesen (Skelettmuskel, Herz, Leber, Gehirn, Niere), wo es als Antwort auf einen physiologischen Stressor (körperliche Aktivität, Kälteeinwirkung, Nahrungskarenz) exprimiert wird^{10,11,12,1,13}. Deshalb sind Expression und Funktion von PGC-1 α gewebespezifisch. Derzeit ist PGC-1 α das am besten untersuchte aller PGC-1s.

Die Retina ist ein Gewebe mit sehr hohem Energiebedarf, da dort die Photorezeptoren Licht in ein vom Gehirn verwertbares Signal umwandeln¹⁴. Die Rolle von PGC-1 α in der Netzhaut wurde bis jetzt jedoch nicht analysiert:

Das erste Projekt befasste sich deshalb mit der Expression und Funktion von PGC-1 α und teilweise auch der von PGC-1 β in der Maus Retina: Zuerst analysierten wir dort das basale Expressionsmuster von PGC-1 α und PGC-1 β . Anschliessend wurden Mäuse, welchen das PGC-1 α Gen fehlt (PGC-1 α Knockout = KO) und Wildtyp (WT) Kontrolltiere mit hochfrequentem Licht bestrahlt beziehungsweise dunkel exponiert. Dann wurden Morphologie (Histologie), Funktion (ERG- Elektretinogramm) und Genexpression (Microarray, semi- quantitative real time PCR) der Mausretinae analysiert. Die PGC-1 α KO Mäuse wiesen einen starken Lichtschaden der Photorezeptorstrukturen sowie verstärkte Apoptose auf im Vergleich zu den WT Kontrolltieren. Analog dazu wurde bei einigen lichtexponierten KO Tieren eine veränderte ERG Antwort festgestellt. Die Microarrayergebnisse zeigten eine Expressionsminderung von DNA Reparatur- und Phototransduktionsgenen sowie verstärkte Expression von Entzündungs- und Apoptosegenen. Abschliessend konnten wir in einem *in vitro* Modell zeigen, dass die Ueberexpression von PGC-1 α Apoptose verringert.

Zur spezifischen Funktion von PGC-1 β im Skelettmuskel ist ebenfalls wenig bekannt: Wir versuchten deshalb im zweiten Projekt, dessen Rolle im Glucose Stoffwechsel und der Bestimmung der Skelettmuskelfasertypen zu klären. Des weiteren hatten wir uns zum Ziel gesetzt, die PGC-1 β spezifischen Zielgene in diesem Gewebe zu identifizieren. Aus diesem Grund versuchten wir, eine skelettmuskelspezifische Knockdown Maus für PGC-1 β zu generieren: Unterschiedliche short hairpin RNAs (shRNAs) und Kontrollen, sogenannte scrambled shRNAs gegen Maus PGC-1 β wurden entsprechend verschiedener Designmodi generiert (shRNA vs shRNA-mir) und deren Knockdown Effizienz und Spezifität wurde anschliessend in Zellkultur getestet. Die geeignetste shRNA wurde dann in einen Vektor kloniert, welcher für die Herstellung von Adeno-Assoziiertem Virus (AAV) verwendet wurde.

Wir produzierten AAV des Serotyps AAV2/6, da dieser einen spezifischen Tropismus für Skelettmuskel besitzt. Injektionsmenge, Weg und Dauer bis zur Expression der shRNA wurde mittels eines Virus, der grün fluoreszierendes Protein (GFP) exprimiert, optimiert. Der shRNA enthaltende Virus wurde dann in den Maus tibialis anterior Muskel injiziert und nach einer Inkubationszeit von 3 Wochen extrahiert. Anschliessend wurde der Muskel auf die Expression von Entzündungsmarkern analysiert. Semi-quantitative real time PCR Analysen zeigten ebenfalls, dass PGC-1 β als auch dessen Zielgene signifikant in ihrer Expression reduziert waren. Ein *in vivo* Test eines skelettmuskelspezifischen Promotors, welcher die Expression der shRNA steuern sollte, führte jedoch zu keiner signifikanten Reduktion von PGC-1 β .

Zusammengefasst konnten wir zeigen, dass PGC-1 α in lichtinduzierter Apoptose in der Retina eine protektive Rolle einnimmt (Projekt 1).

In Projekt 2 zeigten wir, dass die Reduktion von PGC-1 β im Skelettmuskel zu einer verminderten Expression von Genen führt, welche OXPHOS steuern.

2. Summary

Peroxisome proliferator-activated receptor γ coactivator- 1 (PGC-1) designates a family of coactivators consisting of PGC-1 α , PGC-1 β and PRC^{1,2,3}. By associating with transcription factors like nuclear receptors, they induce transcription of target genes that are responsible for mitochondrial biogenesis⁴, glucose uptake⁵, gluconeogenesis⁶, oxidative phosphorylation^{7,8} and β -oxidation of fatty acids⁹. Originally identified in brown adipose tissue¹, these coactivators are predominately expressed in tissues with high energy requirements (skeletal muscle, heart, liver, brain, kidney) upon stimulation with physiological stressors (exercise, cold, fasting)^{10,11,12,1,13}. PGC-1's expression and function is therefore highly tissue specific. PGC-1 α is to date the best studied of all family members.

One of the tissues high in energy demand is the retina; its photoreceptors convert light into a signal that can be interpreted by the brain¹⁴. However, thus far the physiological role of PGC-1 α has never been studied there. In the first project of this thesis, we consequently analyzed PGC-1 α and to a certain extent also PGC-1 β expression and function in mouse retina: We first assessed expression patterns of PGC-1 α and PGC-1 β . Second, we subjected mice with a global deletion of the PGC-1 α gene (PGC-1 α knockout = KO) and wildtype (WT) control mice to high intensity light compared to a dark setting and studied their retinae's morphology (histology), function (electroretinogram) and gene expression levels (microarray, real time PCR). We found the PGC-1 α KO mice to display increased apoptosis and disrupted retinal photoreceptor structure compared to the wildtype (WT) control animals upon light exposure. The corresponding light damage could also be confirmed by ERG in some animals. Microarray analysis revealed downregulation of DNA repair and phototransduction as well as an upregulation of inflammatory and apoptotic pathways, respectively in the KO animals. Finally, we confirmed in an *in vitro* setting that overexpression of PGC-1 α helped alleviate apoptosis.

The role of PGC-1 β in skeletal muscle has not been thoroughly studied either: More specifically, we wanted to address its role in glucose metabolism/ insulin sensitivity and fiber type composition as well as to identify exclusive target genes of PGC-1 β in this tissue in the second project. For this purpose, we aimed at generating a skeletal muscle specific knockdown mouse: Different small hairpin RNAs (shRNAs) and control, scrambled shRNAs against mouse PGC-1 β were designed according to different design principles (shRNA vs shRNA-mir) and tested for their knockdown efficiency and specificity in cell culture. The most promising one was then inserted into a vector backbone used to generate adeno-associated virus (AAV). We decided to produce the AAV serotype AAV2/6, as it displays specific tropism for skeletal muscle (AAV2/6). Injection quantity, route and duration until onset of shRNA expression were optimized with a virus expressing green fluorescent protein (GFP). The virus carrying shRNA was then injected into the mouse tibialis anterior muscle and after 3 weeks of incubation time analyzed for inflammatory gene expression. Semi- quantitative real time PCR analysis revealed that expression of PGC-1 β as well as of

its downstream target genes was significantly reduced. *In vivo* testing of a skeletal muscle specific promoter, however, did not lead to a significant reduction of PGC-1 β levels.

In summary, we showed that PGC-1 α has a protective role in light induced apoptosis in the retina (project1).

In project 2, we showed that a reduction of PGC-1 β in skeletal muscle leads to diminished expression of genes implicated in OXPHOS.

3. Introduction

3.1. The PGC-1 family of coactivators

Eukaryotic gene expression is a tightly regulated process that is governed by altering the state of chromatin: It is either decondensed by histone acetyl- transferases (HATs) or condensed by histone deacetylases (HDACs). Upon decondensation, chromatin is rendered more accessible and allows for transcription to occur¹⁵.

Transcription factors bind to DNA promoter or enhancer regions and thus steer the rate of conversion from DNA to RNA. Thereby, they associate with chromatin remodeling cofactors (coactivators or corepressors) which either have intrinsic HAT or HDAC properties or recruit either of these. Cofactors also associate with various other chromatin remodeling enzymes. This process either drives or impedes transcriptional activity. Cofactors split into two classes:

Class I cofactors enzymatically modify DNA tertiary structure, by acetylation (class I coactivators) or by deacetylation of histones (class I corepressors). Class II cofactors (coactivators or corepressors) associate with RNA polymerase II, however, they lack the enzymatic activity to modify histones. As such, they require interaction with class I coactivators^{16,17}.

The peroxisome proliferator activated receptor γ coactivator – 1 (PGC-1) designates a family of such class II coactivators that regulate transcription¹.

The PGC-1 family is composed of three members present in all mammals: PGC-1 α , PGC-1 β and PGC-1 related coactivator (PRC) (for reviews see^{18,19}).

3.2. Structural features of PGC-1 α

PGC-1 α , PGC-1 β and PRC share common structural modules that enable their tight interaction with the transcriptional machinery:

These include first, an activation domain (AD) at the N-terminus which recruits several HAT complexes like the 3'-5'- cyclic adenosine monophosphate (cAMP) response element-binding protein (CREB)- binding protein (CBP), p300 and steroid receptor coactivator-1(SRC-1)²⁰. Three LXXLL motifs locate adjacent to the AD and enable binding of many transcription factors.

Second, the C-terminus contains a RNA binding domain that attracts the thyroid receptor-associated protein/ vitamin D receptor-interacting protein/ mediator complex (TRAP/ TRIP). This complex facilitates direct interaction with the transcription initiation machinery²¹. This region also interacts with the switch/ sucrose non-fermentable (SWI/SNF) chromatin-remodeling complex through its interaction with the mammalian chromatin remodeling associated factor BAF60a²².

Third, adjacent to this domain lies the highly conserved nuclear localization signal as well as serine-arginine rich region that coordinates transcription and pre-mRNA splicing jointly with the RNA binding domain^{23,24}.

Fourth, the mid region between the two termini features a repression domain where silent information regulator T1 (SIRT1) and the MYB binding protein (P160) can attach¹⁹. Interestingly, this region is only present in PGC-1 α and PGC-1 β , yet absent in PRC (**Fig.1**).

These structural elements equip PGC-1 with the necessary tools to attract and assemble various chromatin remodeling and histone-modifying enzymes and thus steer transcription actively. In line with its function as transcriptional activator, it can also deter repressor proteins from attaching²⁵.

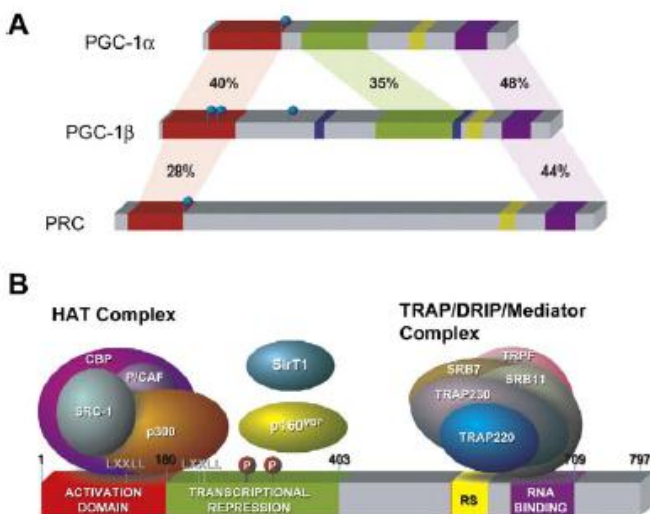


Fig.1: (A): Sequence homology of PGC-1 α , PGC-1 β and PRC (B) Structural domains and protein complexes associating with PGC-1 α : red= activation domain, yellow= arginine/ serine rich domain, purple= RNA binding domain, green= transcriptional repression domain.

Source: ¹⁹

This crucial role of PGC-1 in transcriptional regulation is substantiated by its high degree of conservation across chordate species, including primates, rodents, ruminants, birds, amphibians, and fishes. Even in *Drosophila*, a PGC-1 homologue called Spargel was recently identified²⁶. Nevertheless, PGC-1 fulfills different functions in different species, such as lower and in higher vertebrates. Such a functional ramification across lineages results from duplication and insertion events²⁷.

3.3. The discovery of PGC-1 α

The first function attributed to PGC-1 α was that of being a transcriptional coactivator of peroxisome proliferator- activated receptor γ (PPAR γ)¹. PPAR γ is a member of the PPAR nuclear receptor family.

PPAR γ regulates adipogenesis in brown adipose tissue (BAT) and white adipose tissue (WAT): PPAR γ 's differential activation of transcriptional targets in these two tissues revealed that PGC-1 α is an interaction partner of PPAR γ in BAT^{1,28}.

Three major findings helped to elucidate the main role of PGC-1 α :

First, BAT is able to perform thermogenesis owing to its increased number of mitochondria compared to WAT. Second, PGC-1 α was identified in highly oxidative tissues^{4,29,30}. Third, ectopic overexpression of PGC-1 α was shown to drive the expression of mitochondrial genes, both nuclear and mitochondrially encoded⁴, leading to increased mitochondrial biogenesis and oxidative phosphorylation (OXPHOS).

3.4. Binding partners

In subsequent studies, PGC-1 α was found to be a coactivator of a myriad of different classes of transcription and chromatin remodeling factors:

Nuclear receptors

A well-studied class of transcription factors is nuclear receptors: These are activated upon binding of ligands like steroid or thyroid hormones to their surface and act as transcription factors on genes that are implicated in metabolic and developmental processes¹⁷: PGC-1 α coactivates thyroid hormone receptors (TR)¹, estrogen receptors (ER)¹ and estrogen related receptors (ERRs)^{31,8} which promote OXPHOS and are also involved in enhancing angiogenesis. Besides the PPARs^{1,32}, liver X receptors (LXR)³³ are also crucial in promoting fatty acid oxidation and transport and are also binding partners of PGC-1 α .

The involvement of PGC-1 α in dopaminergic neuron and osteoblast regulation is attested by its association with nuclear receptor subfamily 1(NURR1)³⁴.

Retinoid X receptors (RXR) α , β and γ are involved in retinoic acid signaling and also constitute members of the nuclear receptor family bound by PGC-1 α ³⁵.

For activation by PGC-1 α to occur, some nuclear receptors need not be bound to a ligand, as is the case of ERR α , hepatocyte nuclear factor 4 (HNF4) or farnesoid X receptor (FXR)^{36,37,38}. These nuclear receptors are implicated in oxidative phosphorylation, insulin release and bile acid synthesis steps, respectively. Unliganded transcriptional activation ensures rapid response to physiological requirements.

Chromatin remodeling factors

As a recruiting agent for factors involved in transcription, PGC-1 α also regulates chromatin remodeling factors like host cell factor C1 (HCFC1)³⁹ and BRG1-associated factor 60a (BAF60A)²².

Transcription factors

Among the classical transcription factors controlled by PGC-1 α are nuclear respiratory factors 1 and 2 (NRF1 and NRF2), primary drivers of mitochondrial biogenesis as well as myocyte enhancer factor2 (MEF2) which steers skeletal muscle fiber type determination^{3,40}. It also associates with GA-binding protein transcription factor (GABP) which controls cytochrome C oxidase expression and mitochondrial transcription factor A (TFAM) which participates in mitochondrial genome replication⁴¹.

Another important target of PGC-1 α is the forkhead/ winged helix protein family member (FOXO1) which drives hepatic gluconeogenesis⁴².

PGC-1 α thus activates transcription factors that control processes as diverse as mitochondrial biogenesis and remodeling, skeletal muscle fiber type determination, angiogenesis, hepatic gluconeogenesis and fatty acid oxidation.

Its most prominent role, however, is to steer transcription factors implicated in OXPHOS, which garnered PGC-1 α the name of *master regulator* of oxidative metabolism.

Subsequent analysis revealed that PGC-1 α is highly expressed in tissues with high energy requirements like skeletal muscle, heart, liver, brain, liver, pancreas, kidney, BAT and WAT^{40,12,43,6,11,44,1}.

Stressors like exercise, cold or fasting seem to be the common denominators of the events that lead to PGC-1 α activation across different tissues^{10,11,12,1,13}.

As PGC-1 α has tissue specific expression patterns/ function and its role is best studied in skeletal muscle, we will look at its upstream and downstream regulation in this tissue:

3.5. PGC-1 α in skeletal muscle

3.5.1. Mechanisms upstream of PGC-1 α

3.5.1.1. Transcriptional regulation

In skeletal muscle, physiological stimuli like physical activity, changes in temperature and metabolic demands partly converge in similar metabolic outcomes (**Fig.2**):

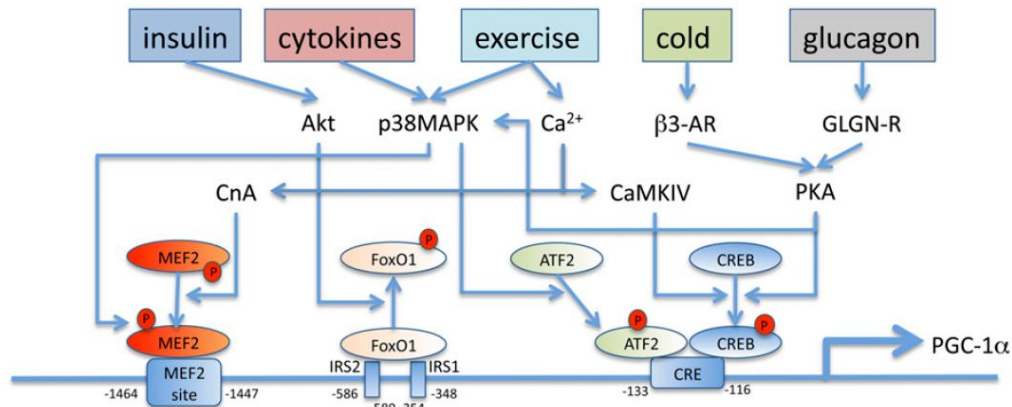


Fig.2: Regulation of PGC-1 α transcription: The PGC-1 α promoter contains binding sites for MEF2, FOXO1, ATF2 and CREB. These factors promote PGC-1 α transcription. They are, in turn, modulated by different signaling pathways: insulin, cytokines, exercise, cold and glucagon. P= phosphorylation site. GLGNR= glucagon receptor
Source: ⁴⁵.

During physical activity, an action potential in the central nervous system (CNS) signals to the α -motorneuron and then to the skeletal muscle, where calcium release finally mediates muscle contraction, a process where actin and myosin filaments slide within each other by consuming adenosine triphosphate (ATP). Calcium activates calcium/ calmodulin dependent protein kinase (CaMKIV) and calcineurin A (CnA). CnA then activates MEF2C and MEF2D leading to transcription of PGC-1 α which is further enhanced by a feedback stimulation of MEF2C and MEF2D by PGC-1 α ⁴⁶. CaMKIV is phosphorylated by calcium and then activates PGC-1 α via CREB¹¹.

Physical activity also leads to release of interleukins (IL-6, IL-8, IL-15, brain-derived neurotrophic factor BDNF, fibroblast growth factor-21 FGF21 and leukemia inhibitory factor LIF) some of which are implicated in glucose homeostasis and β -oxidation of fatty acids⁴⁷. These factors are also called cytokines, if released from the muscle, they are termed myokines. Myokines as well as exercise itself promote activation of p38 MAPK. P38 MAPK in turn activates MEF2 and activating transcription factor2 (ATF2) which induce PGC-1 α ⁴⁸.

During exercise, the adenosine monophosphate (AMP)/ ATP ratio in the cell is high meaning that the cell is energy deprived: AMP activated protein kinase (AMPK) is thus activated to restore energy homeostasis by increasing fat oxidation, mitochondrial biogenesis and glucose uptake. AMPK transcription is specifically induced by the AMPK activator AICAR and AMPK likewise activates PGC-1 α via phosphorylation^{49,50}.

The lack of energy encountered during physical activity triggers a rise in glucagon levels and protein kinase A (PKA) activation in liver. Likewise, cold exposure, sensed by β -adrenergic signaling receptor (β -

AR) leads to increased cAMP and PKA activity¹. PKA then targets CREB which in turn activates PGC-1 α expression^{1,51}. This effect is potentiated via stimulation of p38 MAPK⁵².

Insulin, the antagonist of glucagon favors activation of anabolic pathways. As PGC-1 α is primarily implicated in catabolic pathways, it seems that insulin inhibits PGC-1 α transcription: Insulin signals to AKT leading to phosphorylation of FOXO1. Thereupon, FOXO1 is excluded from the nucleus and cannot promote transcription of PGC-1 α any more⁵³. Contrary to this finding, Puigserver et al found that FOXO1 does not activate, but is coactivated by PGC-1 α ⁴².

3.5.1.2. Posttranslational regulation

Besides transcriptional regulation, posttranslational modification of PGC-1 α confers a second, faster regulation mode to this coactivator. The respective residue that undergoes modification determines if PGC-1 α is activated or repressed (**Fig.3**):

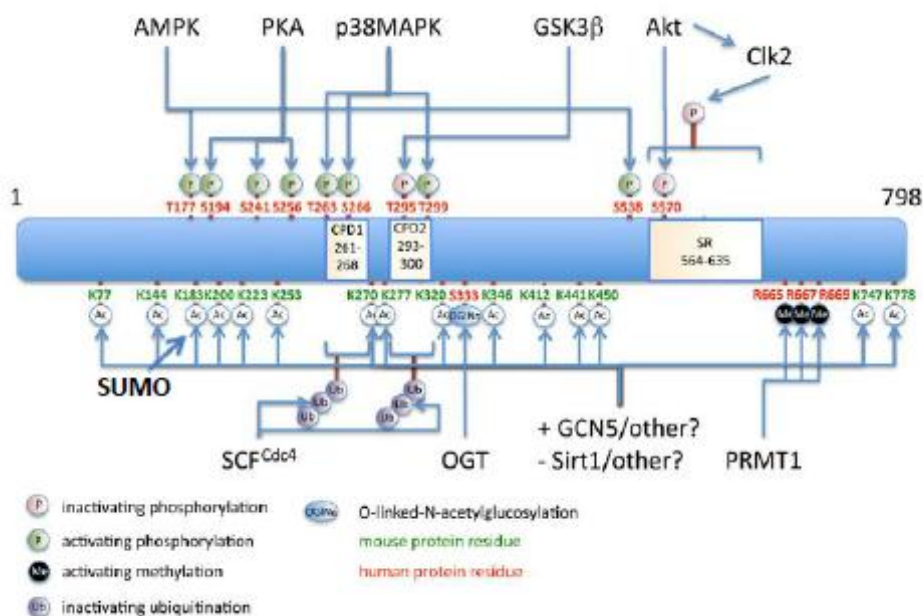


Fig.3: Posttranslational modifications of PGC-1 α

Source:⁴⁵.

Among the first posttranslational modifications of PGC-1 α to be identified was phosphorylation: AMPK⁵⁴, PKA and p38MAPK⁵⁵ activate the coactivator upon phosphorylation, whereas the serine-threonine protein kinase AKT and Cdc2-like kinase2 (CLK2)⁵⁶ repress PGC-1 α 's activity.

Phosphorylation of PGC-1 α by AMPK is a prerequisite for activation of PGC-1 α : Upon energy deprivation, the cellular levels of nicotinamide dinucleotide (NAD⁺) increase through AMPK. This leads to increased

activity of silent information regulator 1 (SIRT1) which deacetylates and thus activates PGC-1 α ⁵⁷. This deacetylation must be preceded by phosphorylation of PGC-1 α by AMPK. Upon caloric excess, the acetyltransferase general control of amino acid synthesis5 (GCN5) acetylates PGC-1 α which has an inhibitory effect⁴⁵.

PGC-1 α is known to have a short half- life of about 2.3 hours⁵⁵. Proteasomal degradation of PGC-1 α in this context plays a huge role via glycogen synthase kinase 3 β (GSK3 β)⁵⁸.

Recently, PGC-1 α has been found to be sumoylated which decreases its activity via a possible interaction with the corepressor receptor interacting protein 140 (RIP140)⁵⁹.

PGC-1 α also undergoes methylation by protein arginine methyl-transferase1 (PRMT1) enhancing its transcription as well as glycosylation by O-linked N-acetylglucosamine (O-GlcNAc) transferase (OGT). The functional role of the latter modification, though, is not known to date^{60,61}.

3.5.1.3. Splicing mediated regulation

Other than the rapid control of PGC-1 α via posttranslational modification or the slower, transcriptional control of PGC-1 α , there is a third option of modulating its activity:

Assembly of different exons yields mRNAs that are different in size and exon composition: These different splice forms may be the result of specific stimuli: PGC-1 α was first found to be subject to alternative splicing mechanisms in BAT in response to cold⁶². A similar splicing pattern was identified in skeletal muscle: The resulting splice variant was exercise- induced, lacked exon8 and yielded a functional, albeit smaller PGC-1 α protein¹⁰. Some years on, PGC-1 α was found to harbor two versions of exon1: exon1a and exon1b: Coupling of either of these exons with exon2 generates diverse isoforms of PGC-1 α which are stress inducible in skeletal muscle, BAT or liver^{63,64}.

Recently, an N-terminal splice variant of PGC-1 α , containing a stop codon after exon6 was described. This variant seems to be relatively stable and its cellular localization (nuclear vs cytoplasmic) and thus activity are determined by phosphorylation⁶⁵.

3.5.2. Mechanisms downstream of PGC-1 α

Increased levels of PGC-1 α in skeletal muscle entail a myriad of different physiological outcomes; some of the most important ones are as follows:

Exercise means increased ATP demand: Cells can increase their ATP levels via glycolysis, OXPHOS and β -oxidation of fatty acids: The latter two require oxygen but supply the organism with a higher yield of ATP than non-oxidative forms of energy generation:

OXPHOS and oxidation of fatty acids take place in mitochondria: Upon exercise, these organelles reorganize by fusion or fission and increase their number and size to increase performance. The increase in number, termed mitochondrial biogenesis is potently stimulated by PGC-1 α which also upregulates mRNA content of components of the electron transport chain, like cytochrome oxidases COXI, COXII, COXIV, ATP synthase and cytochrome c (CYT c)⁴⁰. These are both mitochondrially (e.g. COXI, COXII) as well as nuclear- encoded (e.g. COXIV, CYT c).

Mitochondria are organized into subsarcolemmal (SSL) and intermyofibrillar (IMF) mitochondria that differ in their location, biochemical properties and speed of substrate utilization⁶⁶.

Generation of metabolites for OXPHOS takes place in the tricarboxylic acid (TCA) cycle: This cycle requires acetyl-CoA which is delivered by β -oxidation of fatty acids and glycolysis and thus couples carbohydrate and fat metabolism: In this cycle, PGC-1 α increases citrate synthase (CS) activity¹³. To further increase TCA cycle activity, PGC-1 α also mediates uptake of free fatty acids (FFAs) from the blood into the muscle via the CD36 fatty acid translocase (CD36), it upregulates carnitine palmitoyltransferase 1 (CPT1) and medium-chain acyl-coenzyme A dehydrogenase (MCAD) which mediate β -oxidation of fatty acids⁶⁷.

Another argument for preferential oxidation of FFAs for ATP generation is that PGC-1 α increases glucose uptake via the GLUT4 transporter⁵. Yet, the glucose is not shuttled into glycolysis but into generation of lipids via fatty acid synthase (FAS). These lipids concomitantly serve as substrates for β -oxidation of FFAs⁶⁸. PGC-1 α thus seems to be involved in catabolic and anabolic skeletal muscle metabolism. Furthermore, PGC-1 α promotes glycogen synthesis to assure energy provision for sustained exercise⁶⁹.

Increased OXPHOS necessitates increased oxygen supply to the skeletal muscle: PGC-1 α thus promotes angiogenesis and increases myoglobin levels in this tissue^{40,70}. Myoglobin contains an oxygen binding prosthetic group called heme. PGC-1 α increases heme biosynthesis by inducing the expression of its rate limiting enzyme, δ -aminolevulinatase synthase1 (ALAS-1)⁷¹.

OXPHOS also leads to increased levels of reactive oxygen species (ROS), which are generated through incomplete reduction of an oxygen molecule: The resulting oxygen radical is detoxified via enzymes like superoxide dismutase (SOD2) whose transcript levels are increased by PGC-1 α ⁷². PGC-1 α also employs a second strategy in reducing cellular ROS levels: It increases mRNA expression of uncoupling proteins UCP2 and UCP3⁷³. These dissipate the proton gradient created during oxidative phosphorylation.

Decreased ROS confer a higher degree of protection against DNA damage and inflammatory events to the cell: Mice overexpressing PGC-1 α in skeletal muscle display reduced levels of tumor necrosis factor α (TNF α) and interleukin-6 (IL-6) in serum and skeletal muscle⁷².

Given the numerous metabolic adaptations to stress that PGC-1 α expression enables, it is understandable that this coactivator is rapidly inducible upon exercise in rodents and humans^{10,74}. Yet, a

mouse model of sustained, skeletal muscle specific overexpression of PGC-1 α mediates not only metabolic, but also functional changes:

Structurally, skeletal muscle is composed of different fiber types according to their metabolic profile and contractile isoform: It is made up of so called fast-twitch and slow-twitch fibers: Fast-twitch fibers in rodents contain type IIB and IIX myosin heavy chains (MHCs) that mainly use glycolysis for energy generation. They share a white phenotype, low myoglobin concentration and tire rapidly. They thus are equipped for short term, acute bouts of exercise. Rodent slow-twitch fibers contain type I and IIA MHCs and mainly use OXPHOS for energy provision. They appear red in color, have high myoglobin content and are effective in sustained, long term exercise⁷⁵.

Upon skeletal muscle specific overexpression, PGC-1 α promotes the conversion of fast into of slow-twitch fibers⁴⁰ in mice. Consequently, these mice have increased running endurance, yet reduced peak performance^{67,69}.

PGC-1 α improves endurance muscle performance not only in the basal state, but is also beneficial in disease models: First, its ectopic expression prevents muscle fiber atrophy caused by denervation⁷⁶. Second, in a mouse model of *Duchenne muscular dystrophy*, characterized by a mutation in the dystrophin gene, PGC-1 α ameliorates muscle histology, serum creatine kinase (CK) levels and running performance⁷⁷.

In summary, PGC-1 α is a versatile coactivator that mediates a vast program of skeletal muscle plasticity (**Fig.4**). (See ⁴¹ for a more detailed review).

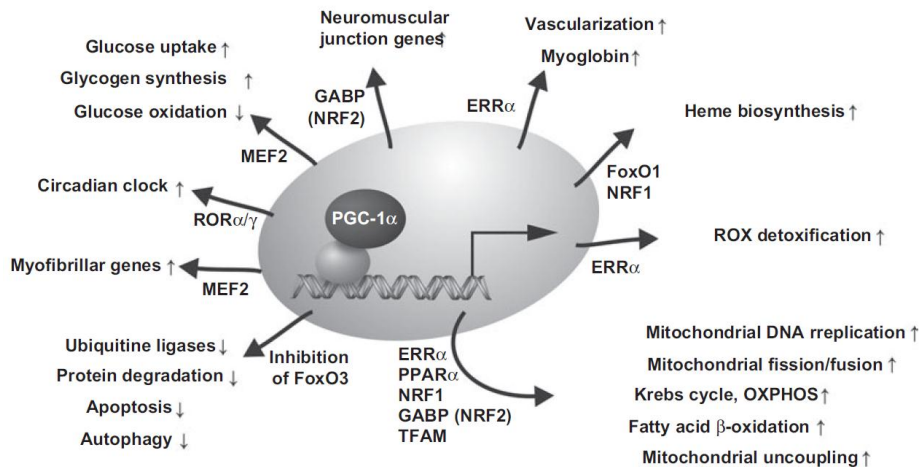


Fig.4: PGC-1 α induces a pleiotropic response in skeletal muscle upon exercise

Source: ⁴¹.

4. The role of PGC-1 α in retina

4.1. Introduction

4.1.1. Retina structure

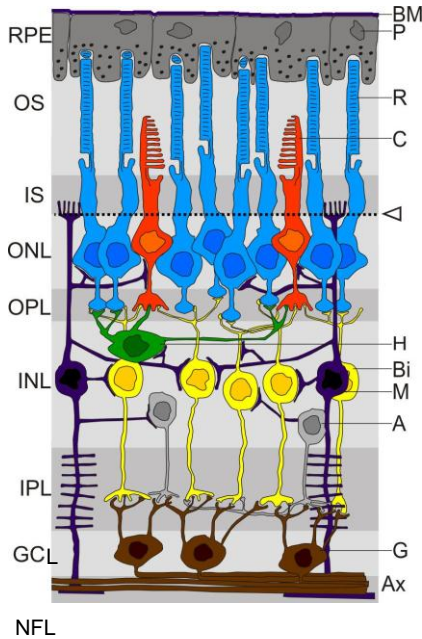


Fig.5: Retina structure: abbreviations: left hand side: cell layers; right hand side: cell types;
RPE= retinal pigment epithelium
OS= outer segment
IS= inner segment
ONL= outer nuclear layer
OPL= outer plexiform layer
INL= inner nuclear layer
IPL= inner plexiform layer
GCL= ganglion cell layer
NFL= nerve fiber layer
BM= basal membrane
P= pigment epithelial cell
R= rod
C= cone
H= horizontal cell
Bi= bipolar cell
M= Müller cell
A= amacrine cell
G= ganglion cell
Ax= axon

Source:

<http://de.wikipedia.org/w/index.php?title=Datei:Retina.jpg&filetimestamp=20080814113451>

Epiretinal layer



The vertebrate retina translates the information of a photon of light into an electrical signal. It is a complex layer at the innermost part of the eyeball and is made up of 8 distinct cell types that allow for visual perception. Six of these cell types are neuronal cells: Ganglion, amacrine, bipolar, horizontal cells (= interneurons) and rod and cone photoreceptors.

Two retinal cell types are non-neuronal: Müller cells and retinal pigment epithelial (RPE) cells.

The 8 distinct cell types are distributed across functionally diverse compartments: Three of these compartments are rich in cell bodies and consequently, cell nuclei: The outer nuclear layer (ONL), inner nuclear layer (INL) and the ganglion cell layer (GCL).

The vertebrate retina is inverted, meaning that light penetrates the eye at the neuronal cell layers until it reaches the photoreceptors which process the signal. This information is then conveyed back to the interneurons which in turn transmit it to other neuronal cells and to the brain¹⁴:

The RPE locates next to the chorioidea that contains blood vessels responsible for nutrient supply of the retina. Phototransduction takes place in the adjacent rod and cone photoreceptors, that are specialized in mediating vision in darkness/ mesopic conditions and light conditions, respectively. Photoreceptors are composed of an outer segment (OS) made up of stacks of membrane disks. These disks contain cone or

rod opsin linked to 11-*cis* retinal. Upon illumination, the 11-*cis* retinal moiety changes its confirmation to all-*trans* retinal and dissociates from opsin. This process is termed “bleaching”. All-*trans* retinal is shuttled into the RPE which regenerates 11-*cis* retinal for use in the OS. The RPE also phagocytes used photoreceptor disks that are not functional any more in a process called “disk shedding”. The photoreceptor OS is connected to the inner segment (IS) via a connecting cilium. The IS contains mitochondria and endoplasmic reticulum and thus constitutes the photoreceptors’ metabolically active compartment.

The cell bodies of rod and cone photoreceptors convey information via glutamate release to bipolar cells and then to ganglion cells. Glutamate has either activating (on bipolar cells) or repressing (off bipolar cells) effects on them. Horizontal cells mediate vision when the photoreceptors’ periphery is illuminated. As such, they are at the interface between photoreceptors and bipolar cells. Amacrine cells are mediators between rod bipolar and on/ off bipolar cells. Rod and cone signaling thus converges in activation of on/ off bipolar cells and ganglion cells. Müller cells are glia cells that span across the retina and thus occupy a stabilizing function. The nerve fiber layer (NFL) contains several axons of ganglion cells and lies adjacent to the epiretinal layer which forms a tight delimitation against the vitreous body¹⁴.

4.1.2. Phototransduction

Photoreceptor rods and cones mediate vision in a similar way: Rods are more light- sensitive and better equipped for visualizing movement. Cones are less light sensitive yet generate color vision. While rods contain only one type of rhodopsin, there are three different, wavelength-specific cone types in humans: L-cones (blue), M-cones (green) and S-cones (red)⁷⁸.

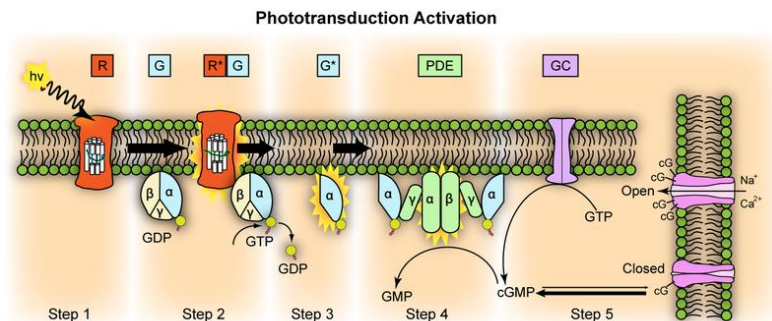


Fig.6: Phototransduction process in the retina in light (simplified)

Depicted is an outer membrane disk in a rod. Step 1: photon (hv) is absorbed and activates rhodopsin R by conformational change in the disk membrane to R*. Step 2: Next, R* makes repeated contacts with transducin G, catalyzing its activation to G* by the release of bound GDP in exchange for GTP. Step 3: G* binds inhibitory γ subunits of the phosphodiesterase (PDE) activating its α and β subunits. Step 4: Activated PDE hydrolyzes cyclic guanosine monophosphate (cGMP) to 5'cGMP. cGMP levels fall which closes cyclic nucleotide gated channels ($\text{Na}^+/\text{Ca}^{2+}$ channels), the cell hyperpolarizes, transmitter release is decreased. Step 5: Guanylyl cyclase (GC) restores cGMP levels.

Source: <http://commons.wikimedia.org/wiki/File:Phototransduction.png>

4.1.2.1. In darkness

Photoreceptor cells dispose of different ion channels to mediate vision by changing their membrane potential:

cGMP gated sodium channels enable sodium inflow into the cell and thus depolarize it. Nongated potassium channels lead to an outflow of potassium, thus hyperpolarizing the cell.

In darkness, photoreceptors are depolarized through an inward flow of sodium: This mechanism triggers the opening of calcium channels and the release of vesicles containing the neurotransmitter glutamate into the synaptic cleft. Photoreceptors thus signal to bipolar cells via glutamate which likewise transmit the signal to ganglion cells. ON bipolar cells hyperpolarize in response to high glutamate levels whereas OFF bipolar cells depolarize. Thus, in darkness, ON bipolar cells are inhibited and OFF bipolar cells are activated⁷⁸.

4.1.2.2. In light

Initiation

In light, phototransduction occurs via the photopigment Rhodopsin (rods) or Cone opsin (cones). It consists of the molecule opsin bound to 11-*cis* retinal. Upon interaction with a photon of light, 11-*cis* retinal undergoes isomerization into all-*trans* retinal which cannot accommodate into the opsin binding pocket any more. Consequently, opsin dissociates as meta-rhodopsin II and activates the G protein transducin. The GDP bound transducin dissociates from guanine diphosphate (GDP) and binds guanine triphosphate (GTP) with its α subunit while the β and γ subunits dissociate. Transducin activates phosphodiesterase (PDE) which cleaves cyclic guanine monophosphate (cGMP) into 5'GMP. Decreasing cGMP levels lead to closure of sodium channels which hyperpolarizes the cell. Voltage gated calcium channels close and calcium levels drop. In response, glutamate levels also drop as they require calcium for vesicle fusion. Low glutamate levels cause depolarization of ON bipolar cells and hyperpolarization of OFF bipolar cells⁷⁸.

Termination

The visual cycle is terminated via GTPase activating protein (GAP) which transforms GTP into GDP, halting the action of the PDE. Guanylyl cyclase activating protein (GCAP) dissociates from its bound calcium ions and activates guanylyl cyclase (GC) which transforms 5'GMP into cGMP. This increase in cGMP levels reopens the cell's sodium and calcium channels.

In parallel, the decrease in calcium levels during phototransduction leads to dissociation of calcium from recoverin and rhodopsin kinase. Consequently, rhodopsin kinase phosphorylates meta-rhodopsinII, deactivating it. Arrestin further deactivates meta-rhodopsinII and restores the dark current⁷⁸.

Regeneration (Visual cycle)

All-*trans* retinal is reduced to all-*trans* retinol and is then shuttled to the RPE where it is recharged: It is first esterified by lecithin-retinol acyltransferase (LRAT) and then converted to 11-*cis* retinal by the isomerohydrolase RPE65. Consequently, it is shuttled back to the photoreceptor for resuming the phototransduction process.

4.1.3. PGC-1 α in retina

The implication of PGC-1 in visual function has not been thoroughly studied thus far, yet several cues warrant its analysis in retina:

PGC-1 α and PGC-1 β are primarily expressed in tissues with high energy requirements (see chapter 3.4 and recent review⁷⁹). The retina is one of the most energy demanding organs per gram of tissue⁸⁰.

PGC-1 α and PGC-1 β are expressed in a circadian- rhythm specific fashion throughout the day^{81,82}. PGC-1 α governs transcription of the clock gene BMAL1, whose ablation leads to defective retinal activity in response to a light flash⁸³.

PGC-1 α is reduced in age and metabolic conditions like type II diabetes in skeletal muscle⁸⁴. These conditions also predispose towards development of retinal pathologies like age-related macular degeneration (AMD) and diabetic retinopathy, respectively⁸⁵. AMD involves increased generation of reactive oxygen species (ROS), inflammatory response and endoplasmic reticulum associated stress leading to apoptosis, all of which are associated with decreased PPAR γ levels⁸⁶. PGC-1 α , on the other hand, is known to promote ROS detoxification as well as decreasing expression levels of inflammatory genes⁷². Furthermore, photoreceptor phagocytosis in the retina involves PPAR γ activation⁸⁷.

4.1.4. Apoptotic pathways

Apoptosis or programmed cell death is a highly regulated process: It is required during development as well as cellular stress situations to ensure tissue viability and function. Impaired as well as increased apoptotic signaling can be implicated in a variety of diseases (cancer, autoimmune disease, neurodegenerative diseases)^{88,89}. Stimuli like DNA damage, temperature insults (heat or cold exposure), hypoxia, oxidative stress, virus infection or energy deprivation can lead to induction of apoptosis via a defined sequence of events⁹⁰. Unlike necrosis, where the cell contents is released in an uncontrolled fashion into the cytosol and thus promotes inflammation and compromise of neighboring cells, apoptosis occurs in distinct phases: the cell shrinks, shows deformation and loses contact to its adjacent cells, chromatin condenses, the plasma membrane blebs or buds, and finally the cell is fragmented into

compact membrane-enclosed structures, called 'apoptotic bodies' which contain cytosol, the condensed chromatin, and organelles^{91,92}.

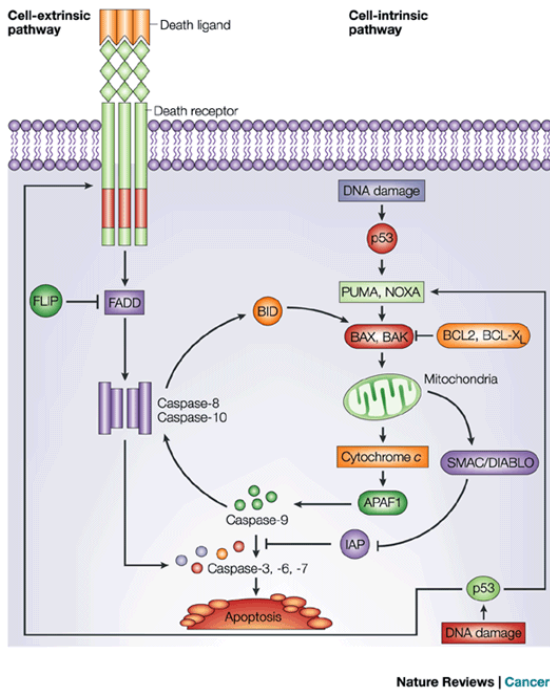


Fig.7: Intrinsic and extrinsic apoptotic pathways

Source: ⁹³.

The pathways leading to apoptosis are diverse (**Fig.7**):

The intrinsic pathway starts with internal cellular insults like hypoxia, DNA damage or energy deprivation. The tumor suppressor p53 is subsequently phosphorylated and stabilized via the DNA damage checkpoint mediators Ataxia Telangiectasia mutated protein (ATM) and Checkpoint Factor-2 (CHK2). P53 then represses anti apoptotic BCL2. BCL2-associated X protein (BAX), BCL2 antagonist (BAK), NADPH oxidase activator 1 (NOXA) and BH3 interacting domain death agonist (BID) are further targets of p53 which propagate the apoptotic signal. Their apoptogenic properties lead to release of SMAC/ DIABLO which inactivates the inhibitor of apoptosis (IAP) molecule. In parallel, cytochrome c is extruded by the mitochondria which binds to apoptotic peptidase activating factor 1 (APAF1) and to pro-caspase 9, generating the “apoptosome”. As a consequence, caspases 3, 6 and 7 ultimately execute apoptosis via cleavage of cytosolic and nuclear proteins^{94,93}.

The extrinsic pathway commences with binding of a death ligand to a death receptor located on the damaged cell's surface. Different ligands have been characterized, ranging from Fas Ligand (FASL) or TNF related apoptosis inducing ligand (TRAIL)^{95,96}.

Typically, this leads to ceramide release and lipid raft fusion which results in large scale clustering of the death receptors. Several apoptotic proteins like FAS associated death domain (FADD) then bind to the receptors which triggers recruitment of caspases 8 and 10. These caspases then integrate with the intrinsic pathway via activation of BH3 interacting domain death agonist (BID)⁹⁵.

Besides intrinsic and extrinsic pathways, there are also alternative apoptotic pathways that do not involve caspase activation: Among the non caspase proteases are the calcium dependent calpains, cathepsins and serine proteases like granzyme A. Among caspase independent endonucleases there are Cyclophyline A/ apoptosis inducing factor (AIF), Granzyme A Activated DNase (GAAD), leucocyte elastase inhibitor (LEI)⁸⁸.

Programmed cell death may also involve mechanisms of autophagy which is a degradation mechanism for cell organelles, ubiquitin-proteasomal degradation steps or tissue specific mechanisms as cell shedding or cornification^{88,97}.

In conclusion, apoptosis is not a one canonical process but involves an interplay of diverse mechanisms which may be tissue specific.

4.1.4.1. Apoptosis in retina

Apoptosis in the retina occurs as a result of degenerative diseases that are acquired (like AMD, glaucoma and diabetic retinopathy) or hereditary conditions (like *Retinitis pigmentosa* or *Leber's congenital amaurosis*)^{98,99}, retinal development and physiological stressors (excessive light exposure, ROS). All of these stimuli lead to apoptosis of retinal cells. According to the employed stimulus, apoptosis varies in time of onset, severity and duration and nature of cells that are primarily affected (e.g. photoreceptors in *retinitis pigmentosa* versus ganglion cells in glaucoma)¹⁰⁰. Owing to this multitude of stimuli, retinal apoptosis does not only involve the classical intrinsic and extrinsic pathways⁸⁸:

Exposure to excessive amounts of light is an established model for studying photoreceptor apoptosis. Contrary to disease models, light exposure can be well dosed and is a monofactorial model:

Different molecules are involved in the light induced apoptotic induction, transduction, execution and clearance phases, respectively:

Light damage induction requires a functional visual cycle: This cycle is interrupted in the absence of 11-*cis* retinal and the photoreceptors are resistant to light damage: Absence of RPE65, which regenerates 11-*cis* retinal thus prevents light damage induced apoptosis¹⁰¹. In accordance with that, absence of Rhodopsin prevents light induced apoptosis¹⁰¹.

Likewise, absence of the retinoid chaperone cellular retinaldehyde-binding protein (CRALBP) which fosters rhodopsin regeneration protects mice from light damage¹⁰².

The amount of light absorption by rhodopsin is also critical in determining how much damage occurs in the light- exposed retina: As blue light likely regenerates rhodopsin from its bleaching intermediates, it can

provide a higher number of bleachable rhodopsin molecules than green light: Blue light exposure thus causes more light damage¹⁰³.

Compromise in termination of the phototransduction cascade via ablation of rhodopsin kinase and/ or arrestin also renders mouse retina more vulnerable to light damage^{104,105}.

Transducin- deficient mice are as sensitive as WT mice towards acute bright light exposure, however, prolonged moderate light exposure is not harmful for these animals¹⁰⁵.

Consequently, damage induced by acute light exposure is mediated by rhodopsin bleaching¹⁰¹ whereas damage by moderate light exposure requires a functioning phototransduction process¹⁰⁵.

The light induced death signal is propagated via the transcription factor activator protein1 (AP-1). AP-1 consists of different members of the c-FOS or c-FOS and c-JUN proteins which partly fulfill redundant functions. c-FOS was shown to be involved in light induced apoptosis¹⁰⁶.

Interestingly, the classical apoptotic protein, p53, does not seem to be involved in light-induced apoptosis in retina¹⁰⁷.

The execution and termination phases in retinal apoptosis may be mediated in part by caspases. Caspase inhibition however was not shown to be protective¹⁰⁸. Most likely, caspases are important in apoptosis during retinal development whereas caspase independent apoptosis seems to be associated with retinal disease conditions¹⁰⁰: Retinal cell death may also occur via autophagy or ubiquitin- proteasomal degradation⁸⁸.

Protection strategies against light induced retinal cell death target the above mentioned phases:

Inhibition of nitric oxide synthase (NOS) is a very effective tool in the early stage of apoptosis¹⁰⁸.

In the late stage of apoptosis, besides a range of growth factors and erythropoietin¹⁰⁹, one of the most important protective responses to light induced retinal apoptosis in Müller cells is the induction of leukemia inhibitory factor (LIF). Upon light insult, it activates JAK-STAT signaling (JAK= janus kinase2, STAT1 and 3= signal transducers and activators of transcription1 and 3)¹¹⁰. Its absence leads to accelerated retinal degeneration¹¹¹.

4.1.4.2. Apoptosis and PGC-1 α

PGC-1 α has been linked to apoptosis in different contexts and tissues:

In skeletal muscle, absence of PGC-1 α is associated with reduced content of IMF and SSL mitochondria as well as reduced CYT c mRNA expression levels¹¹². However, CYT c release from subsarcolemmal mitochondria of PGC-1 α KO mice is increased¹¹³.

Likewise, p53 knockout animals have reduced mitochondrial content and diminished protein levels of PGC-1 α . Subsarcolemmal CYT c release is increased, whereas intramyofibrillar CYT c release is

decreased. Total apoptosis measured by nucleosomal fragmentation, however, is decreased in this setting¹¹⁴.

As no other measurement of apoptosis was used in¹¹³ and no apoptotic trigger was employed in both¹¹³ and¹¹⁴, it is hard to pinpoint the implication of PGC-1 α in skeletal muscle apoptosis.

An apoptotic trigger was employed by Liang et al who looked at the effects of potassium deprivation in cerebellar granule neurons leading to c-Jun kinase (JNK9) activation: The increase in this inflammatory mediator negatively regulates the PGC-1 α promoter. PGC-1 α overexpression on the other hand seems to decrease apoptosis¹¹⁵.

During the course of this PhD project, Zheng et al showed that lovastatin, a cholesterol lowering drug, also influences the diabetic retina: Lovastatin decreases ROS production and displays anti-inflammatory effects, reduced Poly ADP ribose polymerase (PARP) and p38 MAPK protein levels correlating with increased PGC-1 α levels⁸⁵.

In light of these data, it would be desirable to conclusively show in loss AND gain of function experiments what PGC-1 α 's actual role in retinal apoptosis induction is, using a tissue- specific trigger.

4.2. Project aims

The role of PGC-1 in retina should thus be studied with regard to seven major questions:

- Retinal expression patterns of PGC-1 α and PGC-1 β
- Localization of PGC-1 α and PGC-1 β in the different retinal compartments
- Relevance of PGC-1 α and PGC-1 β for retinal development
- Expression of PGC-1 α and PGC-1 β in retinal disease models
- Retinal response to a physiological stressor in the absence of PGC-1 α as well as its functional and morphological analysis
- Implication of PGC-1 α in retinal apoptosis

4.3. Manuscript

PGC-1 α determines light damage susceptibility of the retina

Anna Egger¹, Marijana Samardzija², Vithiyajali Sothilingam³, Naoyuki Tanimoto³, Christina Lange², Silvia Salatino¹, Lei Fang⁴, Marina Garcia-Garrido³, Susanne Beck³, Michał J Okoniewski⁵, Albert Neutzner⁴, Mathias W. Seeliger³, Christian Grimm² & Christoph Handschin¹

¹ Biozentrum, Division of Pharmacology/Neurobiology, Biozentrum, University of Basel, Basel, Switzerland

² Laboratory for Retinal Cell Biology, Department of Ophthalmology, University of Zurich, Zurich, Switzerland

³ Division of Experimental Ophthalmology, Institute for Ophthalmic Research, University of Tübingen, Tübingen, Germany

⁴ Department of Biomedicine, University Eye Clinic, University Hospital Basel, Basel, Switzerland.

⁵ Functional Genomics Center UNI ETH Zurich, Zurich, Switzerland

Correspondence should be addressed to: Christoph Handschin, Division of Pharmacology/Neurobiology, Biozentrum, University of Basel, Klingelbergstrasse 50-70, CH-4056 Basel, Switzerland, *Phone*: +41 61 267 2378, *Fax*: +41 61 267 2208, *Email*: christoph.handschin@unibas.ch

Abstract

The peroxisome proliferator-activated receptor gamma coactivator 1 (PGC-1) proteins are key regulators of cellular bioenergetics and are accordingly expressed in tissues with a high energetic demand. We now show that PGC-1 α and PGC-1 β are found at high levels in the mouse retina, most prominently in the photoreceptors. PGC-1 α knockout mice suffer from a striking deterioration in retinal morphology and function upon detrimental light exposure. Gene expression analyses revealed dysregulation of all major pathways involved in retinal damage and apoptosis, repair and regeneration in the PGC-1 α knockouts. The light-induced increase in apoptosis *in vivo* in the absence of PGC-1 α was substantiated *in vitro*, where overexpression of PGC-1 α showed strong anti-apoptotic effects. Finally, we found that retinal levels of PGC-1 expression are reduced in different mouse models for *retinitis pigmentosa*. Our findings thus imply that PGC-1 α might be an attractive target for therapeutic approaches targeted at retinal degeneration diseases.

Introduction

The vertebrate retina translates information of a photon of light into an electrical signal. It is a complex, 7-layered compartment at the innermost part of the eye and is made up of 8 distinct cell types, five of which are neuronal cells. Photons hit photosensitive cells (photoreceptors), which enable phototransduction by conformational change of the photopigment rhodopsin. Distinct photoreceptors allow for vision in light (cone cells) and dark (rod cells) conditions. Subsequent photopigment recovery occurs in the adjacent retinal pigment epithelium (RPE)¹⁴. The light information is transmitted from the photoreceptors via interneurons (amacrine cells, horizontal cells, bipolar cells) to ganglion cells, which then relay an electric action potential to the optical nerve and ultimately the visual cortex in the brain.

PGC-1 (peroxisome proliferator-activated receptor γ coactivator-1) designates a family of coactivators that comprises PGC-1 α , PGC-1 β and PGC-1-related coactivator (PRC). These coactivators dock to specific nuclear receptors and other transcription factors, thereby promoting the transcription of target genes, for example those implicated in mitochondrial biogenesis and oxidative phosphorylation (OXPHOS)^{19,18,116,117}. PGC-1 α and PGC-1 β are mainly expressed in tissues with a high energetic demand, such as skeletal muscle, liver, pancreas, heart, kidney, brain and brown adipose tissue (BAT)^{19,18,116,117}. The expression of PGC-1 α and PGC-1 β is further regulated in these organs by developmental stimuli and physiological stressors like cold, fasting and exercise. PGC-1 α and PGC-1 β accordingly regulate tissue-specific functions such as adaptive thermogenesis in brown adipose tissue, gluconeogenesis in the liver or endurance exercise adaptation in skeletal muscle^{19,18,116,117}.

Interestingly, despite the well-established link between PGC-1 expression and cellular energetics, the expression and function of the PGC-1 coactivators in the retina, one of the most energy demanding vertebrate organs⁸⁰, has not been studied so far, even though a number of cues warrant the analysis of this coactivator family in this organ.

The high demand on ATP for physiological retinal function is assured by both glycolysis and oxidative phosphorylation: Neurotransmission relies on glycolysis, sodium transport employs glycolysis and oxidative phosphorylation, whereas phototransduction is mainly fuelled by oxidative phosphorylation to meet energetic demands¹¹⁸. In phototransduction, rods and cones are comparable in their energy expenditure in dark conditions, while cones have greater energy demands in the light¹¹⁹. Thus, most of the metabolic processes that are important for retinal function are most probably strongly regulated by the PGC-1 coactivators in analogy to other tissues, in particular substrate uptake, fatty acid oxidation and oxidative phosphorylation.

Inversely, pathological conditions of the retina such as age-related macular degeneration and diabetic retinopathy are associated with excess generation of reactive oxygen species (ROS), inflammation and endoplasmic reticulum stress, which result in apoptosis and tissue degeneration^{86,85}. PGC-1 α affects these processes by promoting ROS detoxification⁴³, ameliorating endoplasmic reticulum stress¹²⁰ and modulating tissue as well as systemic inflammation^{121,122}. Finally, photoreceptor outer segment renewal involves activation of PPAR γ ⁸⁷, a functional interaction partner of the PGC-1 coactivators in various tissues¹.

Thus, to investigate the potential role of PGC-1 α in the retina, we assessed the expression patterns of PGC-1 α and PGC-1 β in retinal development, adult retina and mouse models for degenerative retinal diseases. Furthermore, we investigated the consequences of genetic ablation of PGC-1 α in the retina in terms of changes in gene expression, morphology and function in the basal, dark condition and upon light-induced retinal stress and damage. Finally, we validated some of our findings in retinal cells *ex vivo* with acutely altered levels of PGC-1 α . Our findings indicate a crucial role for PGC-1 α in tissue protection, in part by inhibition of apoptosis.

Results

PGC-1 α and PGC-1 β are highly expressed in murine retina

Real-time qPCR-based expression analysis revealed highest PGC-1 α and PGC-1 β levels in tissues with a great energetic demand. Accordingly, PGC-1 α and PGC-1 β were found at elevated levels in skeletal and cardiac muscle, brain and kidney. Both coactivators were more moderately expressed in liver and lung.

Strikingly, the highest expression levels of all tissues studied were observed in the retina for PGC-1 α and PGC-1 β (**Fig. 1a**).

To assess the differential expression pattern of PGC-1 α and PGC-1 β in distinct retinal compartments, we used laser capture microdissection to separate the different retinal cell layers and subsequently quantified expression via qPCR. PGC-1 α and PGC-1 β showed their highest expression in the outer nuclear layer (ONL) that harbors rod and cone photoreceptors (**Fig. 1b**). Although markedly lower compared to ONL, expression of both coactivators was also found in the inner nuclear layer (INL), which contains bipolar, horizontal, amacrine and Müller glia cells, and the ganglion cell layer (GCL), where ganglion and amacrine cells are located (**Fig. 1b**).

To distinguish between rod and cone-specific expression of the PGC-1 coactivators within the ONL, we determined PGC-1 α and PGC-1 β levels in neural retinal leucine zipper (*Nrl*) knockout animals, which lack rod photoreceptors but retain cone morphology and function¹²³ and the rd10 mouse model where rod degeneration is followed by cone degeneration until all photoreceptors are lost by day 60¹²⁴. The significant reduction of PGC-1 α and PGC-1 β transcript levels in *Nrl* knockout mice (**Fig. 1c**) and the rd10 animal model (**Fig. 1d**) implies that both coactivators are expressed in rods and cones.

Genetic ablation of Pgc-1 α does not compromise morphology and function in the dark adapted, unstressed mouse retina

PGC-1 α global knockout animals¹²⁵ were used to study the function of PGC-1 α in the retina. First, we analyzed basal morphology of 7 week- old PGC-1 α knockout (KO) and C57 BL/6 WT control mice. Both KO and WT animals revealed an intact, regularly shaped retinal structure (**Fig. 2a**). To assess basal retinal function, the mice were kept in the dark and then subjected to an electroretinogram (ERG), which tracks the electrical responses of retinal cells to a light stimulus. The resulting a and b waves reflect the function of the outer and inner layer, respectively. ERG responses were recorded in scotopic (darkness) and photopic (illuminated) conditions to analyze rod and cone function, respectively. In all of these experimental contexts, the PGC-1 α KO mice showed regular a and b waves undistinguishable from the WT control animals (**Fig. 2b**). Finally, in addition to the morphological and functional studies, we investigated whether genetic ablation of the PGC-1 α gene in the retina affects global gene expression patterns with gene expression microarrays. Gene ontological analysis revealed primarily a reduction in metabolic pathways in the KO animals, foremost oxidative phosphorylation and citrate cycle (**Fig. 2c**), similar to results in loss-of-function experiments with PGC-1 α in other tissues. Inversely, cytoskeleton remodeling, transforming growth factor beta (*Tgfb*) and *Wnt* signaling were the most prominent pathways expressed at a higher level in KO compared to WT mice (**Fig. 2c**).

Absence of PGC-1 α increases light-damage susceptibility

While in most organs, the effects of genetic ablation on morphology and function are relatively mild, stress conditions like exercise, cold or fasting greatly exacerbate the phenotype of PGC-1 α knockout mouse models^{121,125}. Thus, triggered by our observation of a small effect of PGC-1 α knockout on retinal morphology and function in the dark, we sought to study the repercussions of PGC-1 α ablation after employing a physiological, retina-specific stressor. For this purpose, PGC-1 α KO and WT control mice were exposed to 15.000 lux of white light for 2hrs, which corresponds to direct sun light exposure. After a 24hrs recovery period, morphologies of PGC-1 α deficient and WT control retinæ were analyzed. In stark contrast to the dark-adapted mice (**Fig. 2**), PGC-1 α KO and WT control mice responded markedly differently to a strong light insult. First, most of the rod inner (RIS) and outer (ROS) segments

were completely destroyed and most nuclei were pyknotic in the ONL of PGC-1 α KO mice (**Fig. 3a**). Thus, most photoreceptors have lost their light absorption (ROS) and energy-production (RIS) sites. In contrast, the corresponding regions in WT exhibited only occasional pyknotic nuclei (**Fig. 3a**) and only one out of six wild type animals showed measurable retinal damage, which, however, was still less intense than in PGC-1 α KOs (data not shown). In either of the genotypes, the INL and GCL layers were unharmed consistent with previous data showing that light damage causes selective death of photoreceptor cells¹⁰¹ (**Fig. 3a**).

Given the nature and extent of retinal degeneration observed in the KO animals, it seemed highly likely that these morphological changes would translate into loss of retinal function. Light- exposed PGC-1 α KO mice displayed a blunted scotopic ERG compared to the WT mice with a significant reduction in b wave amplitude 10 days post insult (**Fig. 3b**). This timeframe was chosen as retina clears injured photoreceptors and returns back to a basal state within 10 days⁸⁸. The photopic response in KO animals remained similar to WT mice, which is consistent with the notion that cones remain unharmed in an acute light- damage paradigm, at least at early timepoints after light damage¹²⁶.

Subsequent to the ERG analysis, animals were subjected to spectral domain optical coherence tomography (SD-OCT), which allow for highly sensitive cross sectional analysis of retinal layers, respectively, and thus reveal retinal detachment as well as delicate structural impairments. Cross sectional retinal analysis showed that the KO mice that had a reduced scotopic ERG response also displayed a thinning of the ONL compared to WT controls. (**Fig. 3c- ABC**).

Light-exposed PGC-1 α KO animals exhibit reduced expression of phototransduction genes, increased expression of apoptotic and inflammatory markers

To elucidate the deficits in gene expression in the light-stressed PGC-1 α KO animals, we compared gene expression microarrays of WT and KO mice in the control, dark-adapted state and after light exposure, respectively. Interestingly, the influence of the environmental conditioning from dark to light exposure was similar in the two genotypes in regard to the number of regulated genes. However, most of the 2914 genes regulated in the KO animals between dark and light were different from the 2524 genes in the WT animals or were modulated at a significantly higher level. Thus, light- exposed PGC-1 α KO and WT mice differed in the expression of 1774 genes, 897 of which were elevated and 877 of which were decreased in KO compared to the WT mice, more than three times the number of genes as observed in the corresponding dark accommodated mouse comparison (**Fig. 4a, Suppl. Fig. 1e**). The top regulated genes (**Suppl. Table 1a**) and the most affected pathways (**Suppl. Table 1b**) that were downregulated in KO mice compared to WT animals still included metabolic processes as observed in the dark condition. Strikingly however, various key processes in retinal function, damage and repair, in particular visual perception, photoreceptor function, DNA damage and repair were now lower in the KO animals compared to controls (**Fig. 4b, 4c and Suppl. Fig. 1a-c**). Phototransduction pathway analysis showed that PGC-1 α KO mice displayed diminished expression of retina specific genes in the illuminated state (for example KO light vs WT light: *Nrl*, *Nr2e3*, *Arr3*, *Scn4a*, *Cnga1*) (**Fig. 4b, 4c, Suppl. Table 1b**). Similarly, the expression of many anti-apoptotic genes was reduced in the animals with an ablated PGC-1 α gene, including *Fas* (**Fig. 4b, 4c and Suppl. Table 1**). Inversely, many inflammatory and pro-apoptotic genes were expressed at a higher level in light-exposed KO mice compared to controls, such as *Bcl2* and *A2M*, respectively (**Fig. 4b, 4c**). Interestingly, genes involved in extrinsic or intrinsic apoptosis were upregulated in the PGC-1 α KO vs WT animals; however, no specific apoptotic pathway was preferentially affected (Suppl. Table 2a). Finally, only the WT animals exhibited an increase in oxidative phosphorylation gene expression pattern comparing dark adapted to light exposed mice (**Suppl. Table 1b**: WTli vs WTda up; KOli vs KOda up).

PGC-1 α expression alleviates apoptosis in retinal cells

Light exposure of the retina leads to damage and induction of apoptotic pathways. Based on our observation in light exposed animals, we tested whether PGC-1 α function is directly involved in the regulation of early events in photoreceptor apoptosis and we therefore quantified cell death in PGC-1 α KO and WT control animals following light exposure. In this experimental context, the generation of free nucleosomes was detected in both genotypes, but at significantly higher levels in the PGC-1 α KO than in the WT control animals (**Fig. 5a**). Thus, the deterioration of the KO retina upon light exposure involves an increase in apoptotic events.

To circumvent the potentially confounding effects of a global, life-long absence of PGC-1 α in the KO mice that may be compensated *in vivo*, we investigated the effect of acutely modulated PGC-1 α in ARPE-19 cells, a retinal pigment epithelial cell line.

In these cells, we studied cytochrome *c* release as an early event in intrinsic, mitochondria-related apoptosis. ARPE-19 cells were transduced with adenovirus encoding GFP as control or PGC-1 α expression cassettes, respectively. Importantly, despite the induction of cytochrome *c* expression by PGC-1 α that has been reported in other experimental contexts (**Fig. 5b**), no change in cytochrome *c* release was observed in ARPE-19 cells with ectopic elevation of PGC-1 α (**Fig. 5c**). As expected, treatment of the ARPE-19 cells with actinomycin D or camptothecin caused elevated cytochrome *c* release and thus apoptosis in GFP-expressing control cells. However, when the cells were additionally expressing PGC-1 α , this resulted in a significant reduction in cytochrome *c* release that was statistically undistinguishable from cytochrome *c* release in vehicle- treated control cells. (**Fig. 5b**).

PGC-1 α and PGC-1 β are reduced in rd10 and VPP models of degenerative retinal disease

A wide array of retinal disease conditions is associated with increased apoptosis of photoreceptors, including *retinitis pigmentosa*, a multi- genetic hereditary retinal disease that is caused by mutations in genes implicated in photoreceptor and RPE function. *Retinitis pigmentosa* (RP) causes progressive vision loss by the degeneration of rods and cones⁹⁹. Animal models to study RP include the rd10, the VPP and the *Nrl* KO mouse^{124,127,128}. Since apoptotic and other pathways involved in retinal damage in *retinitis pigmentosa* were affected by the PGC-1 α gene knockout in light- exposed mice, we investigated whether the expression levels of PGC-1 α were altered in these mouse models with age-dependent disease progression of retinal degeneration. In the WT animals, PGC-1 α augmented with increasing age similar to *Rho* (*Rhodopsin*), a marker of rod differentiation. In contrast, after an initial rise, PGC-1 α expression reverted back to initial levels in the rd10 mouse (**Fig. 6a, b**). A similar decrease was observed for PGC-1 β expression in the rd10 animals, where PGC-1 β levels remained consistently lower compared to those of WT animals, even after the initial spike of PGC-1 β expression around the age of 15 days (**Fig. 6c**). Any remaining amount of both coactivators was probably due to their presence in the GCL and INL which remained intact in all of the used models (**Fig. 1b**).

The VPP mouse suffers from a degeneration of rods and cones caused by three rhodopsin mutations (V20G, P23H, and P27L [VPP])¹²⁷. Both the rd10 and the VPP mouse models thus recapitulate the damage in rods and cones that is observed in human *retinitis pigmentosa*. Interleukin-1 β (*Il-1 β*), served as a control gene that is upregulated in the VPP mouse due to the inflammation in this model¹²⁹ (**Fig. 6d**), similar to what was shown for the inflammatory marker monocyte chemoattractant protein 1 (*Mcp-1*)¹¹¹. Both PGC-1 α and PGC-1 β were expressed at a lower level in the VPP mouse compared to WT animals. Strikingly, convergence of both PGC-1 α and PGC-1 β expression in VPP and WT animals coincided with the relief of the inflammatory response in the VPP model implied by the strong decrease in *Il-1 β* expression between day 42 and day 52. Thus, the apoptotic events seen in the VPP model that precede the inflammation directly correlated with reduced levels of PGC-1 α and PGC-1 β (**Fig. 6d, e, f**). Interestingly, PGC-1 β was likewise reduced in the light- exposed PGC-1 α knockout mice, which also exhibited retinal damage and dysfunction, as shown in the present manuscript (**Supp. Fig. 1e**).

Discussion

The PGC-1 coactivators are key regulators of mitochondrial biogenesis and oxidative metabolism. Hence, our present observation of high expression of both PGC-1 α and PGC-1 β in the retina, a tissue with one of the highest energy demands, is not surprising. Moreover, the intraretinal expression pattern showing high levels of both coactivators in rod and cone photoreceptors reflects the high energetic requirement of phototransduction that to a large extent is met by oxidative phosphorylation¹¹⁸. Interestingly however, dark-adapted mice with an ablation of the PGC-1 α gene in the retina display normal retinal morphology and function, even despite a notable reduction in metabolic gene expression in this experimental context. Lack of a prominent phenotype in PGC-1 α loss-of-function settings in basal, unstressed conditions has also been observed in other organs in tissue-specific knockout mice^{13,121,71} and in global knockout animals^{125,112}. Importantly, a more striking phenotypic dysregulation in these animal models is often induced by external stimuli such as fasting, cold exposure or exercise. Similarly, the absence of a functional PGC-1 α gene has much more dramatic consequences in light-exposed compared to dark-adapted animals. Light stress and the resulting cellular damage in the retina results in a cascade of events aimed at destruction of damaged cells through apoptosis, removal of cellular debris, repair of DNA damage and restoration of phototransduction through increased expression of cone- and rod-specific genes (**Fig.6g**). These processes require a considerable amount of energy, witnessed in the increased expression of genes implicated in oxidative phosphorylation in the WT light versus WT dark up (**Suppl.Table 1b**). For example, components of the NADH dehydrogenase (*Ndufa*) and the *cytochrome c* oxidase (*Cox*) complexes are upregulated in this context. The PGC-1 α KO animals, however, likely fail to meet the increased energy need (**Suppl.Table1**: KO li vs WT li down) and thus restoration of tissue homeostasis and function is hampered (**Fig. 6g**). In addition, apoptosis and the inflammatory response are enhanced in light-damaged retinæ of PGC-1 α knockout animals, while DNA damage repair and photoreceptor recovery are impaired in these mice. Interestingly, a recent study analogously implied that PGC-1 α dysregulation may be implicated in irradiation-caused DNA damage in the liver¹³⁰. As a consequence, light-exposed retinæ of PGC-1 α knockout animals show morphological aberrations, specifically a destruction of the RIS and ROS and consequent thinning of the ONL. As a result, light perception is significantly impaired in these mice, as suggested in particular by the reduced the rod-dependent, scotopic b-wave amplitude. Taken together, our data indicate an important role for PGC-1 α in the protection against light-induced retinal damage.

The interpretation of our data obtained in global PGC-1 α knockout animals could potentially be hampered by several drawbacks of this model. First, total ablation of the PGC-1 α gene in many cases results in different, sometimes diametrically opposed phenotypic changes compared to those in tissue-specific knockouts¹³¹. For example, hepatic gluconeogenesis is constitutively elevated in one global PGC-1 α knockout mouse model¹²⁵, whereas the fasting-dependent induction of gluconeogenesis is significantly blunted in liver-specific knockouts⁷¹. Similarly, fiber-type distribution in global knockout is unchanged compared to control mice, while AMP-dependent protein kinase (AMPK) is activated in this context^{125,132}. In contrast, a fiber-type switch towards glycolytic muscle fibers has been observed in muscle-specific PGC-1 α knockouts that also exhibit normal AMPK activation^{13,121}. In both cases, the tissue-specific knockout models exhibit the phenotype that is expected based on *in vivo* gain-of-function experiments^{40,6}. Second, in a global PGC-1 α knockout mouse, PGC-1 α is obviously not only absent in retinal cells, but also other structures involved in light perception and vision. For example, PGC-1 α knockout animals suffer from marked neurodegenerative events in the central nervous system¹²⁵. Neuronal deficits, in particular in the visual cortex where PGC-1 α expression has been reported¹³³, but also the optic nerve, would obviously also affect vision in these mice. Finally, it is difficult to interpret etiology and causality underlying the pathological phenotype in the global PGC-1 α knockout animals with a life-long absence of a functional PGC-1 α gene. To circumvent all of these potentially confounding problems of global, non-inducible PGC-1 α gene ablation and to test whether apoptosis is directly affected by PGC-1 α and not altered as a consequence of an energy crisis, we tested whether acute modulation of PGC-1 α levels in an isolated system of RPE cells recapitulates our observations made in light-exposed PGC-1 α knockout mice exhibiting increased levels of apoptosis *in vivo*. Our experiments in the ARPE-19 cell line clearly show a strong anti-apoptotic effect of ectopically expressed PGC-1 α against two different pharmacological triggers of apoptosis, actinomycin D and camptothecin. PGC-1 α expression has been associated with

decreased apoptosis in different cellular contexts, including skeletal muscle¹¹³, aortic endothelial cells¹³⁴ and decreased retinal capillary cell apoptosis after statin treatment⁸⁵. In contrast, PGC-1 α regulates intestinal epithelial cell fate in part by promoting apoptosis in the intestinal epithelial surface¹³⁵. We now show for the first time that loss-of-function of PGC-1 α results in increased apoptosis in the retina *in vivo* and that increased levels of PGC-1 α exert an anti-apoptotic effect in retinal pigment epithelial cells.

Our tissue culture data thus not only confirm the direct involvement of loss-of-function of PGC-1 α on apoptosis in the ONL *in vivo*, but together with the observation of reduced PGC-1 α and PGC-1 β expression in mouse models for *retinitis pigmentosa* also indicate that elevation of PGC-1 α might be a valid approach to prevent retinal damage and also promote recovery in retinal diseases through increase in ATP generation.

Future studies should thus aim at elucidating the therapeutic efficacy of normalization of PGC-1 α levels with viral vectors or pharmacological tools on retinal degeneration in *retinitis pigmentosa* and other retinal pathologies.

Acknowledgements

We thank our colleagues in the laboratory for discussions and comments on the manuscript. This project was funded by the Swiss National Science Foundation, the SwissLife “Jubiläumsstiftung für Volksgesundheit und medizinische Forschung”, the Roche Research Foundation, the United Mitochondrial Disease Foundation (UMDF) and the University of Basel.

Author contributions

A.E. designed and performed experiments, analyzed the data and wrote the manuscript. M.S. performed *in vivo* experiments. V.S., S.B., M.G-G. and N.T. performed ERG measurements. M.W.S. supervised the study. M.O. and S.S. performed bioinformatics analyses. C.L., L.F. and A.N. performed *in vitro* experiments. C.G. performed experiments and supervised the study. C.H. designed experiments, wrote the manuscript and supervised the study.

Competing financial interests

The authors declare no competing financial interests.

Figure legends

Figure 1. PGC-1 α and PGC-1 β are strongly expressed in rods and cones in the outer nuclear layer of the murine retina.

Relative mRNA expression levels of PGC-1 α and PGC-1 β in different mouse tissues evaluated by semi-quantitative real time PCR. β -actin was used as housekeeping gene (HKG). P value was calculated using two tailed Student's T test: * = $p < 0.05$; *** = $p < 0.001$. + SEM (a) Relative mRNA expression in different tissues from 3 month old wild type male C57BL/6j mice (TA= tibialis anterior). n=4 (b) Relative mRNA expression levels of PGC-1 α and PGC-1 β in different retinal layers from 3 month old wild type male C57BL/6 mice: ONL= outer nuclear layer, INL= inner nuclear layer, GCL= ganglion cell layer. n=4 (c) + (d) Relative mRNA expression levels of PGC-1 α and PGC-1 β in two retinal disease models: Retina was isolated from *Nrl*^{-/-}, rd10 and age matched control C57BL/6j WT mice. n=3. (c) Expression of PGC-1 α and PGC-1 β in *Nrl*^{-/-} mice at 2 months of age. Data were normalized against C57BL/6j WT mice. (d) Expression in rd10 mice at 5-6 months of age.

Figure 2. Regular morphology and function in PGC-1 α KO mouse retina.

Dark adapted, 13 week old PGC-1 α KO and C57BL/6j WT were subjected to morphological analysis and electroretinogram (ERG). (a) Representative retinal morphologic sections from the lower central retina of 13 week old PGC-1 α KO and C57BL/6j WT mice: RPE= retinal pigment epithelium, ROS= rod outer segments, RIS= rod inner segments, ONL= outer nuclear layer, INL= inner nuclear layer, GCL= ganglion cell layer. (b) [A] Scotopic (dark-adapted) and [B] photopic (light-adapted) single-flash ERGs with increasing light intensities recorded from PGC-1 α KO and C57BL/6j WT control mice. The vertical line crossing each trace shows the time point of the light flash. +SEM of n=4. [C] Scotopic and [D] photopic b-wave amplitudes from PGC-1 α KO and C57BL/6 control mice as a function of the logarithm of the flash intensity. Boxes indicate the 25% and 75% quartile range, whiskers indicate the 5% and 95% quantiles. (c) Microarray analysis of PGC-1 α KO and C57BL/6j WT control mice. Shown are the top 10 pathways up/downregulated in their mRNA expression of PGC-1 α KO and C57BL/6j WT mice, dark exposed. n=3; * = $p < 0.05$; ** = $p < 0.01$; *** = $p < 0.001$. Statistical significance was calculated using ANOVA test, Benjamin Hochberg corrected. Thresholds for changes in gene expression set at 1.2 (20% above control) or 0.80 (20% below control).

Figure 3. Aberrant morphology and compromised function of PGC-1 α KO mouse retina under light stress conditions.

PGC-1 α KO and C57BL/6j WT, aged 13 weeks, were exposed to 15.000 lux of white light for 2 hours and after 10 days of recovery subjected to morphological and functional analysis (a) Representative retinal morphologic sections from the lower central retina of PGC-1 α KO and C57BL/6j WT mice. (b) [A] Scotopic

(dark-adapted) and **[B]** photopic (light-adapted) single-flash ERGs with increasing light intensities recorded from PGC-1 α KO and C57BL/6j WT control mice. The vertical line crossing each trace shows the time point of the light flash. **[C]** Scotopic and **[D]** photopic b-wave amplitudes from PGC-1 α KO and C57BL/6 control mice as a function of the logarithm of the flash intensity. **(c)** Optical coherence tomography (SD-OCT): **[A]** comparison of two representative OCT horizontal slices of PGC-1 α KO and C57BL/6j WT control mice. **[B]** Magnification of these SD-OCT horizontal slices: left side: C57BL/6, right side: PGC-1 α KO; GC= ganglion cell layer, IPL= inner plexiform layer, INL= inner nuclear layer, OPL= outer plexiform layer, ONL= outer nuclear layer, OLM= outer limiting membrane, IS/OS=inner segment/outer segment, RPE= retinal pigment epithelium **[C]** Topography of retinal thickness of C57BL/6 (side) and PGC-1 α KO (right) mice calculated from 61 equidistant SD-OCT slices (green= dense; blue= less dense).

Figure 4. Microarray: Ablation of PGC-1 α affects gene expression changes relative to apoptosis, inflammation, protein folding and phototransduction. Microarray analysis of light exposed PGC-1 α KO and C57BL/6j WT control mice. +SEM for n=3 **(a)** number of genes changed significantly between genotypes and conditions: thickness of arrow relates to number of genes changed. **(b)** Heat map: expression patterns of a representative selection of genes involved in apoptosis, inflammation, DNA repair and phototransduction. Green= upregulated; red= downregulated; black= unchanged. **(c)** Semi-quantitative real time PCR validation examples of pro apoptotic, anti apoptotic, inflammatory and phototransduction genes changed significantly in the microarray. 18SrRNA was used as HKG. P value was calculated using two tailed Student's T test: * = p<0.05; ** =p<0.01. + SEM of n=3; Koli= PGC-1 α knockout, light condition, Koda= PGC-1 α KO, dark condition, Wtli= C57BL/6 WT, light conditions, Wtda= C57 BL/6 WT, dark condition.

Figure 5. PGC-1 α alleviates retinal apoptotic response upon light stress *in vivo* and *in vitro*. Relative quantification of cell death. P value was calculated using two tailed Student's T test: * = p<0.05; ** = p< 0.01; ***= p<0.001 **(a)** PGC-1 α KO and C57BL/6j WT mice were exposed to 15'000 lux of white light for 2 hrs. After 24hrs, retina was extracted and analyzed for free nucleosomes as a measure of cell death via ELISA. +SEM of n=11 (WT) and n=15 (PGC-1 α KO). **(b)** Retinal pigment epithelial cells ARPE-19 were transduced with adenovirus carrying GFP or mouse PGC-1 α . Semi-quantitative real time PCR of PGC-1 α and its targets *Cox5b* (cytochrome c oxidase subunit Vb) and (cytochrome c) in PGC-1 α versus GFP transduced ARPE-19 cells. 18SrRNA was used as HKG. +SEM of n=6 **(c)** ARPE-19 cells were transduced with adenovirus carrying GFP or PGC-1 α , treated with apoptosis inducers actinomycin D or camptothecin and then analyzed for cell death via immunostaining of released cytochrome c. ACT= Actinomycin D, CAMP= Camptothecin. 18SrRNA was used as HKG. +SEM of n=6.

Figure 6. PGC-1 α and PGC-1 β are reduced in rd10 and VPP retinal degeneration models Retina from rd10 and VPP mice was isolated at different PNDs (postnatal days) and checked for expression of genes via semi- quantitative real time PCR. β -actin was used as HKG. +SEM of n=3 per time point. **(a)-(c)** rd10 mouse model: Rhodopsin (*Rho*) was used as control gene diminished in this condition. **(d)-(f)** VPP mouse model: Interleukin 1- β (*Il-1 β*) was used as control gene marking the duration of the inflammatory response phase. **(i)** Loss of the PGC-1 α gene in mice affects all the steps of the major cascade of events in light-induced retinal damage, repair and regeneration and consequently results in abnormal retinal morphology and function.

Suppl. Fig1. Gene expression analysis of WT and PGC-1 α KO mice in light and dark. **(a)** Microarray analysis of light and dark exposed PGC-1 α KO and C57BL/6j WT control mice; Gene expression changes in the four comparisons: 18sRNA was used as HKG. +SEM for n=3; * = p<0.05; ** = p< 0.01; *** = p<0.001. Statistical significance was calculated using two tailed Student's T test **(b)** phototransduction genes, **(c)** pro and anti apoptotic genes, **(d)** inflammatory genes and **(e)** PGC-1 α and PGC-1 β gene expression.

Suppl. Table1. Microarray analysis of light and dark exposed PGC-1 α KO and C57BL/6j WT control mice: top genes and pathways. **(a)** Top 10 genes most highly up-/downregulated in their mRNA expression of PGC-1 α KO and C57BL/6j WT mice, dark vs light exposed. **(b)** Top 10 pathways up-

/downregulated in their mRNA expression of PGC-1 α KO and C57BL/6j WT mice, dark vs light exposed. n=3; * = p<0.05; ** = p< 0.01; *** = p<0.001. Statistical significance was calculated using ANOVA test, Benjamin Hochberg corrected. Thresholds for changes in gene expression set at 1.2 (0.2x upregulated) or 0.87 (0.2x downregulated).

Suppl. Table2. Microarray analysis of light and dark exposed PGC-1 α KO and C57BL/6j WT control mice. significant changes in genes involved in apoptosis, DNA repair, inflammation and phototransduction. green= upregulated; red= downregulated **(a)** pro and anti-apoptotic, DNA repair genes **(b)** phototransduction and protein folding genes **(c)** ECM breakdown and inflammatory genes

Suppl. Table3. List of primers used for semi- quantitative real time PCR

Methods

Animals

All animal experiments were performed according to procedures approved by the veterinary authorities and according to the statement of “The Association for Research in Vision and Ophtalmology” for the use of animals in research. Wildtype C57 BL/6 NRj mice were purchased from Janvier (Le Genest St. Isle, France). C57 BL/6 PGC-1 α global KO mice were a kind gift of Bruce M. Spiegelman, Dana- Farber Cancer Institute and Department of Cell Biology, Harvard Medical School (Boston, MA). Rd10 (= retinal degeneration 10) mice were purchased from Jackson Lab (Bar Harbor, Maine). VPP (= mutant opsin transgene) mice were obtained from Muna Naash, University of Oklahoma (Oklahoma City, Oklahoma). *Nrl* (Neural retinal leucine zipper) KO mice were purchased from the University of Michigan (Ann Arbor, Michigan). Mice were maintained in a 12h : 12h light-dark cycle (60lux).

Light exposure

Six to thirteen- week old male C57 BL/6 PGC-1 α global KO mice and wildtype C57 BL/6 NRj mice were dark adapted overnight (16hrs). Pupils were dilated with 1% cyclogyl (Alcon, Cham, Switzerland) and 5% phenylephrine (Ciba Vision, Niederwangen, Switzerland) for 45 min. before light exposure. Mice were exposed to 15'000 lux of light for two hours. Following overnight recovery in darkness, mice were analyzed at time points indicated in the results section. Mice that were dark adapted and not exposed to light served as controls.

Morphology and cell death detection ELISA

For morphology, eyes were fixed in 2.5% glutaraldehyde in 0.1M cacodylate buffer (pH 7.3) at 4°C overnight. The superior and inferior retinae were prepared, washed in cacodylate buffer, incubated in osmium tetroxide for 1 hour, dehydrated graded in alcohol series. Epon 812 sections (0.5 μ M) from the lower central retina were counter-stained with methylene blue.

Cell death was quantified 24hours after light exposure in isolated retinas using the ELISA-based cell death detection kit (Roche Diagnostics, Mannheim, Germany).

Laser capture microdissection

Mice were sacrificed, eyes enucleated, embedded in tissue freezing medium (Leica Microsystems Nussloch, Germany) and frozen in 2-methylbutane bath cooled by liquid nitrogen. Retinal sections (20 μ M) were fixed (5 min. acetone), air-dried (5 min.) and dehydrated (30sec 100% ethanol, 5 min. xylene). Microdissection was performed using an Arcturus XT Lasercapture device (Molecular devices, Silicon Valley, CA).

Gene Expression Studies

RNA was isolated by pooling 2 retinas from 1 animal using the miRNeasy Mini Kit from Qiagen. 1 μ g of RNA was employed for cDNA synthesis using Super Script Reverse Transcriptase II (Invitrogen) and

random hexamer primers (Promega, Madison, USA). Real-time PCR analysis (Power SYBR Green Master Mix, Applied Biosystems, Carlsbad, California, USA) was performed either by using the LightCycler 480 Sybr Green I Master Kit and a LightCycler 480 instrument (Roche, Mannheim, Germany) or by Power SYBR Green Master Mix using the StepOnePlus sequence detector (Applied Biosystems, Carlsbad, California, USA). Relative expression levels were calculated with the $\Delta\Delta C_t$ method and normalized to the expression of β -actin or 18S ribosomal RNA (18SrRNA) with primers indicated in Suppl. Table 3.

Cell culture and adenoviral infection

ARPE-19 cells were seeded at 2×10^5 cells per well of a 12 well plate in 50% F-12/ 50% DMEM medium supplemented with 1% Penicillin/ Streptomycin. 24h afterward, cells were infected with adenoviral constructs encoding GFP and PGC-1 α , respectively.

Apoptosis induction and cell death detection

48h after adenoviral infection, cells were treated with Z-VAD-FMK (Peptanova, Sandhausen, Germany) for 60min to prevent cell detachment. Apoptosis inducers Camptothecin or Actinomycin D (final concentration: 20 μ M) were added. 24h later, cells were fixed with 4% paraformaldehyde in PBS, washed with PBS and stained with anti-cytochrome c (BD biosciences). Released cytochrome c was quantified using fluorescence microscopy.

ERG measurements

Electroretinograms (ERGs) were recorded according to previously described procedures¹³⁶. Mice that were light exposed as described above were analyzed 10 days after light damage. Non-exposed mice served as controls. All mice were dark- adapted overnight prior to ERG analysis. Mice were then anaesthetized with ketamine (66.7 mg/kg body weight) and xylazine (11.7 mg/kg body weight). Pupils were dilated and single flash ERG responses were obtained under dark-adapted (scotopic) and light-adapted (photopic) conditions. Light adaptation was accomplished with a background illumination of 30 candela (cd) per square meter starting 10 min before recording. Single white-flash stimulus intensity ranged from -4 to 1.5 log cd*s/m² under scotopic and from -2 to 1.5 log cd*s/m² under photopic conditions.

Spectral domain optical coherence tomography (SD-OCT)

Eyes were subjected to SD-OCT using the commercially available Spectralis™ HRA+OCT device from Heidelberg Engineering featuring a broadband superluminescent diode at $\lambda = 870$ nm as low coherent light source¹³⁷.

Gene expression profiling

RNA was isolated as described above (Gene expression studies) and 4.25 μ g of cDNA from the mouse retinae was hybridized to the Affymetrix Gene Chip Mouse 1.0 ST at the in-house microarray facility service. Microarray CEL output files were analyzed at the Functional Genomics Center Zurich, Winterthurerstrasse 190, CH-8057 Zurich. Statistical significance was calculated using ANOVA test, Benjamin Hochberg corrected. Thresholds for changes in gene expression set at 1.2 (0.2x upregulated) or 0.87 (0.2x downregulated). $p \leq 0.05 = *$, $p \leq 0.01 = **$, $p \leq 0.001 = ***$.

Figures

Fig. 1

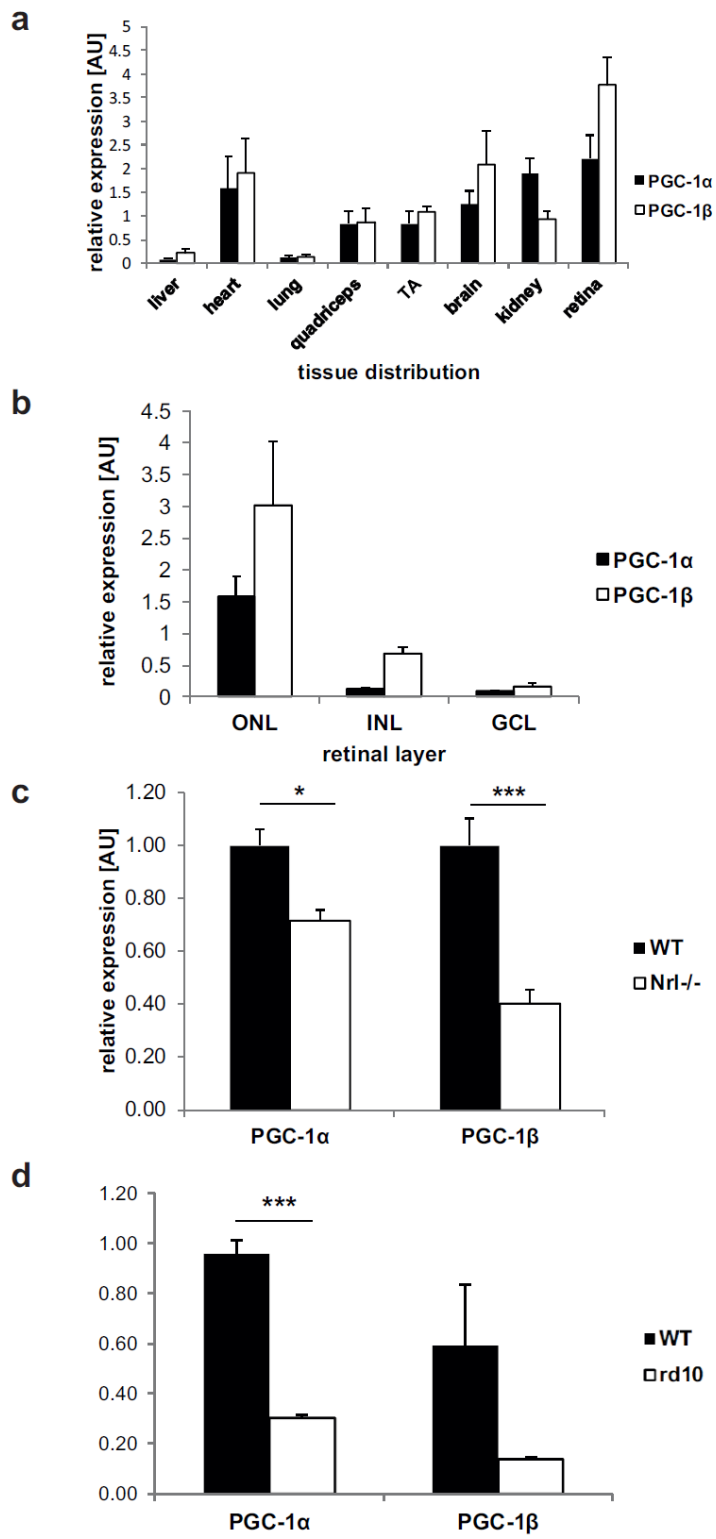
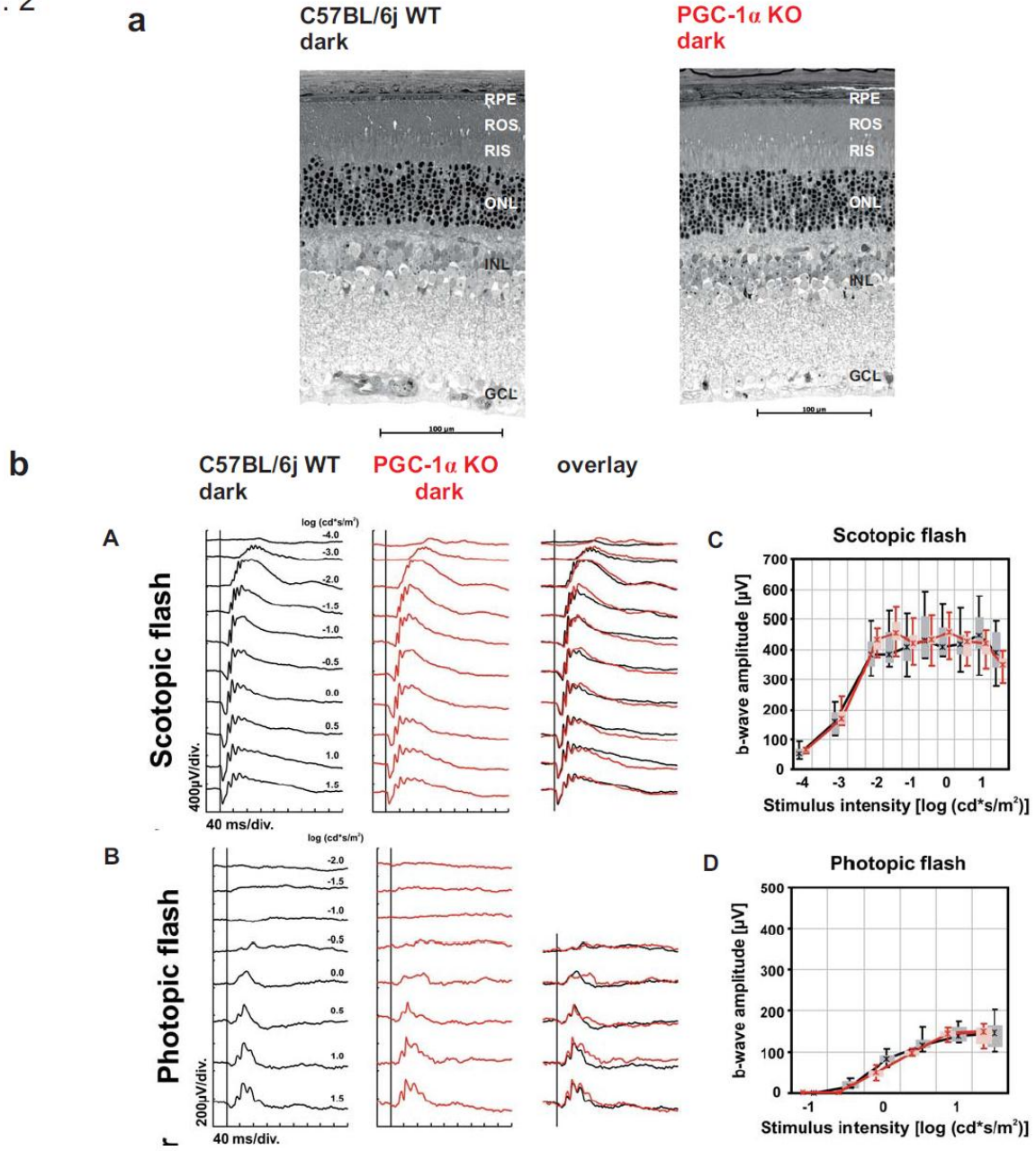


Fig. 2



C

KO dark vs WT dark down	
pathway name	pValue
Oxidative phosphorylation	5.02E-16
Ubiquinone metabolism	4.8E-09
TCA	2.06E-05
Transcription_Transcription regulation of aminoacid metabolism	0.000839
Transcription_Role of VDR in regulation of genes involved in osteoporosis	0.002058
Aminoacyl-tRNA biosynthesis in cytoplasm	0.002839
Aminoacyl-tRNA biosynthesis in cytoplasm/ Rodent version	0.003044
Leucine, isoleucine and valine metabolism	0.005915
Cytoskeleton remodeling_Neurofilaments	0.006587
Unsaturated fatty acid biosynthesis	0.011499

KO dark vs WT dark up	
pathway name	pValue
Cytoskeleton remodeling_TGF, WNT and cytoskeletal remodeling	3.09E-07
Transcription_Androgen Receptor nuclear signaling	9.85E-07
Immune response_MIF - the neuroendocrine-macrophage connector	1.25E-06
Development_GM-CSF signaling	2.11E-05
Development_WNT signaling pathway, Part 2	3.6E-05
Development_Ligand-independent activation of ESR1 and ESR2	4.54E-05
Cytoskeleton remodeling_Cytoskeleton remodeling	4.58E-05
PGE2 pathways in cancer	5.03E-05
Development_TGF-beta-dependent induction of EMT via SMADs	5.2E-05
Development_Endothelin-1/EDNRA transactivation of EGFR	6.58E-05

Fig. 3

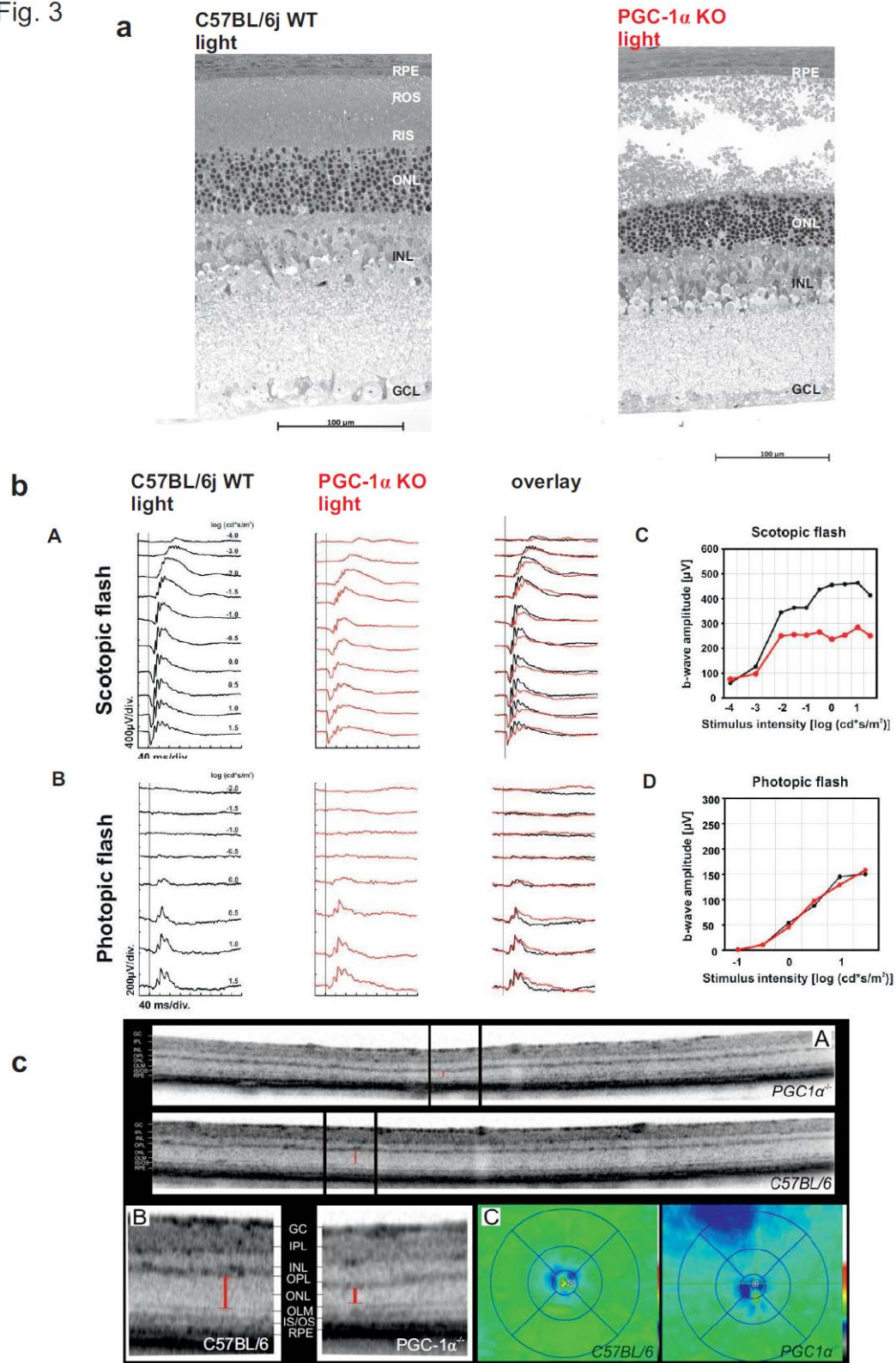


Fig. 4

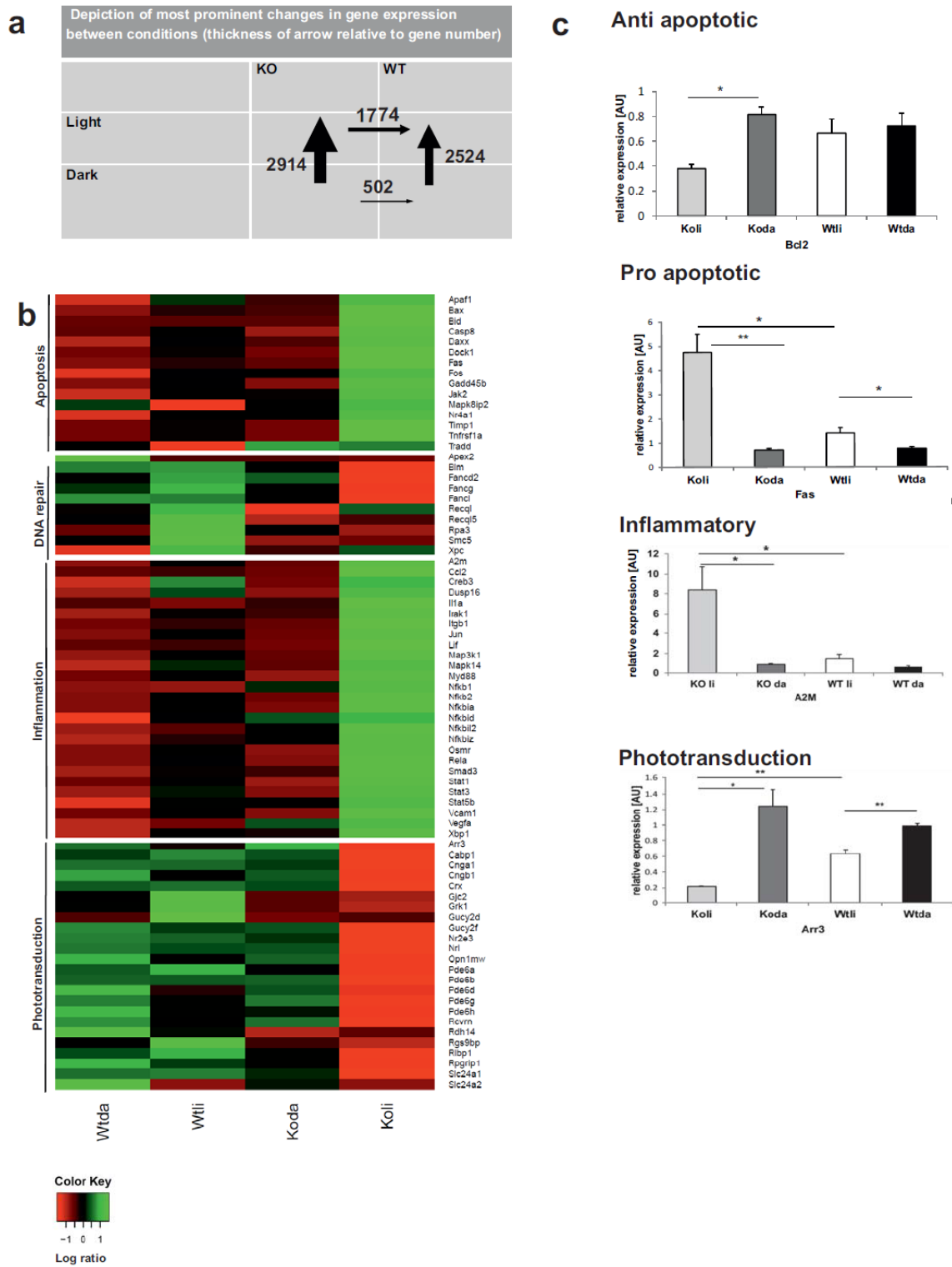


Fig. 5

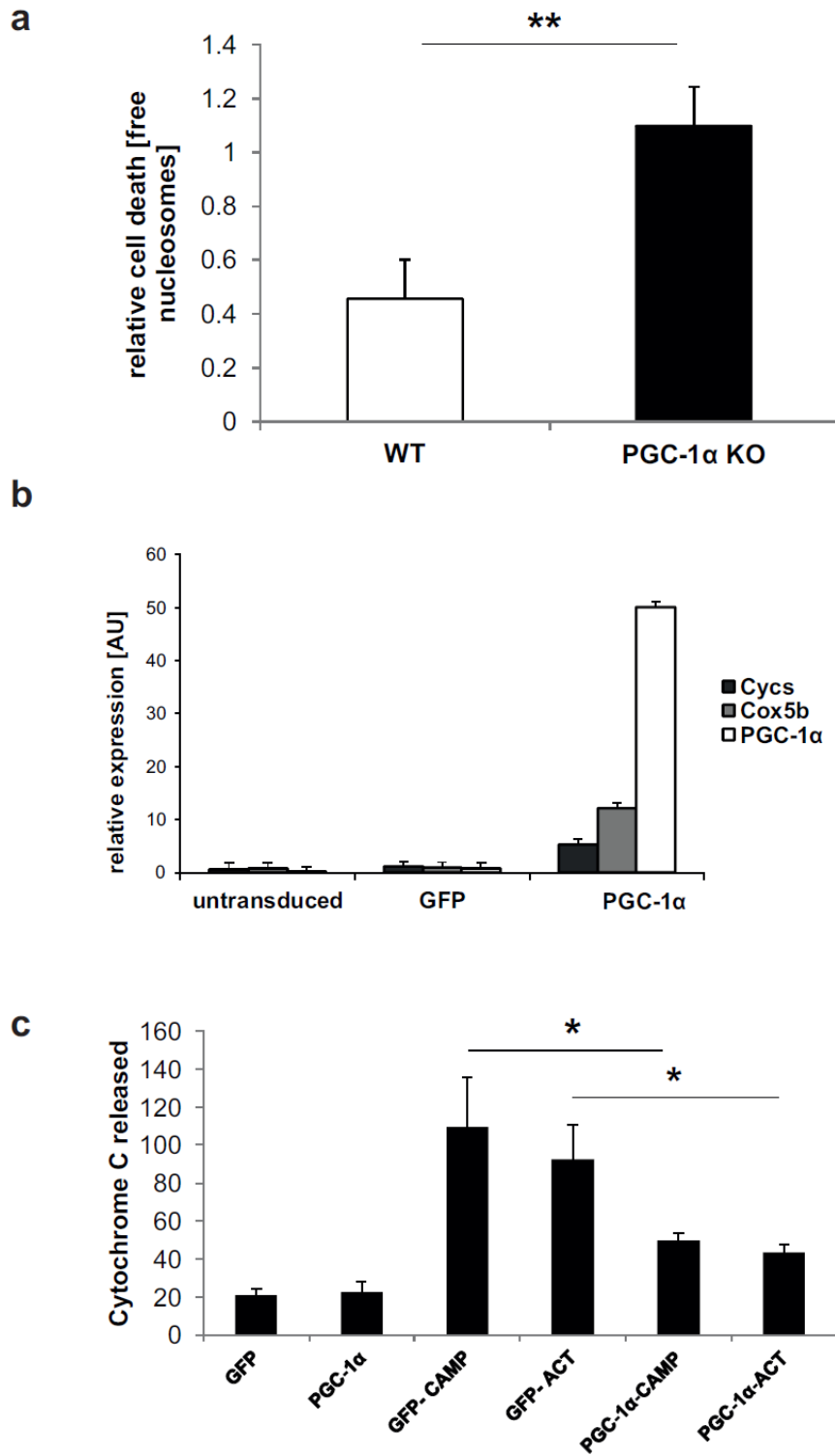
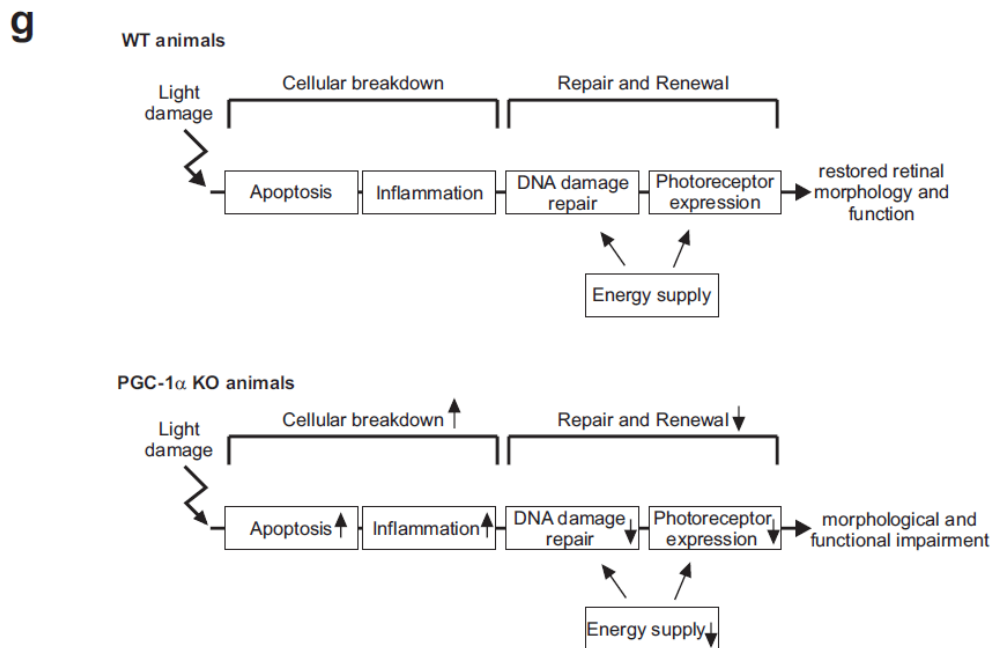
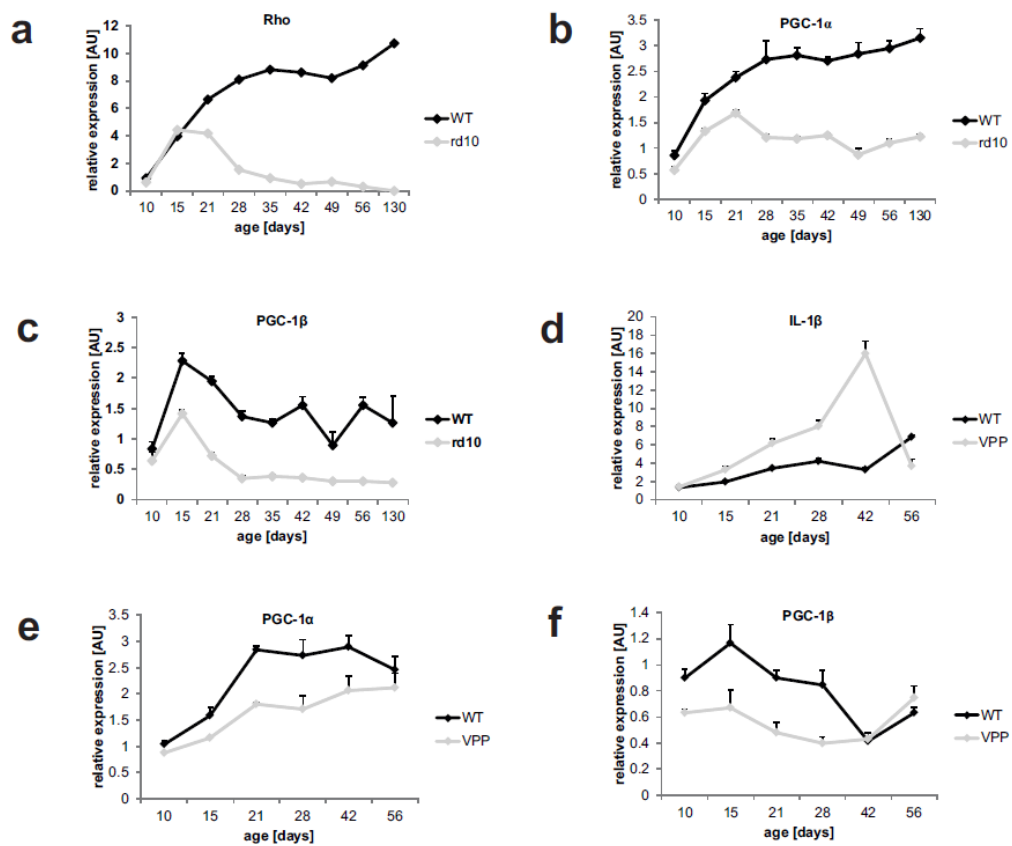
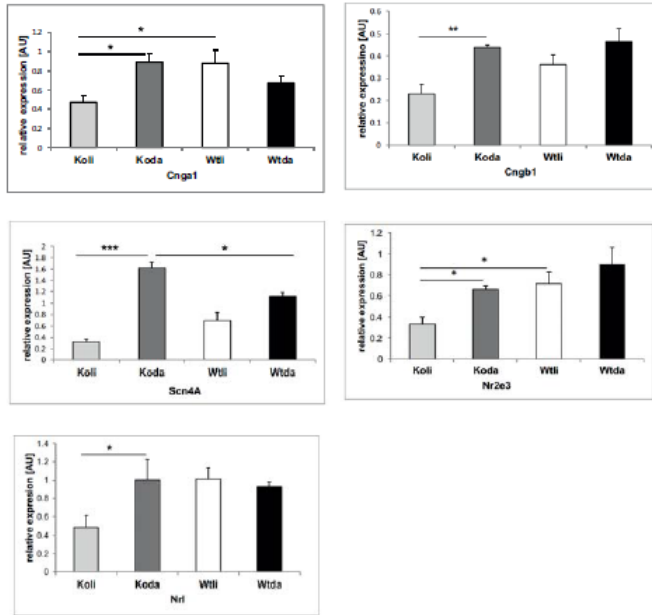


Fig. 6



Suppl. Fig.1

a Phototransduction

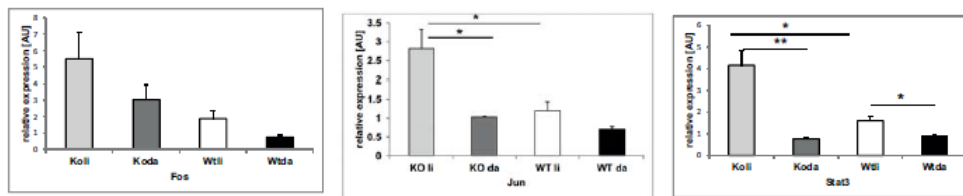


e

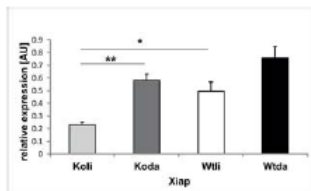
number of genes changed: light vs dark		
	KO	WT
↑	1410	1002
↓	1504	761

number of genes changed: KO vs WT		
	light	dark
↑	897	167
↓	877	335

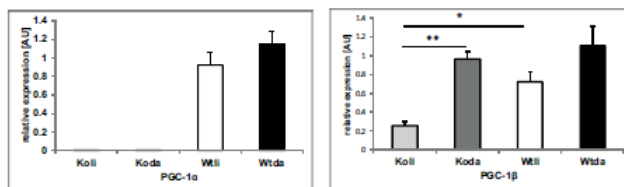
b Pro apoptotic



c Anti apoptotic



d PGC-1 α and PGC-1 β



Suppl. Table 1

a

KO II vs KO da down				KO II vs KO da up				KO da vs WT da down				KO da vs WT da up			
gene ID	gene name	p val	ratio	gene ID	gene name	p val	ratio	gene ID	gene name	p val	ratio	gene ID	gene name	p val	ratio
ENSMUSG000000086503	AL669964.8	2.06E-08	0.005687	ENSMUSG000000090949	Elf2s3y	2.35E-07	54.80594	ENSMUSG00000042210	Abhd14a	2.07807E-05	0.193843	ENSMUSG000000006177	Kk1b22	0.019040589	14.68375
ENSMUSG00000000154	Eps81	0.000298	0.310375	ENSMUSG000000068457	Uty	2.81E-07	35.7843	ENSMUSG00000075751	SNORD115	0.00054873	0.249685	ENSMUSG000000035296	Sox9	4.08404E-05	6.80034
ENSMUSG000000031966	Glb113	0.042325	0.345601	ENSMUSG000000069045	Ddx3y	2.86E-06	13.24099	ENSMUSG00000048758	Rpl29	0.001339296	0.252996	ENSMUSG000000007299	Cryod	0.0352007	4.578664
ENSMUSG000000019233	Akg1z1	0.01099	0.395672	ENSMUSG000000056673	Kdm5d	2.16E-07	9.542699	ENSMUSG00000044573	Acp1	0.000374379	0.021788	ENSMUSG000000038418	Egr1	0.000184156	3.668763
ENSMUSG000000005519	Immu-mil-183	0.00074	0.411426	ENSMUSG000000021081	Serpina3n	6.69E-06	7.656752	ENSMUSG00000034248	Sic25a37	0.000491299	0.389097	ENSMUSG000000075930	SNORD115	0.000895339	3.569132
ENSMUSG000000022899	Sic15a2	0.042768	0.434437	ENSMUSG000000015312	Gadd45b	0.001278	7.013121	ENSMUSG00000074407	AC124577.1	0.006958778	0.421765	ENSMUSG000000075766	SNORD115	0.000175157	3.650665
ENSMUSG000000060890	Ahr3	0.001724	0.447277	ENSMUSG00000000982	Cd3	0.002205	6.726247	ENSMUSG00000087178	AC102121.3	0.00196835	0.429943	ENSMUSG000000042073	Abhd14b	0.000281255	3.07212
ENSMUSG0000000063590	Gcm5c31	0.011673	0.453493	ENSMUSG000000028270	Gbp2	2.86E-05	6.570339	ENSMUSG00000015666	Hspa8	0.000325941	0.459106	ENSMUSG000000036217	I18	0.001231077	2.637179
ENSMUSG000000001027	Scn4a	0.001642	0.453723	ENSMUSG000000041782	Lad1	0.000118	5.721613	ENSMUSG000000067536	Dnahc7b	0.001128195	0.470338	ENSMUSG000000056199	AC130827.2	0.002466451	2.45678
ENSMUSG000000074930	RP23-224B9.1	0.003755	0.454678	ENSMUSG000000030111	A2m	0.001193	5.562193	ENSMUSG000000066705	Fxyd6	0.000461585	0.478773	ENSMUSG000000052143	AC156940.1	1.64301E-05	2.258559
WT II vs WT da down				WT II vs WT da up				KO II vs WT II down				KO II vs WT II up			
gene ID	gene name	p val	ratio	gene ID	gene name	p val	ratio	gene ID	gene name	p val	ratio	gene ID	gene name	p val	ratio
ENSMUSG000000086503	AL669964.8	3.37E-07	0.005715	ENSMUSG000000090949	Elf2s3y	1.00932E-07	60.1737237	ENSMUSG000000031966	Glb113	0.011341	0.200791	ENSMUSG000000060177	Kk1b22	0.01315403	14.15191
ENSMUSG000000048758	Rpl29	0.000464	0.167101	ENSMUSG000000068457	Uty	1.6419E-07	37.7391677	ENSMUSG00000071984	Fndc1	0.017437	0.420968	ENSMUSG000000029816	Gpmmb	0.000035759	5.8861178
ENSMUSG000000042210	Abhd14a	6.49E-07	0.208578	ENSMUSG000000069045	Ddx3y	1.24419E-05	14.3921267	ENSMUSG00000074407	AC124577.1	0.0135833	0.423098	ENSMUSG000000030111	A2m	0.000305459	4.1088189
ENSMUSG000000045573	Acp1	9.95E-05	0.218836	ENSMUSG000000066973	Kdm5d	3.44951E-06	8.3423296	ENSMUSG00000072844	GS30011006Rk	0.005516	0.457092	ENSMUSG00000000982	Cd3	0.01009673	3.8950643
ENSMUSG00000000154	Eps81	0.00327	0.318603	ENSMUSG000000035296	Sox9	3.30198E-05	7.0014513	ENSMUSG000000025450	AC163689.1	0.001251	0.477925	ENSMUSG000000015312	Gadd45b	0.00889059	3.8511659
ENSMUSG000000034248	Sic25a37	0.000923	0.413001	ENSMUSG000000042073	Abhd14b	1.02711E-05	3.23125644	ENSMUSG00000015656	Hspa8	0.003025	0.480434	ENSMUSG00000029822	Lcn2	0.00337735	3.8338973
ENSMUSG000000076867	A630098A13Rik	0.005688	0.439523	ENSMUSG000000020932	Glbpe	0.01813089	2.4320601	ENSMUSG00000035296	Sox9	0.008462	0.483232	ENSMUSG000000021091	Serpina3n	0.0162945	3.6072455
ENSMUSG000000025794	Rpl14	0.020493	0.464948	ENSMUSG00000038418	Egr1	0.00673996	2.36133213	ENSMUSG00000005233	Spz25	0.034111	0.511731	ENSMUSG000000023078	Kk113	0.01890613	3.2663722
ENSMUSG000000005594	Timp1	0.006139	0.467175	ENSMUSG00000004855	Cxd10	0.00021406	2.3193745	ENSMUSG000000003712	Hic2	0.002234	0.514729	ENSMUSG000000041782	Lad1	0.00512352	3.0985626
ENSMUSG000000021229	Dct	0.034269	0.480081	ENSMUSG000000071984	Fndc1	0.00851626	2.1922718	ENSMUSG000000027360	Hic3	0.002264	0.538682	ENSMUSG000000000987	Ccd4a	0.01043177	2.8783082

b

KO vs KO da down	pathway name	pValue	KO vs KO da up	pathway name	pValue	KO da vs WT da down	pathway name	pValue	KO da vs WT da up	pathway name	pValue
Neurophysiological process: Visual perception		2.9E-09	Apoptosis and survival: Endoplasmic reticulum stress response pathway		1.0E-14	Oxidative phosphorylation		5.05E-16	Cytoskeleton remodeling: TGF, Wnt and cytoskeletal remodeling		3.08E-07
Protein folding, literature references and signal transduction of G-proteins (G) heterotrimeric G-protein		5.6E-06	Cytoskeleton remodeling: Cytoskeleton remodeling		5.3E-15	Uridylate metabolism		4.8E-09	Transcription: Androgen Receptor nuclear signaling		8.93E-07
Cellular Response: NF-AT signaling in Cardiac Hypertrophy		5.8E-08	Immune response: Oxidative nitric oxide synthase (iNOS) nitrosylates		9.0E-10	TCR		2.9E-05	Transcription: Retinoid Receptor nuclear signaling		1.25E-06
Neurophysiological process: ACIN regulation of the myosin II		4.9E-07	Immune response: Oxidative nitric oxide synthase (iNOS) nitrosylates		2.0E-11	Transcription, Transcription regulation of amino acid metabolism		0.00039	Development: GPCR signaling		2.1E-05
Development: Role of Hsp70 and calmodulin-dependent kinase II (CaMKII) in control of skeletal myogenesis		2.5E-07	Oxidative phosphorylation: TGF, Wnt and cytoskeletal remodeling		6.9E-11	Transcription, Role of VDR in regulation of genes involved in osteoporosis		0.00258	Development: Wnt signaling pathway: Part 2		3.6E-05
Immune response: Fc-gamma R1 (FCGR1) in macrophages		1.9E-05	Cell adhesion: Chemokines and adhesion		1.4E-10	Aminoacyl-tRNA biosynthesis in cytoplasm		0.00339	Development: Ligand-independent activation of ESRR1 and ESRR2		4.54E-05
Cell adhesion: ECM remodeling		2.9E-09	Cellular signaling: G-protein-coupled receptor (GPCR) signaling pathway		9.3E-10	Aminoacyl-tRNA biosynthesis in cytoplasm		0.00344	Cytoskeleton remodeling: Cytoskeleton remodeling		4.53E-05
Neurophysiological process: ACIN and ACN2 in neuronal membrane polarization		3.6E-08	Immune response: ETV5:RelB up CGP (transcript) nucleotide phosphorylation		1.1E-09	Lactation: Lactation and milk metabolism		0.00915	PGE2 pathway in cancer		5.3E-05
Muscle contraction: G-protein coupled receptor (GPCR) signaling pathway		1.3E-05	Apoptosis and survival: BAX transmembrane		2.1E-06	Cytoskeleton remodeling: Neurofilaments		0.00657	Development: TGF-beta dependent induction of EMT via SMOs		5.3E-05
Signal transduction: AMP signaling		1.6E-05	Cellular signaling: Notch signaling		3.3E-08	Urea cycle: Urea cycle and biogenesis		0.01849	Development: Endothelin-1/EDNRB transactivation of EGFR		6.58E-05
WT vs WT da down	pathway name	pValue	WT vs WT da up	pathway name	pValue	KO vs WT II down	pathway name	pValue	KO vs WT II up	pathway name	pValue
Neurophysiological process: ACIN regulation of the myosin II		1.5E-06	Transcription: P53 signaling pathway		1.6E-08	Neurophysiological process: Visual perception		1.4E-09	Cell adhesion: Chemokines and adhesion		7.3E-10
Immune response: Fc-gamma R1 (FCGR1) in macrophages		2.2E-05	Cellular response: Cytokine signaling pathway		3.3E-06	Oxidative phosphorylation		1.2E-05	Cytoskeleton remodeling: TGF, Wnt and cytoskeletal remodeling		1.20E-12
Transcription: Transcription regulation of amino acid metabolism		1.4E-05	Development: P53 signaling in S100 and NF-kB		4.8E-05	Cell cycle: The mitotic phase checkpoint		0.00022	Cytoskeleton remodeling: Cytoskeleton remodeling		1.04E-12
Development: Notch Signaling Pathway		4.0E-05	Development: Role of IL-6 in angiogenesis		2.9E-05	Cell cycle: Chromosome condensation in prophase		0.00339	Reproduction: GPR1 signaling		3.9E-10
Development: Role of Hsp70 and calmodulin-dependent kinase II (CaMKII) in control of skeletal myogenesis		2.5E-07	Immune response: Oxidative nitric oxide synthase (iNOS) nitrosylates		2.8E-05	DNA damage, ATM/ATR regulation of G2/M checkpoint		0.00134	Neurophysiological process: Receptor mediated axon growth regulation		5.89E-10
Cellular Response: NF-AT signaling in Cardiac Hypertrophy		5.8E-08	Development: TGF-beta dependent induction of EMT via RhoA, PDK1 and GSK-3beta		2.9E-05	Cardiac: Hypertrophy: Ca2+/calmodulin-dependent kinase II (CaMKII) signaling in Cardiac Hypertrophy		0.01999	Signal transduction: Calcium signaling		5.89E-10
Transcription: Gene-Dependent Transcription of Retinoid/RetA genes		0.00181	Development: Androgen Receptor nuclear signaling		4.8E-05	Protein folding, literature references and signal transduction of G-proteins (G) heterotrimeric G-protein		0.01022	Development: Regulation of cytoskeleton-actin-myosin interaction (EMI)		4.53E-09
Development: Hedgehog signaling		0.00703	Immune response: Oxidative nitric oxide synthase (iNOS) nitrosylates		8.6E-05	Development: P53 signaling pathway		0.00329	Cell adhesion: Role of Integrins in the Hedgehog-mediated cell adhesion		6.69E-09
Transcription: Notch and NF-kB transcription regulation		0.00704	Development: BAX transmembrane		5.5E-05	Atherosclerosis: Role of VDR in regulation of genes involved in atherosclerosis		0.00324	Development: S100 Signaling		1.13E-08
Protein folding, literature references and signal transduction of G-proteins (G) heterotrimeric G-protein		0.00784	Cytoskeleton remodeling: Neurofilaments		6.1E-05	Uridylate metabolism		0.01817	Cytoskeleton remodeling: Regulation of actin/cytoskeleton by Rho GTPases		1.57E-08

Suppl.Table2

a

<i>Koda vs Wtda comparison1</i>	<i>Koli vs Wtli comparison2</i>	<i>Koli vs KO da comparison3</i>	<i>Wtli vs Wtda comparison4</i>	<i>role</i>
	BCL-2	BLC-2		anti apoptotic
	XIAP		XIAP	anti apoptotic
			BAX	anti apoptotic
		HRK		anti apoptotic
		RPS6KB1		anti apoptotic
		MDM2	MDM2	anti apoptotic
	TIMP1	TIMP1		anti apoptotic
PARK7		PARK7	PARK7	anti apoptotic
FASTK			FASTK	pro apoptotic
	BID	BID		pro apoptotic
		JAK2	JAK2	pro apoptotic
	NR4A1	NR4A1	NR4A1	pro apoptotic
	CRADD	CRADD		pro apoptotic
	TNFSF15	TNFSF15	TNFSF15	pro apoptotic
			TRAF2	pro apoptotic
	CASP7	CASP7		pro apoptotic
	GZMA	GZMA		pro apoptotic
ANP32A	ANP32A			pro apoptotic
	APAF-1	APAF-1	APAF-1	pro apoptotic
	DAXX	DAXX	DAXX	pro apoptotic
	DOCK1	DOCK1		pro apoptotic
	FAS	FAS		pro apoptotic
	GADD45b	GADD45b	GADD45b	pro apoptotic
	p53	p53		pro apoptotic
	TNFRSF1a	TNFRSF1a		pro apoptotic
		TRADD		pro apoptotic
	CASPASE8	CASPASE8		pro apoptotic
		FOS	FOS	pro apoptotic
		ERN1	ERN1	pro apoptotic
		MAPK8ip2	MAPK8ip2	pro apoptotic
			BMF	pro apoptotic
	STAT1	STAT1	STAT1	pro apoptotic
	JUN	JUN		pro apoptotic
	STAT3	STAT3	STAT3	pro apoptotic
			STAT4	pro apoptotic
	STAT5	STAT5	STAT5	pro apoptotic
			LIF	pro apoptotic
	Pxn		Pxn	cell adhesion
POLD4			POLD4	D.N.A. repair
RECQL		RECQL		D.N.A. repair
TREX2		TREX2	TREX2	D.N.A. repair
	BLM	BLM		D.N.A. repair
	FANCD2			D.N.A. repair
	FANCE		FANCE	D.N.A. repair
	FANCG		FANCG	D.N.A. repair
	FANCL		FANCL	D.N.A. repair
	MGMT	MGMT		D.N.A. repair
	MMS21 (NSMCE2)		MMS21 (NSMCE2)	D.N.A. repair
	RPA3			D.N.A. repair
		SMC5		D.N.A. repair
		APEX (REF1)		D.N.A. repair
		ATM	ATM	D.N.A. repair
	BAP1	BAP1	BAP1	D.N.A. repair
			XPC	D.N.A. repair
			POLD3	D.N.A. repair
		POLD1		D.N.A. repair
	RECQL5			D.N.A. repair

Supp.Table2

b	<i>Koda vs Wtda</i>	<i>Koli vs Wtli</i>	<i>Koli vs KO da</i>	<i>Wtli vs Wtda</i>	role
	<i>comparison1</i>	<i>comparison2</i>	<i>comparison3</i>	<i>comparison4</i>	
		HSP90ab1	HSP90ab1	HSP90ab1	protein folding
			DERL-1		protein folding
			eIF2AK3	eIF2AK3	protein folding
				CEBPZ	protein folding
				UBC7	protein folding
			UBE3C	UBE3C	protein folding
		LMNB1		LMNB1	structure; scaffold
AIPL1			AIPL1		phototransduction
		ARR3	ARR3	ARR3	phototransduction
CABP1	CABP1	CABP1	CABP1	CABP1	phototransduction
		CNGA1	CNGA1		phototransduction
CNGB1	CNGB1	CNGB1	CNGB1		phototransduction
		GJC2			phototransduction
			CRX		phototransduction
		GRK1		GRK1	phototransduction
		GUCY2D		GUCY2D	phototransduction
		GUCY2F		GUCY2F	phototransduction
		NR2E3			phototransduction
		NRL	NRL		phototransduction
		OPN1MW	OPN1MW	OPN1MW	phototransduction
		PDE6A		PDE6A	phototransduction
		PDE6B	PDE6B		phototransduction
			PDE6D		phototransduction
		PDE6G	PDE6G		phototransduction
PDE6H	PDE6H	PDE6H	PDE6H	PDE6H	phototransduction
		RBP3	RBP3		phototransduction
		RGS9BP		RGS9BP	phototransduction
RDH14					phototransduction
		RCVRN	RCVRN		phototransduction
		GUCA1A	GUCA1A	GUCA1A	phototransduction
		RGS9	RGS9		phototransduction
		RHOD	RHOD		phototransduction
				RLBP1	phototransduction
RPGRIP1	RPGRIP1	RPGRIP1	RPGRIP1	RPGRIP1	phototransduction
		SLC24A1	SLC24A1	SLC24A1	phototransduction
				Slc24A2	phototransduction

Suppl.Table2

C	<i>Koda vs Wtda</i> <i>comparison1</i>	<i>Koli vs Wtli</i> <i>comparison2</i>	<i>Koli vs KO da</i> <i>comparison3</i>	<i>Wtli vs Wtda</i> <i>comparison4</i>	<i>role</i>
		MMP14	MMP14		ECM breakdown
			MMP9		ECM breakdown
			MIF		inflammatory
			PLG (Angiostatin)		inflammatory
		CDC25C		CDC25C	inflammatory
			CREB3	CREB3	inflammatory
		MAP3K1	MAP3K1	MAP3K1	inflammatory
		IL-1a	IL-1a		inflammatory
				IRAK1	inflammatory
		IRAK2		IRAK2	inflammatory
		ITGBI	ITGBI		inflammatory
		VEGF-A			inflammatory
		A2M	A2M		inflammatory
				CCL2	inflammatory
			CREB3	CREB3	inflammatory
			MYD88		inflammatory
			NFkb	NFkb	inflammatory
		OSMR	OSMR	OSMR	inflammatory
		MAPK14	MAPK14		inflammatory
		DUSP16	DUSP16	DUSP16	inflammatory
			MTA2	MTA2	inflammatory
		OSM		OSM	inflammatory
		RelA	RelA	RelA	inflammatory
		SENP2		SENP2	inflammatory
		SMAD3	SMAD3	SMAD3	inflammatory
				STAT4	inflammatory
		XBPI	XBPI	XBPI	inflammatory
				TLR2	inflammatory
		VCAM1	VCAM1	VCAM1	inflammatory
		OSMR	OSMR	OSMR	inflammatory
	MFN2	MFN2	MFN2	MFN2	mitochondria

Suppl.Table3

Primer name	Sequence 5' => 3'
PGC-1 α _ex3-5-F	AGCCGTGACCACTGACAACGAG
PGC-1 α _ex3-5-R	GCTGCATGGTTCTGAGTGCT AAG
PGC-1 β -F	GGCAGGTTCAACCCCGA
PGC-1 β -R	CTTGCTAACATCACAGAGGA TATCTTG
Gnat1-F	GAGGATGCTGAGAAGGATGC
Gnat1-R	TGAATGTTGAGCGTGGTCAT
β - Actin-F	CAACGGCTCCGGCATGTGC
β -Actin-R	CTCTTGCTCTGGGCCTCG
18S rRNA-F	AGTCCCTGCCCTTTGTACACA
18S rRNA-R	CGATCCGAGGGCCTCACTA
Bcl2-F	ACCGGGAGATCGTGATGAAG
Bcl2-R	ATCTCCAGCATCCCACTCGT A
Fas-F	GCTGGCTCACAGTTAAGAGTTCATAC
Fas-R	ACCCGCCTCCTCAGCTTT
Stat3-F	TGCGGAGAAGCATTGTGAGT G
Stat3-R	TTTTCCAGACGTGTCCAGGCAGATG
Opn1mw-F	TGTACATGGTCAACAATCGG A
Opn1mw-R	ACACCATCTCCAGAATGCAA G
Cycs-F	GGCGTGTCCCTTGGACTTAGA
Cycs-R	TGCCTTTCTCAACATCACCC
Cox5b-F	GCTCCATGGCATCTGGA
Cox5b-R	ATGGGTCCAGTCCCTTCTTT
Rho-F	CTTCACCTGGATCATGGCGT T
Rho-R	TTCGTTGTTGACCTCAGGCTTG
Mcp-1-F	GGCTCAGCCAGATGCAGTTA
Mcp-1-R	CTGCTGCTGGTGATCCTCTT
Il-1 β -F	GCAGGCAGTATCACTCATTG

4.4. Conclusions

In this study, the coactivator PGC-1 α was found to occupy a crucial role in retinal health:

Whereas it is dispensable for retinal morphology and function in an unstressed, dark exposed condition, high intensity light exposure leads to enhanced apoptosis and decreased DNA repair in the absence of PGC-1 α . However, it cannot be concluded from these data whether the coactivator delivers the additional energy required for recovery and DNA repair after a light insult or if PGC-1 α directly steers transcription of genes involved in recovery and DNA repair.

The ERG data also confirm that ablation of PGC-1 α in the light treated animals accounts for compromised phototransduction. In fact, the ERG response of the KO animals was quite variable: This may be due to the process of light exposure where animals can receive unequal amounts of light in accordance with the movements that they make. Furthermore, the ERG is a good device to detect sound functional abnormalities in retina, whereas retinal damage that is restricted to certain areas may not always be detected via an altered Ganzfeld ERG. A longer light exposure could have helped alleviate this problem.

The role of PGC-1 α in retinal development was also investigated:

Lifelong absence of PGC-1 α does not seem to affect morphology at a later stage in life: 10 month old and 3.5 month old PGC-1 α KO animals do not differ in retinal morphology from the respective WT controls in their amount and distribution of SWL and MWL cone opsins. (**Fig. 8A**). SWL seems to be distributed preferentially in the ventral region in the KO and WT animals of 3.5 and 10 months; MWL on the other hand is distributed equally in the dorsal and ventral region in KO and WT animals (**Fig. 8B**) (Data: courtesy of Marijana Samardzija).

Likewise, some important genes involved in retinal function are not markedly changed in their expression between PGC-1 α KO and WT mice in a timecourse experiment (**Fig.9**).

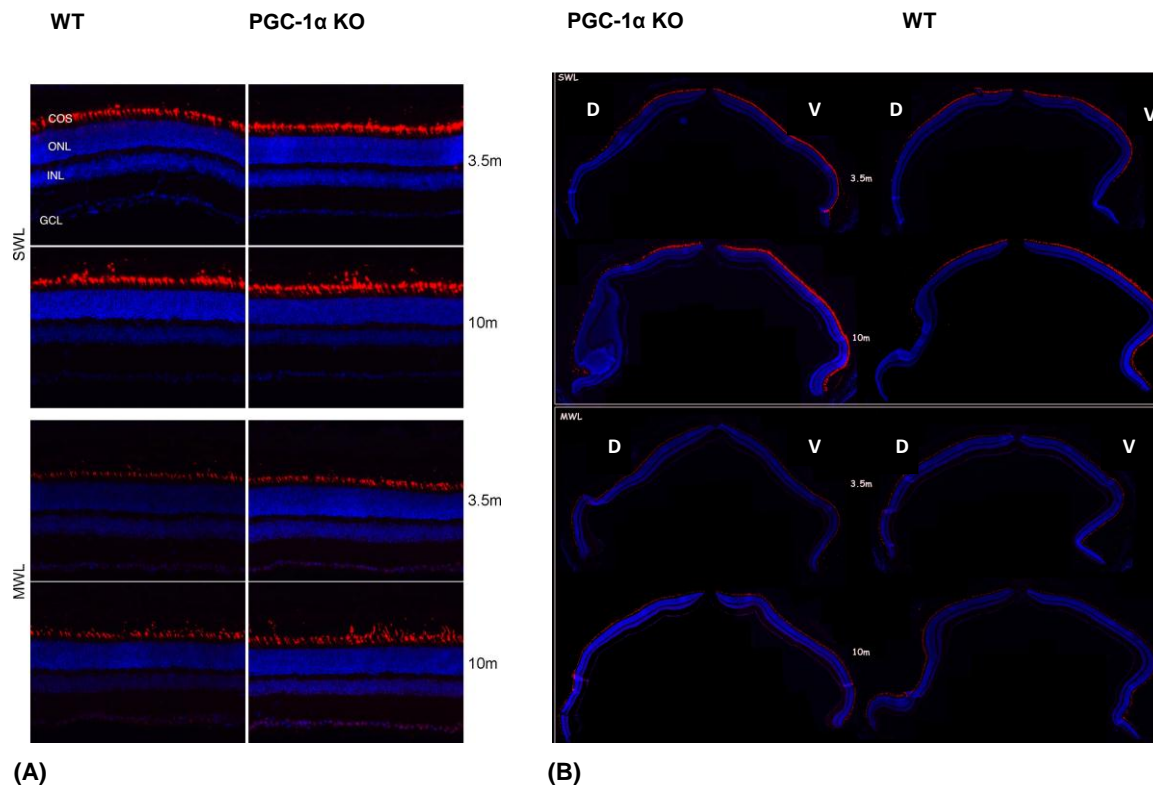


Fig.8: Morphological analysis of 3.5 and 10 month old PGC-1α KO and WT animals

Immunofluorescence staining of mouse retina: blue= DAPI staining, red= opsin staining; 10m= 10 month old animals, 3.5m= 3.5 month old animals (A) retinal sections: SWL= short wave length cone opsin; MWL= mid wave length cone opsin. COS= cone outer segments, ONL= outer nuclear layer, INL= inner nuclear layer, GCL= ganglion cell layer (B) retinal panorama: dorso- ventral orientation. D= dorsal, V= ventral
courtesy of Marijana Samardzija.

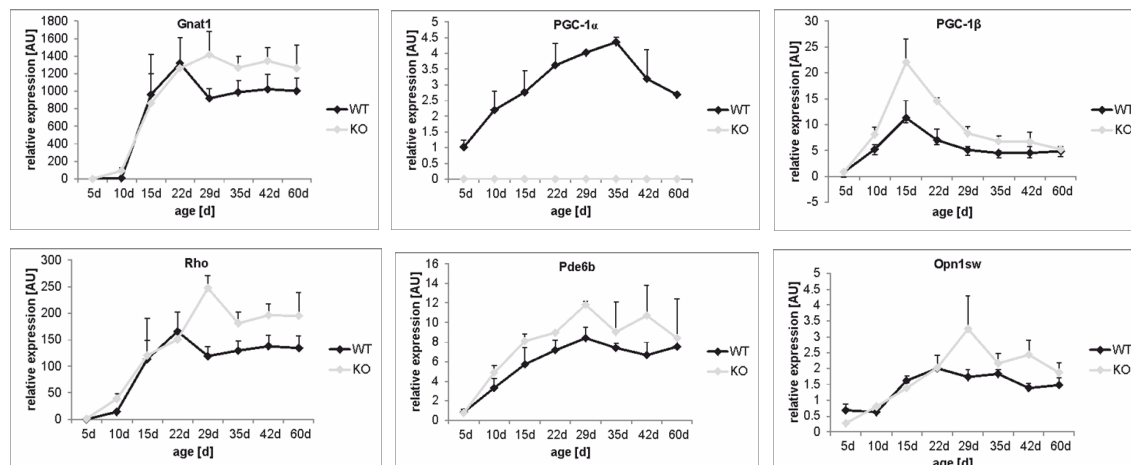


Fig.9: Gene expression in PGC-1α KO and WT mouse retina at different ages. Day5 – Day60. Expression of retinal genes measured by semi-quantitative real time PCR. Normalization against 5day old WT mouse retina.18SrRNA was used as housekeeping gene. n=2. +SEM

On balance, PGC-1α protects murine retina from high intensity light induced damage to photoreceptors.

5. The role of PGC-1 β in skeletal muscle

5.1. Introduction

Most research efforts thus far have focused on elucidating the role of PGC-1 α in different tissues. PGC-1 β , the closely related isoform of PGC-1 α , has not been studied to that extent: First identified in BAT, PGC-1 β coactivates most of the transcription factors also targeted by PGC-1 α involved in OXPHOS such as NRF-1, ERR α and PPAR α ^{39,138}. Like PGC-1 α , it is also expressed in heart, skeletal muscle, liver and pancreatic islets^{139,140,141,142}. Still, it also exhibits non redundant coactivation functions:

In liver, it regulates hepatic lipogenesis as well as lipoprotein secretion by coactivating sterol regulatory element binding protein 1c, 1a (SREBP1c, SREBP1a) and forkhead transcription factor A2 (FOXA2)^{141,143}. Upon induction by dietary fats, PGC-1 β causes a shift of triglycerides and very low density lipoprotein (VLDL) from the liver to the blood by coactivating FOXA2.

PGC-1 β seems to be implicated in glucose homeostasis by reversing hepatic insulin resistance caused by fructose¹⁴⁴.

5.1.1. PGC-1 β in skeletal muscle

The role of PGC-1 β in skeletal muscle has not been defined that clearly. Most information can be gathered from global KO and skeletal muscle specific overexpression mouse models of PGC-1 β : Yet, as PGC-1 is differentially expressed with regard to the tissue (e.g. low expression in liver vs high expression in skeletal muscle) and is strongly associated with the metabolic status (e.g. fed vs fasted conditions) and health status, the global KO models have to be assessed with caution (**Table1**):

PGC-1β manipulation models	
<i>manipulation</i>	<i>phenotype</i>
Systemic ablation ¹⁴⁵	Impaired mitochondrial function, reduced body weight and fat mass, increased thermogenesis, blunted chronotropic response to dobutamine in the heart, HFF leads to hepatic steatosis and reduced plasma triglycerides and cholesterol
Systemic ablation ¹³⁹	Decreased activity in the dark cycle, abnormal hypothermia and morbidity when exposed to cold, HFF leads to hepatic steatosis, increased serum triglyceride and cholesterol
Systemic deletion of exons 3-4, hypomorphic ¹⁴⁶	Mitochondrial dysfunction in liver and skeletal muscle but hepatic insulin resistance, elevated liver triglycerides in the fed state
Skeletal muscle specific overexpression ^{140, 147}	Increased fatty-acid oxidation, hyperphagia, reduced body weight and adipose tissue, increased exercise capacity, increased angiogenesis, increased IIX fiber content

Skeletal muscle specific overexpression ¹⁴⁸	Amelioration of insulin resistance in rats fed a high fat diet, decreased level of long chain acyl CoAs, increased antioxidant defense
Liver and adipose tissue specific Knockdown ¹⁴⁴	Reversal of hepatic insulin resistance caused by fructose, reduction of SREBP expression , increase of whole body insulin stimulated glucose disposal, increased uptake of glucose into adipose tissue
Liver specific overexpression ¹⁴⁹	Hyperlipidemia, increased hepatic triglyceride secretion, SREBP levels unchanged, on HFD decrease of SREBP 1c and plasma triglyceride levels
Skeletal muscle specific KO ¹⁵⁰	Decreased exercise performance, decreased expression of genes implicated in OXPHOS, regular glucose tolerance and insulin sensitivity

Table1: Tissue specific and systemic manipulation models of PGC-1 β

Adapted from⁷⁹.

In an unstressed setting, the PGC-1 β global KO mice are viable, fertile, but display signs of activity reduction^{139,145}. Upon cold exposure, they develop hypothermia¹³⁹.

All three global PGC-1 β KO/ hypomorphic models display reduced expression of OXPHOS genes in skeletal muscle (soleus)^{145,139,146}. Mitochondrial volume and function in soleus is decreased in two models^{145,146}. Interestingly, despite hepatic insulin resistance upon high fat diet (HFD), skeletal muscle of the hypomorphic animals responds to insulin like the control animals¹⁴⁶.

HFD leads to changes in plasma triglycerides and cholesterol: Both Sonoda et al and Lelliott et al reported hepatic steatosis in their KO animals compared to the WT animals upon HFD. However, Lelliott et al witnessed decreased plasma triglyceride and cholesterol levels in the HFD KO animals compared to controls whereas Sonoda described them as increased^{139,145}.

Overexpression of PGC-1 β in skeletal muscle decreases body weight and adipose tissue and increases exercise capacity. A second skeletal muscle specific overexpression model was published during the course of this project (see discussion part).

A skeletal muscle specific knockout model of PGC-1 β was also published during the course of this project by Zechner et al¹⁵⁰ (see discussion part).

5.1.1.1. PGC-1 β and angiogenesis

A skeletal muscle specific PGC-1 β overexpression model has helped to explain its tissue specific function: It induces OXPHOS and mitochondrial biogenesis and it also stimulates angiogenesis via VEGF induction¹⁴⁷.

5.1.1.2. PGC-1 β and fiber type determination

Like PGC-1 α , PGC-1 β is involved in fiber type determination: It causes a strong induction of IIX fibers. IIX fibers are oxidative but have “fast-twitch” biophysical properties and thus constitute intermediates between IIA and IIB fibers. They are transiently recruited during fiber type conversion from IIB to IIA¹⁵¹ and their frequency increases with age¹⁵². At the same time, type I and IIA MHC expression are repressed by PGC-1 β . This inverse correlation between PGC-1 β levels and percentage of type I fibers was also observed by Mortensen et al¹⁵³: They could show that endurance training lowers PGC-1 β expression levels. Strikingly, in transgenic PGC-1 β mice, every fiber in the observed skeletal muscle types is oxidative and the mice can run longer than WT animals. The question arises if this is due to an increase in type IIX fibers.

5.1.1.3. Specific role of PGC-1 β in skeletal muscle

PGC-1 α and PGC-1 β display different regulation patterns in response to physiological stimuli: While PGC-1 α is clearly increased/ decreased upon exercise/ obesity in skeletal muscle, PGC-1 β is not altered upon exercise¹⁵⁴.

This finding raises the question if PGC-1 β fulfills a specific task in skeletal muscle different from PGC-1 α .

5.1.1.4. PGC-1 β and glucose homeostasis

PGC-1 α is implicated in efficient glucose uptake and utilization via induction of GLUT4 transporter expression⁵.

It is a well - known observation that PGC-1 α and PGC-1 β are decreased in skeletal muscle from patients with type II diabetes whereas PGC-1 α is increased in type II diabetes models in liver^{84,7}. This drop in PGC-1 levels may lead to a reduced expression of NRF dependent genes, which is characteristic of insulin resistance⁸⁴. A skeletal muscle specific KO of PGC-1 α leaves peripheral insulin sensitivity unchanged yet impairs glucose tolerance compared to WT animals¹³.

Yet, it is not known how skeletal muscle specific KO animals for PGC-1 β handle glucose uptake.

Furthermore, the two coactivators have different regulatory functions on glucose and fat metabolism in skeletal muscle: Whereas expression of PGC-1 α in muscle is positively related to glucose uptake and oxidation, PGC-1 β expression correlates with non-oxidative glucose metabolism¹⁵⁵.

It would be interesting to know if a combined reduction of PGC-1 α and β is required for overt insulin resistance in skeletal muscle.

Three questions must thus be answered: How does PGC-1 β affect fiber type composition? What are the exclusive targets of PGC-1 β in skeletal muscle? How is PGC-1 β implicated in glucose homeostasis in skeletal muscle?

We therefore conceived a strategy that should allow for temporary reduction of PGC-1 β specifically in skeletal muscle.

5.1.2. Skeletal muscle specific knockdown of PGC-1 β

5.1.2.1. The construct

Over the last decades, a wide array of nucleic acid based constructs for sequence specific gene regulation has been developed: However, none of these has sparked more interest than RNA interference (RNAi):

Initially described in the nematode *Caenorhabditis elegans*¹⁵⁶, RNAi comprises microRNA (miRNA) and small interfering RNA (siRNA) mechanisms:

miRNA is a system of endogenous gene regulation in multicellular eukaryotes that inactivates mRNA. Pri-miRNA constructs consist of 2 imperfectly base paired RNA strands connected via a loop structure that is transcribed by Polymerase II in the nucleus. Upon cleavage with Drosha, the resulting pre-miRNA is released from the nucleus in an exportin-5 dependent fashion, processed by Dicer which yields miRNA. This miRNA is then incorporated into a complex containing an RNA induced silencing complex (RISC) and Argonaute protein2 (AGO2) which recognizes target sites at the 3' untranslated region (UTR) of mRNAs and leads to translational inhibition and mRNA degradation¹⁵⁷.

siRNAs were first discovered in plants as eukaryotic defense system against viruses¹⁵⁸. They consist of double stranded RNAs of around 21BPs size with 2 nucleotides overhang at their 3' ends. They are perfectly complementary to their mRNA target and reduce mRNA levels by mimicking miRNA leading to mRNA cleavage.

shRNAs are exogenous, imperfectly base paired double stranded RNAs that mimic pre-miRNA leading to mRNA degradation. They contain a base paired stem, loop and a 3' terminal UU overhang.

shRNA-mir is a further development of shRNAs which mimics pri-miRNA.

As both shRNA-mir and shRNA enter the silencing cascade far more upstream than siRNA and are usually delivered via vectors, they allow for long-term, stabler knockdown than would be possible with siRNA^{159,160}.

We therefore strived for the generation of a shRNA-mir based vector to knock down PGC-1 β .

One important caveat in dealing with shRNA is its potential toxicity: If shRNA expression is too high, the endogenous exportin-5 system is oversaturated and shRNA delivery, especially *in vivo*, can be toxic or fatal¹⁶¹. This limitation can be overcome by employing polymerase II promoters which are used by the cell

to generate miRNA: In contrast to the ubiquitously expressed, potent polymerase III promoters (U6, H1), polymerase II promoters are often tissue specific and grant more attenuated gene expression¹⁵⁹.

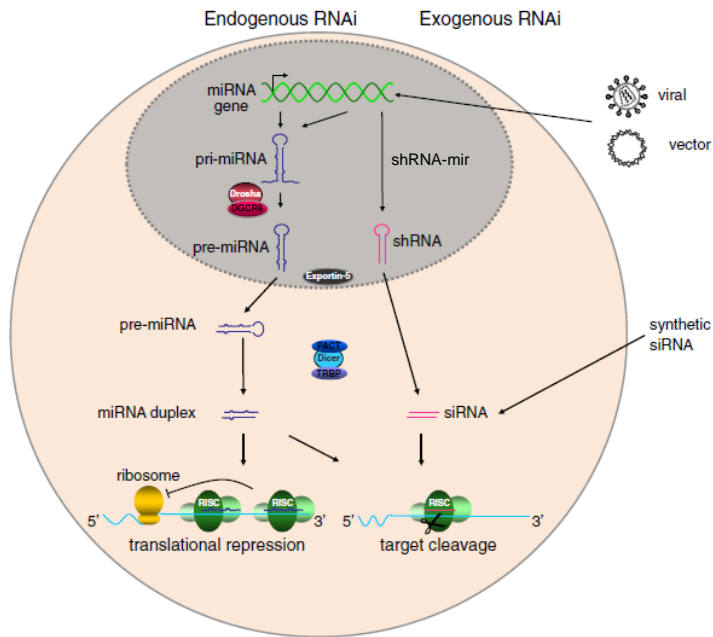


Fig.10: RNAi: Exogenous shRNA and siRNA versus endogenous miRNA pathways
 adapted from¹⁶²

5.1.2.2. The delivery

5.1.2.2.1. Somatic delivery

One possible avenue of administering the shRNA construct is systemic (intraperitoneal or intravenous injection): This necessitates the use of skeletal muscle specific promoters to avoid expression of the construct throughout the body. Furthermore, this approach has two major limitations: First, the shRNA may easily be degraded and diluted upon injection. Second, for efficient knockdown, the shRNA needs to be injected repeatedly. This technique thus lends itself more to being a complementary approach, for example in tumor treatment¹⁶³.

5.1.2.2.2. Transgenic mouse delivery

Tissue specific KO models have paved the way for studying the organ specific function of genes and enabling the generation of animal models that would not thrive were the protein globally ablated. Typically, these models also avail themselves of inducible KO (e.g. tetracycline or tamoxifen controlled) which avoids interference with developmental programs that would further hamper the analysis of the gene of interest¹⁶⁴.

This technique can be combined with delivery of shRNA: Gao et al published the generation of a transgenic RNAi mouse where the shRNA construct is driven by a H1 promoter. This construct is then injected into the pronuclei of mouse one-cell embryos¹⁶⁵. This technique was also used for creating an inducible KO by Dickins et al: They bred transgenic mice harboring a tetracycline responsive RNA polymerase II promoter driving a shRNA targeting p53. Upon crossing with mouse strains expressing tissue specific or general transactivator proteins that can be either activated (tet-on) or repressed (tet-off) by tetracycline, transient expression of shRNA is achieved¹⁶⁶.

5.1.2.2.3. Viral delivery

We strived for a system, which is potentially more time saving and cost effective than the ones mentioned above:

Jointly with stem cell therapy, gene therapy has emerged as a tool for combating acquired or hereditary diseases during the last decades: The generation of a virus harboring the therapeutic gene, its propagation, delivery to the host and ultimately expression has been achieved using a tailored virus attenuated in its original properties (for recent review see¹⁶⁷): Three viral strains, namely adenovirus (AV), adeno-associated Virus (AAV) as well as lentivirus (LV) have been tested in animal models and are starting to be successfully used in clinical trials (e.g.:¹⁶⁸, Amsterdam Molecular Therapeutics: Glybera). Their route of viral delivery can be local or systemic. The present hurdles of gene therapy are mostly host inflammatory responses as well as transduction problems.

As AAV and LV both appeared to be interesting candidates for our approach we scrutinized their potential for our project (**table2**). We eventually opted for the use of AAV:

AAV belongs to the family of parvoviridae and is a single stranded DNA virus. It infects preferentially postmitotic, quiescent cells. In most cases, it does not integrate into the genome but remains episomal and does not lead to pronounced immune response. Furthermore, the wildtype virus is replication – deficient and thus requires a helper AV to replicate itself, making it a safe tool for gene therapy. Structurally, AAV has an icosahedral capsid that can accommodate about 5kB of foreign DNA. The AAV virion consists of two large open reading frames (ORFs) that encode for the replication (rep) and capsid (cap) proteins VP1, VP2 and VP3 controlled by a p40 promoter. Both sides of the genome are flanked by inverted terminal repeats (ITRs) responsible for AAV genome replication¹⁶⁹.

AAV life cycle starts with binding to cellular surface receptors like heparin sulfate proteoglycan (HSPG), fibroblast growth factor receptor-1 (FGFR1), integrin $\alpha\beta 5$ and hepatocyte growth factor receptor (HGRF) and subsequent internalization via clathrin-mediated endocytosis. Second, the AAV is channeled to the nucleus, where it is uncoated and the vector genome is released. This vector genome then has to be completed from single stranded to double stranded DNA to serve as a template for transcription. This very process is the rate limiting step in the use of AAV for gene therapy: It can thus take up to several weeks until the second strand of the genome is successfully synthesized. Another bottleneck is the number of cellular surface receptors that can vary according to the tissue/ cell type used¹⁷⁰.

The standard manufacturing approach of AAV is achieved through triple transfection of three vectors: first, the vector containing the genome plus the transgene flanked by two internal repeats (ITRs), second a helper plasmid that provides replication (rep) and capsid (cap) proteins and third, a helper plasmid of adenoviral origin containing the essential early genes E1, E2A, E4 in cell culture¹⁷¹. 72hrs post transfection, the AA virions can be harvested from the cell lysate¹⁶⁷.

There were two major features of AAV that made us opt for this approach:

First, contrary to LV and AV, AAV displays considerable tissue tropism: 11 different serotypes have been characterized. These serotypes distinguish themselves from one another mainly by their capsid proteins which determine tissue tropism allowing for targeted uptake of the virus into various tissues (photoreceptors and retinal pigment epithelial cells, skeletal muscle, cardiac muscle and liver cells¹⁷² - see **table3**). This feature would allow for targeted uptake of AAV into skeletal muscle irrespective of the route of delivery (systemic or local injection) using AAV6: AAV6¹⁷³ has a strong tropism for skeletal muscle, albeit also cardiac muscle^{174,175} where it has been used for treating severe heart failure¹⁶⁷. AAV2 displays a broad tissue tropism and has been used in clinical trials with muscular, subretinal and intracranial administration¹⁶⁷. It is also the most widely studied and best characterized serotype. However, AAV2 displays a slower onset of protein expression (28 days postinjection) from the gene of interest delivered than does AAV6 (7 days postinjection)¹⁷⁴. We thus tried to combine AAV2 with the capsid from AAV6, generating a so called pseudotyped AAV2/6 that harbors the genetic properties of AAV2 whilst displaying tissue tropism of AAV6.

Second, up to now, infection with AAV has not been associated with considerable immune response. It can, however, lead to some cellular and humoral immune response which engenders neutralizing antibodies. This phenomenon is observed when AAV from the same serotype is administered repeatedly¹⁷⁶. As both PGC-1 α and PGC-1 β are downregulated in disease states that comprise low level, systemic inflammation⁸⁴ and they counter inflammatory response⁷², we sought for a model that does not trigger immune system activation.

However, there are also downsides to the use of AAV: it does not lend itself to the production of high titer virions. Also, transduction efficiency in culture for diverse cell types is more efficient in AV and LV (**table 2**). Finally, the scaling up of AAV production is also not as straightforward as with AV¹⁷⁷.

	AV	AAV	LV
Insert size	7.5kB	5.0kB	8.5kB
Inflammatory response	high	low	Medium to high
Host genome integration	no	no	possible

Transduction efficiency	All cell types nearly 100%	Dividing and non-dividing cells; tropism is serotype specific	Dividing and non-dividing cells
High level of protein expression	yes	no	no
Easy to scale up in production	yes	no	no
Easy to get high titers > 1x10E9	yes	no	no

Table2: properties of AV, AAV and LV: adapted from <http://signagen.com/>

TABLE 1: Hierarchy of transduction efficiency in major tissues of AAV serotype vectors

Tissue	Optimal serotype(s)	References
Liver	AAV8, AAV9	[16,17,68,71]
Skeletal muscle	AAV1, AAV7, AAV6, AAV8, AAV9	[16,17,23,60,63]
CNS	AAV5, AAV1, AAV4	[64-66,123]
Eye		[67]
RPE	AAV5, AAV4	
Photoreceptor cells	AAV5	
Lung	AAV9	[17]
Heart	AAV8	[69]
Pancreas	AAV8	[125,126]
Kidney	AAV2	[124]

Table3: AAV serotypes and their tissue tropism:¹⁷¹

We finally decided to opt for AAV mediated knockdown of PGC-1 β in skeletal muscle.

5.2. Project aims

Before the project start, only global or liver specific KO models as well as skeletal muscle specific overexpression models have been used to explain the roles of PGC-1 β in skeletal muscle. As seen for PGC-1 α , expression of PGC-1 β is tissue specific and systemic effects in global KO animals often hamper analysis of gene function in specific tissues^{13,112}. Thus, in order to specifically assess the function of PGC-1 β in skeletal muscle, it is crucial to limit PGC-1 β ablation to this tissue.

Therefore, the involvement of PGC-1 β in glucose homeostasis and fiber type determination was answered in generating a skeletal muscle specific PGC-1 β knockdown (KD) model using RNAi directed against PGC-1 β . KD rather than KO allows for a moderate to pronounced downregulation of PGC-1 β rather than complete ablation. Delivery of the KD construct was done via systemic and local injections of AAV carrying the KD sequence against PGC-1 β . After testing KD efficiency via qPCR and Western Blot, systemic tests should be carried out to unveil the effects of PGC-1 β reduction on glucose homeostasis. Skeletal muscle fiber type should be characterized via fiber staining.

5.3. Material and Methods

Design and cloning of shRNAs to knock down PGC-1 β

Three different design modi (construct1, construct2, construct3- see results section) were used to generate shRNA-mir against *mus musculus* PGC-1 β (Genbank accession number NM_133249):

All shRNA-mir constructs are hereafter designated as shRNA for simplicity.

The sequences were subjected to BLAST analysis <http://blast.ncbi.nlm.nih.gov/Blast.cgi> to ascertain if they were specific for PGC-1 β .

Subsequently, constructs were cloned into pU6-mir30, pMan, pcDNA3.1(+), pAAV-CMV-MCS and pAAV-CK6-MCS backbones, respectively, using Vector NTI 7.0 (Invitrogen, Carlsbad, California) and Geneious (Geneious, Auckland, New Zealand) softwares. Backbone pSuper already contained the shRNA.

Cloning was carried out according to the handbook “Molecular Cloning: A Laboratory Manual”, Third Edition, Sambrook and Russell, Cold Spring Harbor Laboratory Press, 2001.

Owing to the size of the shRNA constructs (around 70BPs), the shRNAs were ordered as single stranded oligos containing the necessary restriction sites, annealed and inserted into the plasmids containing the shRNA flanking sequences:

shRNA2 and scrashRNA were cloned in pU6-mir30 using the restriction sites XhoI and EcoRI.

shRNA3 was cloned into pMan using the restriction sites for MfeI.

shRNA4 was already contained in the pSuper backbone.

shRNA2 - pU6mir-30 flanking sequence and scrashRNA-pU6mir-30 flanking sequence were cloned into pcDNA3.1(+) via a HindIII restriction site.

shRNA4 of pSuper was also cloned into pcDNA3.1(+) via a HindIII restriction site.

shRNA2 – pU6mir-30 flanking sequence and scrashRNA – pU6mir-30 were inserted into pAAV-CMV using the HindIII restriction site.

GFP was cloned into pAAV- CMV- shRNA2pU6mir via BglII restriction sites.

shRNA2 - pU6mir-30 flanking sequence and scrashRNA-pU6mir-30 flanking sequence were cloned into pAAV-CK6 via SacI and BsmI restriction sites.

Cell lines and respective culture conditions

HEK293 cells were cultivated at 37°C in 5% CO₂. DMEM (high glucose) (Gibco, Invitrogen, Carlsbad, California, order no 10313-039:) supplemented with 10% FBS (Gibco, Invitrogen, Carlsbad, California, order no 10099158), 1% Penicillin/ Streptomycin (Gibco, Invitrogen, Carlsbad, California, order no 15070-063) was used as medium.

Sol8 and C2C12 cells were cultivated similarly to HEK293 cells but 20% FBS was used for Sol8 cell cultivation.

Differentiation of C2C12 and Sol8 cells

C2C12 and Sol8 cells were grown to 90% confluency and then differentiated using regular cultivation medium containing 2% horse serum (Invitrogen, Carlsbad, California, order no 16050114). Medium was changed every 3rd day.

Skeletal muscle primary cells and respective culture conditions

Primary cells from C57 BL/6 mouse skeletal muscle were cultivated in 79% F10 (Gibco, Invitrogen, Carlsbad, California, order no 11550-043) , 20% FBS hyclone (Hyclone Logan, Utah, order no HY-ME-SH30070-02), 1% Penicillin/Streptomycin, 0.1% Fungizone (Invitrogen, Carlsbad, California, order no 15290-018) and 0.01% bFGF (Invitrogen, Carlsbad, California, order no 13256-029).

Differentiation of skeletal muscle primary cells

Skeletal muscle primary cells were grown to 90% confluency and then differentiated using regular cultivation media with 5% horse serum.

Cell line transfections

HEK293 cells were split to 1x10E10 cells per 10cm diameter plate; 12 hours later cells were transfected with plasmids. Plasmids carrying shRNA sequences and control plasmid carrying FLAG tagged mouse PGC-1 β were added to the cells in a molar ratio of 5:1. Calcium Chloride and HBS were used as transfection reagents according to “Der Experimentator: Molekularbiologie/Genomics”, Cornel Mülhardt, Elsevier GmbH, Fifth edition, 2006.

Preparation of cell lysates

48 hours post transfection, cells were harvested and protein was extracted in lysis buffer (10% glycerol, 20mM Tris pH=8, 137mM NaCl, 1% Nonidet P-40, 1mM PMSF, 1x Protease inhibitor mix: Roche Diganostics, Mannheim, Germany, order no 11697498001). Cells were incubated in lysis buffer (300ul of lysis buffer per 1 Mio cells) for 30min. on ice and subsequently centrifuged. The resulting supernatant was frozen at -80°C.

Western Blot

Protein concentration of total protein extracts was analyzed via Bradford assay using bovine serum albumin as a standard (Bradford M et al, 1976).

50-100ug of protein was applied to a polyacrylamide gel and blotted onto PVDF membranes by semi-dry electroblotting (Thermo Scientific, Waltham, Massachusetts, order no OWHEP1). Membranes were stained with Ponceau S to verify equal protein amount per lane. After blocking (1% non fat milk powder, 0.1% Tween 20 in Tris-buffered saline), blots were probed overnight with anti-FLAG antibody (Sigma Aldrich, St.Louis, Missouri, order no F3165) or anti α - tubulin (Cell Signaling, Danvers, Massachusetts, order no 2125) using dilutions 1:2000 and 1:1000, respectively. Detection was carried out using horseradish peroxidase conjugated anti mouse (GE Healthcare, Waukesha, Wisconsin, order no NA931) and anti rabbit (Jackson Immuno Research, West Grove, Piscataway, order no 111-035-144) antibodies. ECL Dura (Thermo Scientific, Waltham, Massachusetts, order no 34075) was used for protein visualization.

AAV production

AAV was produced in three ways: using a commercially available kit, ordering AAV from an industrial production facility and from a university based AAV production facility.

Commercially available kit

AAV Helper Free System (Agilent, Santa Clara, California, order no 240071) was used to produce AAV: AAV2 was produced via triple transfection of AAV293 cells with pAAV-CMV-shRNA2/ pAAV-CMV-scrashRNA/ pAAV-GFP-IRES, pHelper and pAAV-RC according to the protocol guidelines. 20x 10mm diameter cell culture plates were used per construct. Virus was aliquoted and stored at -80°C.

Virus purification was done using Fast Trap- Adeno Associated Virus Purification and Concentration Kit (Millipore, Billerica, Massachusetts, order no FTAA 000 03).

Virus titration was carried out using the QuickTiter™ AAV Quantitation Kit (Cell Biolabs, San Diego, California, order no VPK-145) and AAV2/3 titration ELISA (Progen Biotechnik GmbH, Germany, order no PRATV).

AAV production facility

pAAV-GFP-IRES, pAAV-CMV-shRNA2, pAAV-CMV-scrashRNA and pAAV-CMV-shRNA2-GFP were sent to “Institut de Recherche Thérapeutique, Université de Nantes – INSERM U649” for production and titration of AAV2/6.

University based AAV production facility

pAAV-CK6-shRNA2 and pAAV-CK6-scrashRNA were used to produce and titrate AAV2/6 at “Baker Heart and Diabetes Institute (Baker IDI)”, Melbourne, Victoria according to the facility’s protocol: AD293 cells were triple transfected with pHelper, pCap6 and pAAV-CK6-shRNA2pU6/ scrashRNApU6 constructs. Upon virus harvesting three days posttransfection, the virus was concentrated in a HiTrap heparin column (GE Healthcare, UK) using high pressure liquid chromatography (HPLC) in a preparative Aekta purifier

(GE Healthcare, UK) and sucrose density gradient ultracentrifugation. Virus titration using semi-quantitative real time PCR was followed by virus storage at -80°C.

AAV2 transduction of cell lines and skeletal muscle primary cells

Skeletal muscle cell lines C2C12, Sol8 and kidney cell line HEK293, respectively, were transduced with AAV2 in concentration ranges from 1×10^4 - 1×10^7 vector genomes per cell by adding the virus directly to the cell culture medium. For this purpose, 80.000 cells were split per well of a 12 well plate 14hrs prior to transduction. 48hrs posttransduction, cells were analyzed.

Differentiated C2C12 and skeletal muscle primary cells were cultivated for 3 days using differentiation medium and subsequently transduced with AAV2 virus particles.

Mice

C57 BL/6 JRj WT mice used for injections were purchased from Janvier, Le Genest St. Isle, France.

AAV2/6 injections into tibialis anterior (TA) muscle

C57 BL/6 JRj WT mouse TA was injected with AAV2/6-GFP-IRES, AAV2/6-CMV-shRNA2 , AAV2/6-CMV-scrashRNA, AAV2/6-CK6-shRNA2, AAV2/6-CK6-scrashRNA or PBS as control: Two different concentrations, 1×10^{10} vector genomes (VG) and 5×10^9 VG were used. Virus was diluted in PBS to a total volume of 40ul.

TA muscle was extracted 7, 14, 21 and 28 days postinjection.

TA was prepared for protein or RNA analysis (snap frozen in liquid nitrogen and stored at -80°C) or used for cryosections.

Cryosections

TA was embedded in a carrier (7% gum tragacanth in AD) that was fixed on a cork plate support by dripping it in cooled isopentane amylalcohol for 20 seconds. TA was stored at -80°C prior to preparing 12 μ m thick slices with a cryostat device (Microm HM 560, Thermo Scientific, Massachusetts) and fixing them on superfrost slides (Menzel Gläser, Braunschweig, Germany, order no AA00008032E) Slides were air dried for 30 min. at room temperature and subsequently stored at -20°C.

Immunofluorescence

Cryosection slides were fixed in 4% PFA (Sigma Aldrich, St. Louis, Missouri, order no 76240) in PBS for 10min., washed 3x with PBS in individual glass chambers. Slides were then incubated with blocking solution made up of 2% BSA (Sigma Aldrich, St. Louis, Missouri, order no A9418) , 0.2% Triton-X (Sigma Aldrich, St. Louis, Missouri, order no 93426, in PBS) for 30min., then incubated with the primary antibody for 1 hour, washed 3x with PBS, incubated with the secondary antibody for 1 hour in the dark. Slides were mounted with a coverslip using vectashield (Vector Labs, Southfield, Missouri, order no H-1400) and sealed with nailpolish. Slides were stored at 4°C protected from light until analysis. Confocal microscopy was done on a Leica TCS-NT-SP1 (Leica instruments, Wetzlar, Germany).

Primary antibodies used were anti mouse CD3 (1:400 dilution) (Abd Serotech, Kidlington, UK, order no MCA500GA) and CD68 (1:400 dilution) (Abd Serotech, Kidlington, UK, order no MCA1957GA). Secondary antibody used was goat anti rat IgG Alexa Fluor 488 (dilution 1:1000) (Invitrogen, Carlsbad, California, order no A11006).

Hematoxylin and eosin staining

For hematoxylin and eosin (H&E) staining, cryosection slides were incubated in 1%PFA in PBS for 15min., rinsed in H₂O₂ for 2x2min. and subsequently stained in Mayer's hematoxylin solution (Sigma Aldrich, St. Louis, Missouri, order no MHS16) for 15min. Rinsing in 0.1% HCl for 30sec. was followed by washing in warm tap water for 15min. and then in AD for 30sec. Subsequently, slides were stained in Eosin Y (Sigma Aldrich, St. Louis, Missouri, order no HT110216) for 3min., rinsed with warm tap water for 30sec., dehydrated in 95% EtOH, 100% EtOH (Sigma Aldrich, St. Louis, Missouri, order no 02860) and Xylol (Merck, Whitehouse Station, New Jersey, order no 108681) (2x2min. each) and finally mounted with anhydrous mounting medium.

Semi quantitative real time PCR

RNA was isolated using the miRNeasy Mini kit from Qiagen (Qiagen, Venlo, Netherlands, order no 74104).

Tissue preparation:

Up to 40mg of frozen TA muscle was homogenized in 700µl of Qiazol.

Cell culture preparation:

Cells in 1 well of a 6 well cell culture plate were homogenized with 700µl of Qiazol.

1ug of RNA was used for cDNA synthesis using Super Script Reverse Transcriptase II (Invitrogen, Carlsbad, California, order no 18064-014) and random hexamer primers (Roche, Basel, Switzerland, order no 11277081001). Fast SYBR Green Master Mix (Applied Biosystems, Carlsbad, California, order no 4385612) was added to the cDNA. qPCR was performed using the Step One Plus qPCR machine (Applied Biosystems, Carlsbad, California, order no 4376600).

Relative expression levels for each gene of interest were calculated using the $\Delta\Delta C_t$ method and normalized to the expression 18S ribosomal RNA (18SrRNA).

Semi quantitative real time PCR primers

Primer name	Sequence 5' => 3'
18S rRNA-F	AGTCCCTGCCCTTTGTACACA
18S rRNA-R	CGATCCGAGGGCCTCACTA
Cox5b-F	GCTGCATCTGTGAAGAGGACAAC
Cox5b-R	CAGCTTGTAATGGGTTCCACAGT
Cpt1-F	ATCATGTATCGCCGCAAAC
Cpt1-R	CCATCTGGTAGGAGCACATGG
Cycs-F	GCAAGCATAAGACTGGACCAAA
Cycs-R	TTGTTGGCATCTGTGTAAGAGAATC
Erra-F	GCAGGGCAGTGGGAAGCTA
Erra-R	CCTCTTGAAGAAGGCTTTGCA
GFP-F	TCGAGGTGGTGTACATGAACGA
GFP-R	GCTGTAGAACTTGCCGCTGTT
Mcad-F	AACACTTACTATGCCTCGATTGCA
Mcad-R	CCATAGCCTCCGAAAATCTGAA
Mhcl-F	CCTCCTCACATCTTCTCCATCTCT
MhclIA-F	CCCCGCCCCACATCTT
MhclIA-R	TGACTGATTCTCCCTGTCTGTTAGC
MhclIB-F	CAACCCATATGACTTTGCTTACGT
MhclIB-R	TCCCAGGATATCAACAGCAGTGT
MhclIX-F	GAAGGAGAAGTGGAAAATGAACAGA
MhclIX-R	TGTTTGC GCAGACCCTTGA
Mhcl-R	TGGACTGATTCTCCCGATCTG
PGC-1 α _ex2-F	TGATGTGAATGACTTGGATACAGACA

PGC-1 α _ex2-R	GCTCATTGTTGTACTGGTTGGATATG
PGC-1 α _ex3-5-F	AGCCGTGACCACTGACAACGAG
PGC-1 α _ex3-5-R	GCTGCATGGTTCTGAGTGCTAAG
PGC-1 β -F	GGCAGGTTCAACCCCGA
PGC-1 β -R	CTTGCTAACATCACAGAGGATATCTTG

5.4. Results

Design and cloning of shRNAs to knock down PGC-1 β

Mouse PGC-1 β , NM_133249 has 3 isoforms; two of which have the most widespread tissue distribution. Isoform1, Ppargc1b-001 has 12 exons; isoform 2, Ppargc1b-002 has 13 exons. The third isoform is not protein coding and contains only 2 exons (**table4**).

Thus, the shRNAs against PGC-1 β should be designed to target both isoforms 1 and 2:

Isoform	Transcript ID	Length (base pairs)	Number of exons	Protein ID	Length (amino acids)	Coding properties
Ppargc1b-001	ENSMUST00000075299	3656	12	ENSMUSP00000074771	1014	Protein coding
Ppargc1b-002	ENSMUST00000063307	3330	13	ENSMUSP00000069431	1030	Protein coding
Ppargc1b-003	ENSMUST00000142134	366	2	-	-	No protein product

Table4: PGC-1 β , NM_133249 isoforms: Exon composition, length on mRNA and protein level

We strived for generation of shRNA-mir to make sure that the constructs enter the knockdown cascade at a very early stage (for more ample information, see introduction): For this purpose, we used 3 constructs: Both constructs1 and 2 were designed according to pri-miRNA design rules to form imperfect hairpin structures, containing nucleotides deletions, insertions and exchanges. Construct3, on the other hand was designed as conventional, perfect-match hairpin. For ease of designation, all constructs hereafter – irrespective of their design principles - will be termed as “shRNA”, numbered 1-4.

Construct1:

The most studied miRNA is human micro RNA-30; its precursor, more specifically the pri-miR-30 stem loop should be used as template to insert shRNA driven by a polymerase II or polymerase III promoter¹⁷⁸. shRNA1 targets exon 11, shRNA2 targets exon 6 of PGC-1 β :

shRNA1:

target sequence: 5' ATACACTGACTATGATCCC 3'

5'TCGAGAAGGTATATTGCTGTTGACAGTGAGCGCA**CACTGACTATGATCCC**ACATTAGTGAAGCCACAGATGTAATGTGGGATCATAGTCAGTGTA TGCCTACTGCCTCGG 3'

shRNA2:

target sequence: 5' GTCCTCTGAGGCTGGAGGT 3'

5'TCGAGAAGGTATATTGCTGTTGACAGTGAGCG**GCCTCTGAGGCT**GGAGGTGAAATAGTGAAGCCA
CAGATGTA TTTACCTCCAGCCTCAGAGGA TGCCTACTGCCTCGG 3'

scra shRNA:

5' TCGAGAAGGTATATTGCTGTTGACAGTGAGCG **GGAACAATCAGCATCCCGACCG**
TAGTGAAGCCACAGATGTA **CGGTCGGGATGCT** GATTGTTCTGCCTACTGCCTCGG 3'

(red: mRNA sense sequence, green: mRNA antisense sequence; blue: loop; black: flanking sequences; orange: shRNA enhancing, changed or added nucleotides; yellow background: original shRNA targeting sequence; bold font: nucleotides that were exchanged or added)

Construct2:

We also used the pri-miR-30 to generate shRNA which contains the stem loop structure and even more extensive flanking sequences. For this purpose, we used the pMan vector¹⁷⁹.

Design was carried out according to: <http://www.dharmacon.com/Home.aspx?id=642>

shRNA3 targets exon 9 of PGC-1 β .

shRNA3:

target sequence: 5' GCTTTGAGGTGTTCCGGTGA 3'

5'TGCTGTTGACAGTGAGCG**AGCTTTGAGGTTCTGTTCCGGTGA**GTGAAGCCACAGATGTCACCGAAC
ACCTCAAAGCCTGCCTACTCCTCGGACTTCAAGG 3'

scra shRNA:

5'TGCTGTTGACAGTGAGCG**AAACAATCAGCTCATCCCGGACCG**TGAAGCCACAGATGGGTCCGGGA
TGAGCTGATTGTTTCTGCCTACTCCTCGGACTTCAAGG 3'

Construct3:

We then wanted to compare the knockdown potential of the first two constructs to a control shRNA already tested embedded in the pSuper vector: www.oligoengine.com/products/pSUPER.html¹⁸⁰.

shRNA4 targets exon6 of PGC-1 β .

shRNA4:

Target sequence: 5' GATATCCTCTGTGATGTTA 3'

5 AGCTTGATCCCC**GATATCCTCTGTGATGTTA**TTCAAGA**GATAACATCACAGAGGATA**TCTTTTTA 3

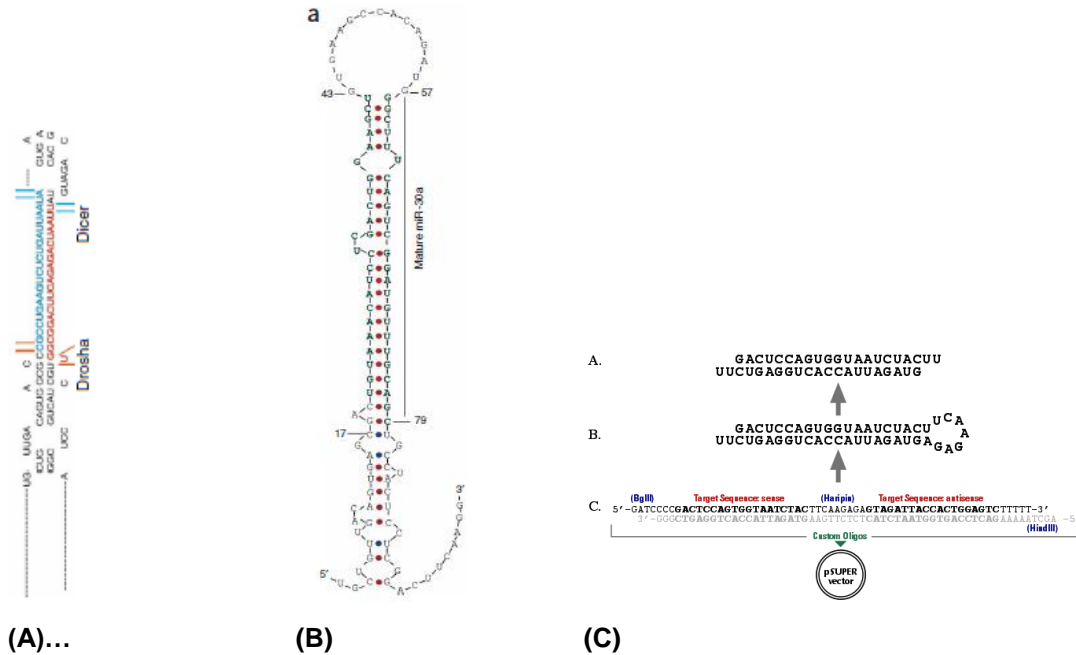


Fig.8: The three constructs used for embedding shRNA: (A): construct1: pri-miRNA¹⁷⁸, (B): construct2: pri-miRNA¹⁷⁹, (C): construct3: shRNA¹⁸⁰.

```

ctcgtccctccccgggggggtcggcgctgactccgcgcgagctgcagcggggctggaagATGGCGGGAA
CGACTCGCGCGCCTGCTGGATGAAGAGCTCTGTCCTTCTCCTCAACTATCTCTGACACCGAGGGTGGGA
CTCTGGAGAGAACACCTGTGTCTGACTTCCAGAGCTTGACTCTCCACGCTGGACCCGATGACTTGGACTC
AGCCACGTGCTTTGGGAGCTGCACTGGTGGCCGGAGACTCAGAGACAGAGCCACCCAGTACAGCCCGATGA
CTCCGAGCTCTCCAGATTGACAGTGAAGTGAAGCTCTCTGGCTGGCTTACGAGACCCCTGGATGACATCCC
CGAAGACGATGTGGGGTGGCTCTCCAGAACTGGTGAAGGGGACACACCATCTGACACCCAGCTCACCC
TGCCTCCTATCTGACCCCGCCAGCCCTGGAGAGCTTCTGTCCTCCAGGCTGACGCTGACGAGCTTTC
ACTCTCTAGAGAGCTCTCTGGCCAGCTCCCGACAGCACTCCCGACAGCACTCTGACGCTCTGAGAGAGGGCCCTG
GTCCACAGCCCTCAGTCTCCAGAGTCAAGCGGCTTGTGCAAGGTGGATGGACCCAGGATAAGAGACCCD
CACACTCGGGGCTCAGAGCCGGCTTGTACGGAACTGCATAAGCACTCACTTCGGTCTGCCCTGCCAGAGT
GAAAGCTGCTCCCAACTCCGACCCCGAGCCCTGGCTCTCTCCAAAGAGAGAGAGAGAGAGTGGGGAGGA
TTGCCAAAGCTTGGCCGATCCAGCTCCCGCAAGCTCTAGCAGAGAGAGAGAGAGAGAGAGAGAGAGAGAG
CCAGCTCCCGAGAGAGTGTAGAGGCAATGGTACAGCTCATTCCTACATGCATACCTACTGCTCCCTCAGAG
GAAGTCCCGCAAGGGCCAGAGCCATCCCGAGCCCTGACAGCACTCTCCAGGCAAGTCAACCCCGATC
CGGCATCCCCCAAGCTTCTGACTGAGTCTCTATCTTAAGGAACTCTGGCCCAAGATATCTCTGTGA
TGTAGCAGCCCTACCGCTGGCATACTGTCTATGCTTCCCTCAGACTCAGTCCAGGCCAGGCCCCCA
GACAGTGGCCCTCCCTCCCTTGGCCAGAGAGAGAGAGAGAGAGAGAGAGAGAGAGAGAGAGAGAGAGAG
GGCTAGCCAGCTGCTCTCTGAGCTGGAGGTGAACGGGATGTTAAACAGCTACAAAGCAAGAGCGGGA
GGAAGATGAGGAGAGAGAGAGAGAGAGAGAGAGAGAGAGAGAGAGAGAGAGAGAGAGAGAGAGAGAGAG
GAAGAGCAGGTGTGGCTGCAATGGACCAAACTAGGGAGAGAGATGGACGCTCCGTGTGCCCTGGCGG
CTCAGAGAGTGAATCCAGAGTGGCTGGCTGGCTGACTTCACTGATGAGCCCTTAGTGTCTCCCTGGAT
GTCTCTGATCAGAGAGAGAGAGAGAGAGAGAGAGAGAGAGAGAGAGAGAGAGAGAGAGAGAGAGAGAGAG
CCCCAGGATCCAGATCCCGCCCTGAAAGCCCTGTGAGAGTGGTGGGAGACACAGATGAAGATCCAAG
CTGCCACAGCCACTTCCAGAGACTCTCCAGTGGCTCATGCTGGCTTGTACAAAGCGACTCTCTGGCAA
GAAGACTTTGAGAGTCCCTGAGCGTGGAGCTTTCCGGCAGCGAGCTCACGCCACCCACACCTCATA
CAAGCCAAAGAGAGAGAGAGAGAGAGAGAGAGAGAGAGAGAGAGAGAGAGAGAGAGAGAGAGAGAGAG
CTCCCGAGGCTCTTCCGCTCACAGCCACCCAGAGCTTCCCAAGCTGCCAAGAGGCCACCCAGAGCGAAG
CGAGCTCTGTCCATTGACGATGCCAACAACCAAGTCTCACAGGCTGGCCAGAGGCCCTCTCTCTG
CTCTTTGGAGACCAAGACTCTCCAGGTGCTCAGCCAGAGGCTGCCCTGACAGGAGAGTGTGCGGTCTG
GGAGCACTGGGTCCACTTGAAGCTTGGCCAGAGAGAGAGAGAGAGAGAGAGAGAGAGAGAGAGAGAGAG
GAGGGAGAGAGAGAGAGAGAGAGAGAGAGAGAGAGAGAGAGAGAGAGAGAGAGAGAGAGAGAGAGAGAG
TCTCAAGAGACTTTGGGCTGCTGGAGACTGCTGGAGGTGAAGACTGGCTCTGTAAGAGAGAGAGAGAG
TGACACCGTATTGAGGACAGCAGCAGCAGTGGCAGGATGACTTCTGCTTGGAGGAGAGAGAGAGAGAG
GAGGGAGGGAGAGAGAGAGAGAGAGAGAGAGAGAGAGAGAGAGAGAGAGAGAGAGAGAGAGAGAGAGAG
GAGCCACCGAGTGAAGAGAGAGAGAGAGAGAGAGAGAGAGAGAGAGAGAGAGAGAGAGAGAGAGAGAGAG
CTGTCCACAGCCACCCGAGAGACTTCAGAGCTGAGAGAGAGAGAGAGAGAGAGAGAGAGAGAGAGAGAG
GCATGCCAGGAGAGAGAGAGAGAGAGAGAGAGAGAGAGAGAGAGAGAGAGAGAGAGAGAGAGAGAGAG
GAGCTCTCGGAACTAAGAGAGAGAGAGAGAGAGAGAGAGAGAGAGAGAGAGAGAGAGAGAGAGAGAGAG
AAGAGGCAAGAGAGAGAGAGAGAGAGAGAGAGAGAGAGAGAGAGAGAGAGAGAGAGAGAGAGAGAGAG
CTGAGAGAGAGAGAGAGAGAGAGAGAGAGAGAGAGAGAGAGAGAGAGAGAGAGAGAGAGAGAGAGAGAG
GGAGTGAAGAGAGAGAGAGAGAGAGAGAGAGAGAGAGAGAGAGAGAGAGAGAGAGAGAGAGAGAGAGAG
CTTACTGAAGAGAGAGAGAGAGAGAGAGAGAGAGAGAGAGAGAGAGAGAGAGAGAGAGAGAGAGAGAGAG

```

Fig11: shRNA target stretches from PGC-1β sequence, mus musculus, NM_133249, adapted from Ace View: <http://www.ncbi.nlm.nih.gov/IEB/Research/Acembly/>. Blue denotes intronic parts; green denotes exonic parts.

Sequences in yellow, red and pink constitute targets of different shRNAs:

shRNA name	Sequence target
shRNA1- pU6mir backbone	Exon 11
shRNA2- pU6mir backbone	Exon 6
shRNA3- pMan backbone	Exon 9
shRNA4-pSuper backbone	Exon 6

Optimization of transfection method and transfection quantity

In order to ascertain which cell culture model should be used for cell culture transfections, HEK293t and C2C12 myoblasts were transfected with 5ug GFP-pcDNA3.1(+) vs 5ug of pcDNA3.1(+) each. Calcium chloride method revealed to be most efficient in HEK293t cells and yielded around 70% transfection efficiency (**Fig.12**).

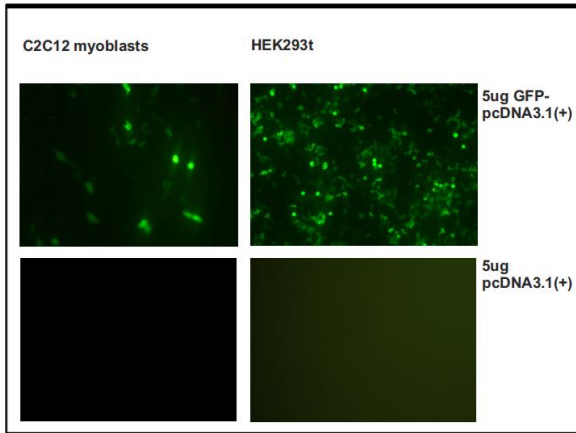


Fig.12: transfection efficiency of calcium chloride transfection method in C2C12 myoblasts and HEK293t cells Plasmids carrying pcDNA3.1(+) or GFP-pcDNA3.1(+). Fluorescence analysis of cells 48hrs posttransfection.

The next step was to determine the necessary transfection quantity of PGC-1 β plasmid: Different amounts of PGC-1 β plasmid were transfected: 5ug of PGC-1 β (data not shown) was regarded as sufficient quantity and used in further experiments (**Fig.13**).

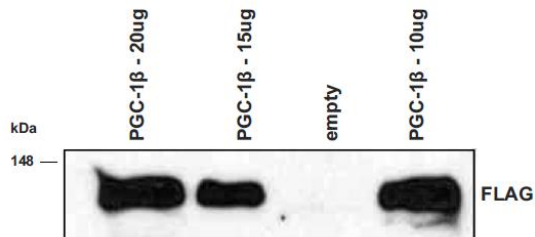


Fig.13: evaluation of necessary quantity of PGC-1 β for transfection

HEK293t cells were transfected with different quantities of PGC-1 β -pcDNA3.1(+) plasmid. Western Blot was done using anti FLAG antibody.

Testing the efficiency and specificity of shRNAs against PGC-1 β

shRNA knockdown efficiency was subsequently tested using PGC-1 β -FLAG plasmid cotransfected with different shRNA constructs. shRNA2pU6mir was found to be the most efficient knockdown construct (**Fig.14**).

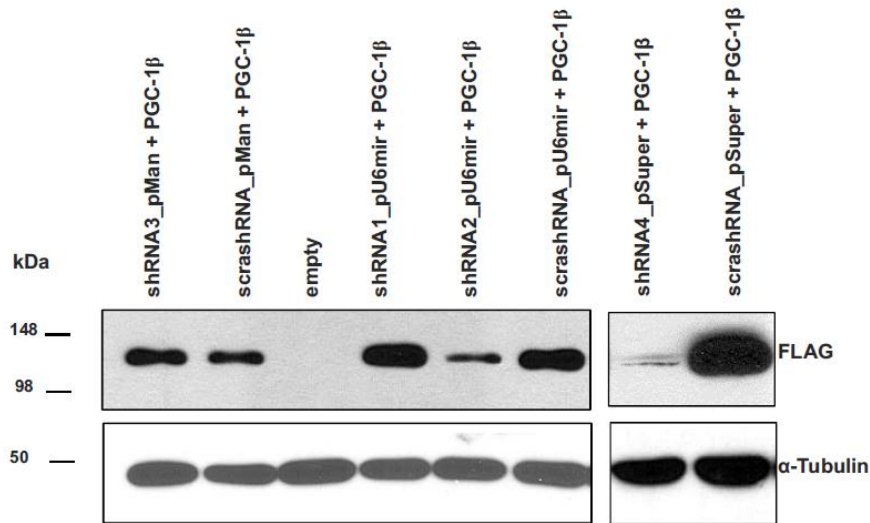


Fig.14: shRNA constructs to knock down PGC-1β

HEK293t cells were cotransfected with PGC-1β-FLAG plasmid together with shRNA constructs cloned in different plasmid backbones:pU6mir, pSuper and pMan carrying Pol III (U6), Pol III (H1) and Pol II (SV40) promoters, respectively. The molar ratio between the shRNA : PGC-1β used was 4:1. Protein extracts were harvested 48hrs post transfection. Western Blot against FLAG and α-Tubulin.

insert	backbone	promoter
shRNA1, shRNA2	pU6mir-30	Pol III (U6)
shRNA3	pMan	Pol II (SV40)
shRNA4	pSuper	Pol III (H1)
PGC-1β plasmid	pcDNA 3.1	Pol II (CMV)

Table5: shRNAs and the respective vector backbones they are embedded in

As the different shRNA constructs are embedded in different vector backbones driven by different promoters, their knockdown efficiency cannot be compared as such (**Table5**). The shRNAs that led to a visible knockdown were thus cloned into pcDNA3.1(+). In this backbone, shRNA2 and shRNA4 were found to be the most efficient constructs in knocking down PGC-1β (**Fig.15**).

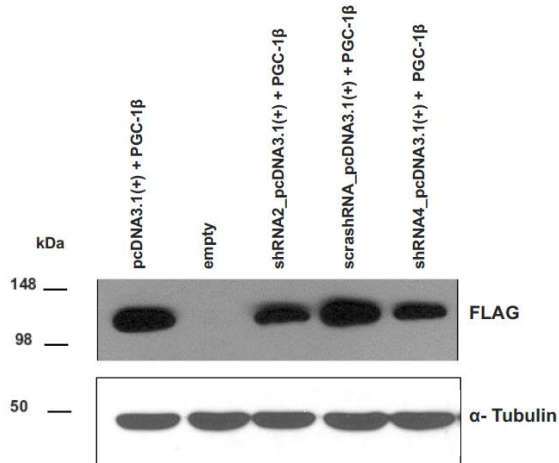


Fig.15: shRNA knockdown efficiency comparison of different constructs

shRNA2, scrashRNA and shRNA4 cloned into pcDNA3.1(+) backbone under the CMV, a Pol II promoter. HEK293t cotransfection. Western Blot against FLAG and α -Tubulin.

We next wanted to rule out possible off target effects of shRNA2 and shRNA4 against PGC-1 α . Consequently, we cotransfected shRNA2 and shRNA4 with PGC-1 α plasmid. As shRNA4 seemed to not only reduce the protein level of PGC-1 β , but concurrently the level of PGC-1 α , shRNA2 was used in further experiments. **(Fig.16)**.

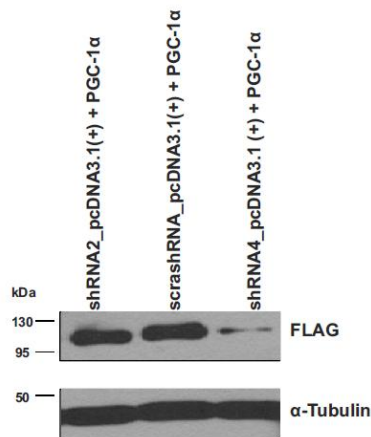
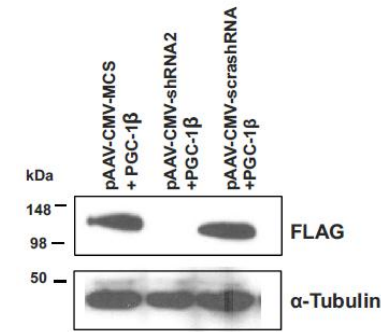


Fig.16: Testing off target effects of shRNA against PGC-1 α

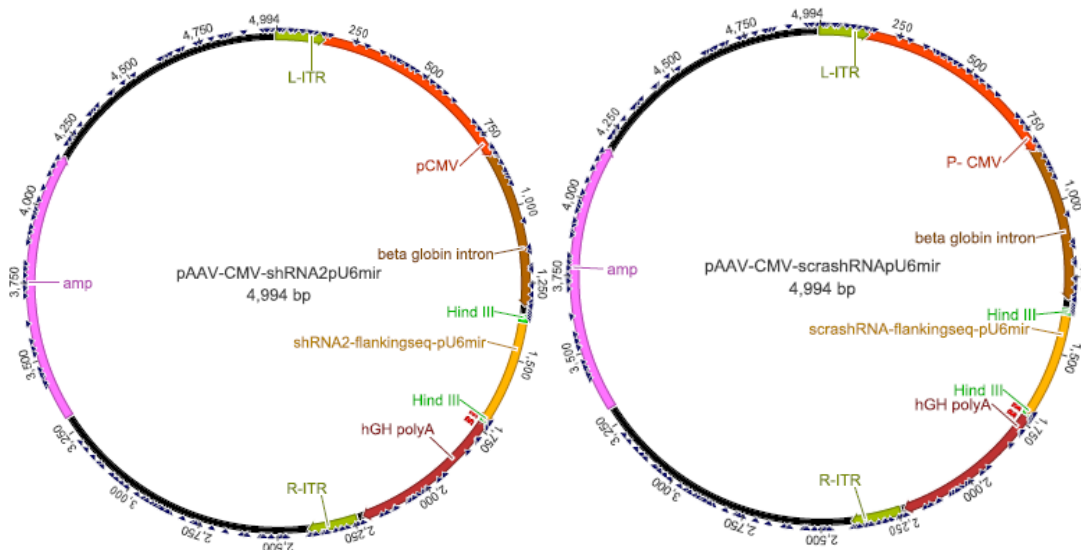
HEK293t cotransfection of the indicated shRNAs together with PGC-1 α . Western Blot against FLAG and α -tubulin.

Cloning of shRNA2 and scrashRNA into pAAV backbones

shRNA2 and scrambled shRNA were consequently cloned into the backbones that are necessary for production of AAV2: The commercially available kit *AAV helper free system* from Agilent was used. Again, the knockdown efficiency of shRNA2 was tested in this new backbone **(Fig.17)**.



(A)



(B)

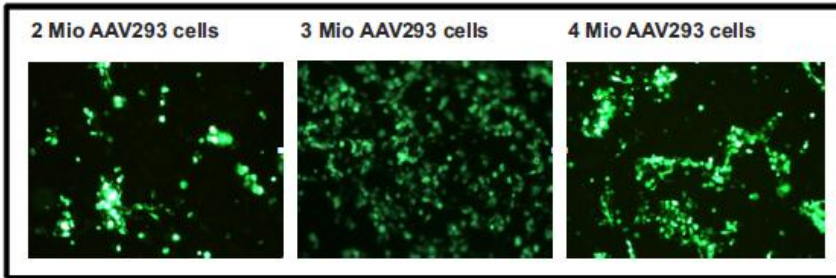
Fig.17: Cloning map of pAAV-shRNA2-CMV and pAAV-CMV-scrashRNA plasmids (B) and shRNA2 knockdown efficiency testing in pAAV-CMV-MCS backbone (A). (B): amp= ampicillin resistance, R-ITR, L-ITR= left and right internal repeats, pCMV= CMV promoter, Hind III= restriction sites, hGH polyA= human growth hormone poly A sequence.

AAV production and purification

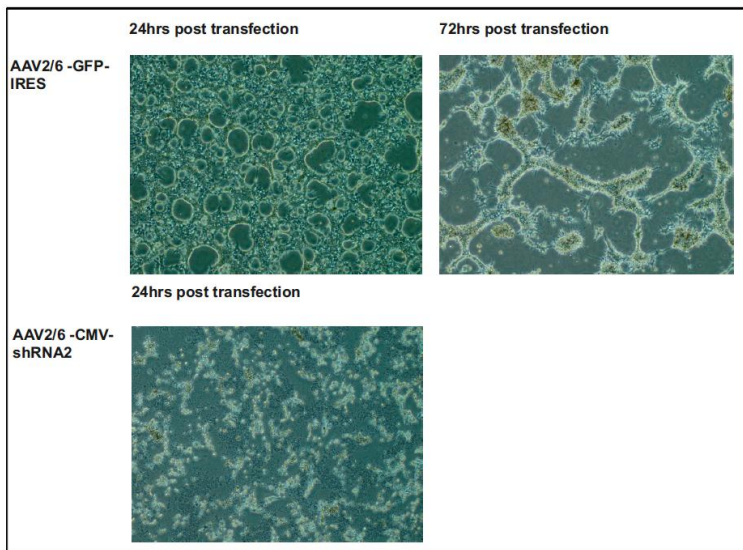
As shRNA2 also led to knockdown in the pAAV-CMV-MCS backbone, it should be used for production of AAV2 by triple transfection. To determine optimal production conditions, we also produced AAV-GFP-IRES:

First, we wanted to assess the morphological changes upon triple transfection: As indicated in the kit, cells detach and round up during AAV2 production (**Fig.18A**) when 3 Mio AAV293 cells are seeded. Second, we ascertained how many cells to seed for highest transgene (GFP) expression: Using 3 Mio cells resulted in best cell detachment and morphological changes associated with virus production. Consequently, AAV2 of shRNA2 and scrashRNA were produced using 3 Mio AAV293 cells. The morphology however did not closely resemble the morphology seen for GFP but showed clear signs of cell

death and debris formation in the case of shRNA2 production. (**Fig.18B**). Yet this phenomenon could be avoided by increasing the number of transfected cells to 4 million. Titer was then checked on the crude viral preparations using Cell Biolabs ELISA titration kit for AAV2 (**Table6**).



(A)



(B)

Fig.18: production of AAV2 using Agilent’s AAV Helper Free System:

(A) Triple transfection of 2, 3 or 4 Mio AAV293 cells with pAAV-GFP-IRES, pHelper and pCap2. Quantification via fluorescence microscopy 72hrs post transfection. (B) triple transfection of 3 Mio AAV293 cells with pAAV-GFP-IRES, pHelper and pCap2, 24hrs and 72hrs post transfection, respectively compared to triple transfection of pAAV-CMV-shRNA2 24hrs posttransfection. Fluorescence analysis.

samples	Titer [VG/ml]
shRNA2- 2 mio cells	$5.8 \cdot 10^9$
shRNA2- 3mio cells	$5.7 \cdot 10^9$
shRNA2- 4mio cells	$6.7 \cdot 10^9$
scrashRNA- 2mio cells	$5.5 \cdot 10^9$

scrashRNA- 3mio cells	4.8. 10 ⁹
scrashRNA- 4mio cells	6.5. 10 ⁹

Table6: titration of AAV2 produced with pAAV-CMV-shRNA2 and pAAV-CMV-scrashRNA constructs employing 2, 3 and 4 Mio AAV293 cells each.

Prior to testing AAV2 in vivo, in vitro experiments should be carried out to confirm the knockdown of PGC-1 β . For this purpose, C2C12 cells were used as the virus should ultimately be injected in mouse skeletal muscle. C2C12 myoblasts were employed as they are undifferentiated and thus easier to transduce than differentiated C2C12 myotubes. C2C12 myoblasts were transduced with different quantities of AAV2-GFP-IRES. 50 hrs post transduction, C2C12 myoblasts were assessed for fluorescence, which revealed that they did not take up the virus (**Fig 19A**).

As C2C12 cells constitute one of many cell culture models of skeletal muscle, other models were also tested: Differentiated C2C12 cells, Sol8 and primary mouse skeletal muscle cells were transduced with AAV2- GFP-IRES, however, none of these cellular models seemed to take up the virus (data not shown). To assess if the virus was functional at all, a cell line from another tissue was used. This cell line had already been successfully transduced with AAV2¹⁸¹. The transduction of HEK293 cells with AAV2-GFP-IRES was successful, but produced a moderate transduction of about 20% of cells only using 1000 μ l of virus (**Fig.19B**). This quantity seemed to be insufficient to check if exogenously added murine PGC-1 β expression is downregulated by the AAV2-CMV-shRNA2.

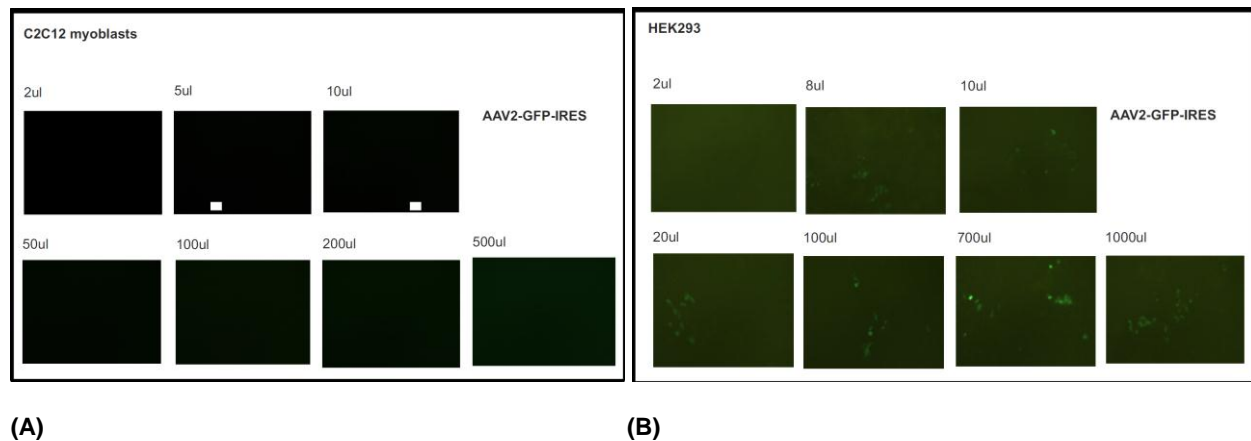


Fig.19: transduction of C2C12 myoblasts (A) and HEK293 cells (B) with different quantities of crude preparations of AAV2-GFP-IRES

Consequently, in order to increase the transduction efficiency of HEK293 cells, AAV2 was subjected to purification using *Fast Trap Adeno Associated Virus (AAV) Purification and Concentration Kit* from Millipore which is based on cation-exchange chromatography. Purification yields around 1ml of functional virus. For this reason, AAV2 was not titrated after this procedure but directly used for transducing cells: HEK293 and C2C12 cells were transduced with different amounts of AAV2-GFP-IRES. Both cell lines took

up the virus this time, with HEK293 taking up more than C2C12 myoblasts (**Fig.20**). The transduction efficiency, however, amounts to only about 30% in HEK293.

Therefore, AAV2 should be tested directly *in vivo* without prior *in vitro* experiments.

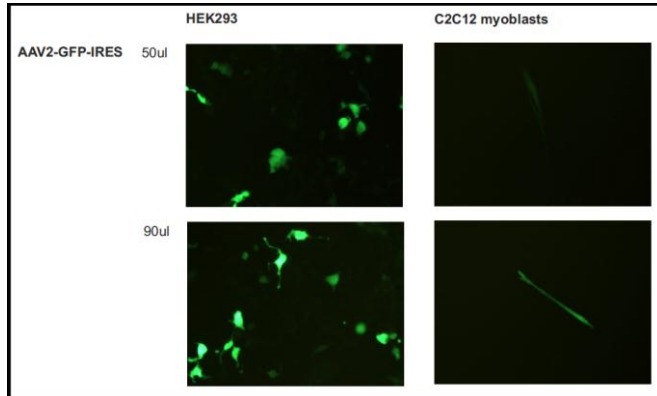


Fig.20: Transduction of HEK293 and C2C12 myoblasts with different quantities of purified AAV2-GFP-IRES. Fluorescence microscopy 50hrs posttransduction.

AAV2/6 production, purification, titration and injection into mouse tibialis anterior (TA)

AAV2/6 was produced with the AAV production core facility in the *Institut de Recherche Thérapeutique, Université de Nantes, INSERM U649*.

Viral titer was determined at INSERM U649 using two strategies: First, mouse embryonic fibroblasts were transduced and the degree of infection used as a means to quantify functional virus. Second, capsid 6 presence was quantified using enzyme linked immunosorbent assay (ELISA) technique, as a means to quantify the number of virions. As infection efficiency is tissue specific, we used the titer generated with ELISA as guidance.

We then wanted to address three major questions:

1. How much virus has to be injected into mouse TA in order to achieve considerable transgene expression?
2. How long do we have to wait for efficient virus transduction?
3. How long remains transgene expression on a stable level?
4. Which is the most favorable route of delivery: local or systemic injection?

AAV2/6- Route of delivery and virus quantity

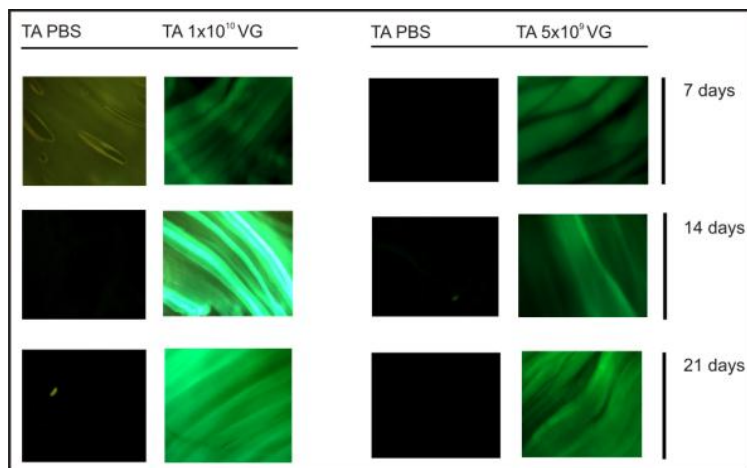
To address the first and second question, we locally injected mouse TA with 5×10^9 and 1×10^{10} vector genomes (VG) of AAV2/6 carrying the GFP-IRES construct as recommended by Paul Gregorevic, *Baker*

IDI: AAV2/6-GFP-IRES was injected into the right leg and phosphate buffered saline (PBS) into the left leg as control setting. We then waited for 7, 14 and 21 days, respectively before extracting the TA. Fluorescence microscopy revealed that GFP expression was most prominent at 14 or 21 days postinjection, respectively. Both quantities, 5×10^9 and 1×10^{10} VG worked for efficient transduction (**Fig.21A**).

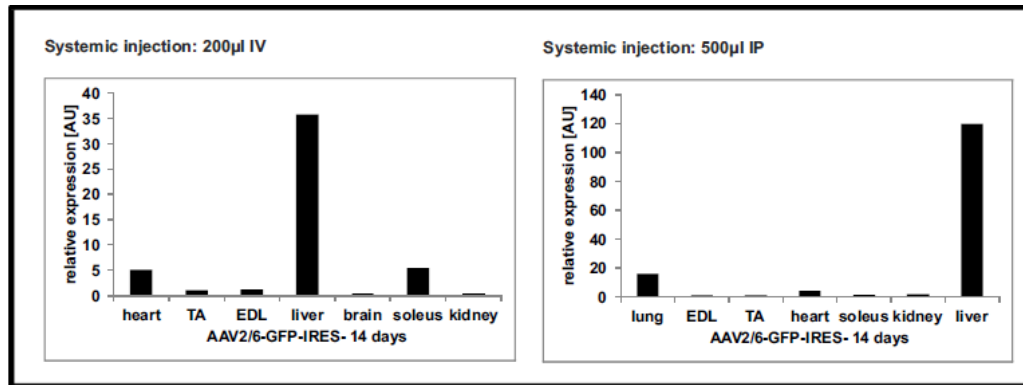
To carry out systemic tests on the injected animals (glucose tolerance test, insulin tolerance test, exercise performance test) we needed to know how long transgene expression remains on a stable level (third question). For this purpose, we would have had to do a timecourse sacrificing mice not only 7, 14 and 21 days postinjection but until at least 2 months postinjection as AAV expression can persist for several months. In fact, according to Zincarelli, expression of both AAV2 and AAV6 seems to stabilize around day 50 to day 80 which would thus constitute the ideal timeframe for experiments^{174,182}.

However, injection timecourses would only make sense if the construct of interest (shRNA2, scrashRNA) is used for this purpose, because due to the different properties of GFP, its detection can only be used as a proof of principle. As the amount of available AAV2/6-CMV-shRNA2 as well as of AAV2/6-CMV-scrashRNA was limited, we decided to only extend our expression test to 21 days postinjection, as this was the presumed peak of AAV6 expression (see also **Fig.21A**)^{174,182}.

Systemic injection was also tested as route of delivery. For this purpose, 2×10^{10} VG (=200 μ l) were injected into mouse tail vein, IV (=intravenous injection). AAV2/6 expression was strongest in liver, heart and soleus, in line with Zincarelli's observations¹²⁰. Intraperitoneal (=IP) injection was tested as another route for systemic delivery: 5×10^{10} VG (= 500 μ l) of AAV2/6-GFP-IRES were injected. As seen in the IV injection, expression was most pronounced in liver and heart as well as in lung. Skeletal muscle displayed even less expression of GFP (**Fig.21B**). The quantities used for IV and IP injections are less than are generally used for this purpose; however, we could not concentrate the viral titer any further^{174,182}.



(A)



(B)

Fig.21: Local, TA targeted (A) and systemic (B) injections of AAV2/6-GFP-IRES into mouse

Injected quantities were 1×10^8 VG, 5×10^{10} VG (A), 6×10^{10} VG (IV) and 1.6×10^{11} VG (IP) (B), respectively. (A) shows fluorescence microscopy after 7, 14 and 21 days, respectively. (B) shows semi-quantitative real time PCR measurements of different organs compared in their expression of GFP 14 days postinjection. IV= intravenously, tail vein injected. IP= intraperitoneally injected. One mouse was used per condition. 18SrRNA was used as housekeeping gene (HKG).

Circadian expression of PGC-1 α and PGC-1 β in skeletal muscle

PGC-1 α and PGC-1 β have long been known to be expressed in a circadian fashion in liver and skeletal muscle⁸¹. In the latter, both are expressed to a similar degree at around 1pm.

We wanted to ascertain the degree of circadian expression of both coactivators in our setting to find a timepoint when both are expressed at a rather high level: This should help us to determine the timepoint when TA should be extracted in order to gain consistent results.

Consequently, we sacrificed two C57BL/6 WT mice at 3 different timepoints and checked the coactivators' expression levels in TA: PGC-1 β levels remained rather stable throughout the day whereas PGC-1 α expression was increased from 1pm to 4.30pm (Fig.22). We thus decided to extract TA in our future experiments starting around 9am as expression difference between PGC-1 α and PGC-1 β is smallest. Furthermore, by administering functional virus into the right leg and control virus into the left leg, we aimed at decreasing intra-individual expression differences. By sacrificing animals at a similar timepoint (9am), we further aimed at decreasing inter-individual expression differences due to circadian rhythm.

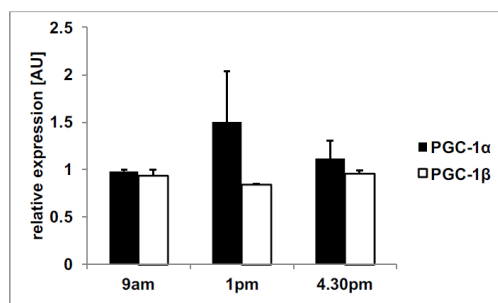


Fig.22: mRNA expression levels of PGC-1 α and PGC-1 β throughout the day

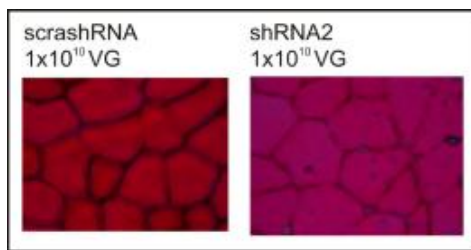
C57 BL/6 mice were sacrificed at different timepoints and mRNA levels of PGC-1 α and PGC-1 β were measured via semi quantitative real time PCR. n=2; +SEM. 18SrRNA used as HKG.

AAV2/6- effects on inflammatory response

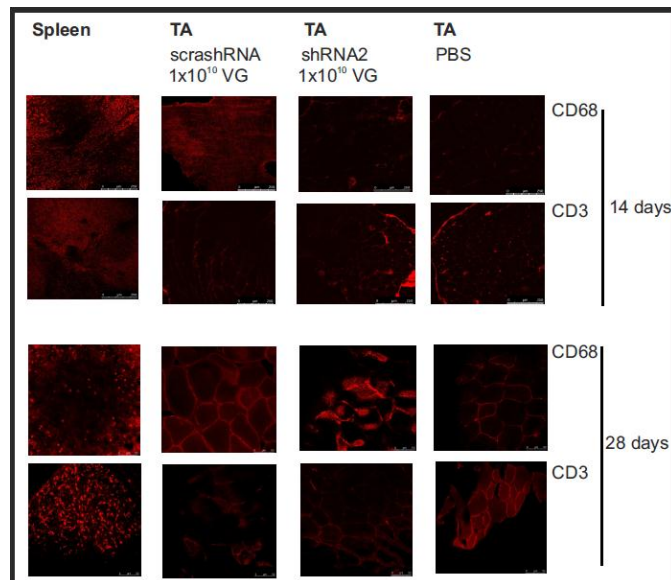
We next asked the question if AAV2/6 delivery fosters inflammatory response. First, immune response due to AAV is tissue specific¹⁸³. Second, it is increased in skeletal muscle that is already injured like in mdx mice which also display lower transgene expression originating from the virus¹⁸⁴.

We thus checked for signs of inflammation using WT mouse spleen as positive control setting. Staining of CD68 (macrophage marker) and CD3 (T cell marker) in TA showed that the difference between virus injected and PBS injected TA was not considerable (**Fig.23B**).

Hematoxylin & eosin staining should reveal if there is muscle damage via yielding centrally localized nuclei. We did not detect these in TA that was treated with either scrashRNA or shRNA2 (**Fig.23A**).



(A)



(B)

Fig.23: Evaluation of inflammatory and target gene effects of AAV2/6 mouse TA local injections:

(A) Immunohistochemistry: Hematoxylin & Eosin staining of mouse TA 28days postinjection with 5x10E9 and 1x10E10 VG of AAV2/6-CMV-shRNA2-CMV or AAV2/6-CMV-scrashRNA. (B) Immunohistochemistry: CD68 and CD3 of mouse spleen and TA, 14 and 28 days postinjection of AAV2/6-CMV-shRNA2, AAV2/6-CMV-scrashRNA or PBS injection into mouse TA.

AAV2/6- knockdown of PGC-1 β - mRNA level

As small scale testing of inflammatory response owing to injection or virus delivery proved negative, we proceeded to AAV2/6-CMV-shRNA2 and AAV2/6-CMV-scrashRNA injections into TA muscle of C57 BL/6 WT mice: 28 days postinjection, mice were sacrificed and checked for gene expression levels of PGC-1 α , PGC-1 β and their downstream target genes. Whereas PGC-1 α levels were not changed, PGC-1 β as well as its target genes Cox5b, Err α , Cyts and Mcad (Acyl-CoA dehydrogenase) were significantly reduced (Fig.24).

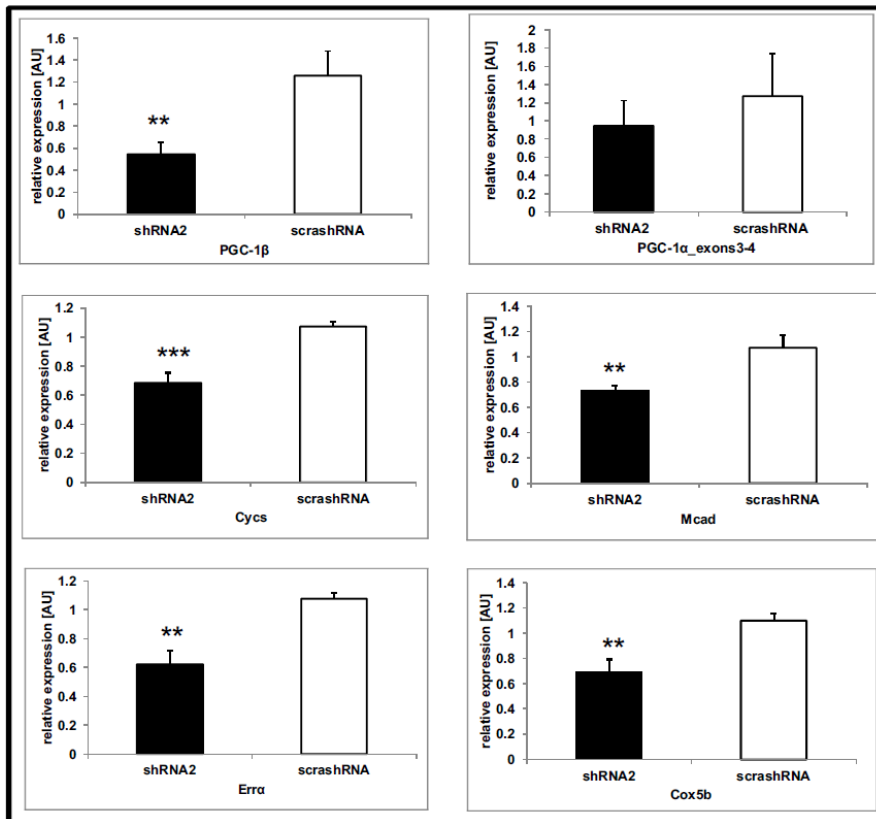


Fig.24: Evaluation of PGC-1 β and target gene knockdown of AAV2/6 mouse TA local injections

AAV2/6 injections into mouse TA using 1×10^6 VG AAV2/6-CMV-shRNA2 or AAV2/6-CMV-scrashRNA as control. Effect on gene expression levels of PGC-1 α , PGC-1 β and its target genes measured via semi-quantitative real time PCR. TA extraction was done 21 days postinjection. n=6; +SEM; paired, 2-tailed T test was used to calculate p value. $p \leq 0.05 = *$; $p \leq 0.01 = **$; $p \leq 0.001 = ***$. 18SrRNA was used as HKG.

AAV2/6- shRNA2- GFP construct

The construct used so far has been AAV2/6-shRNA2-GFP. The *AAV Helper Free System Manual* however indicates that there is not only a maximum insert size of 3kB but also a minimum insert size of 1kB in order to guarantee efficient viral packaging. We thus added a “DNA stuffer sequence” of about 700BP in the form of GFP. We thus hoped to avoid a possible loss of function of the shRNA due to

inefficient packaging. Even though, we did hardly see any difference in shRNA efficiency comparing the AAV2/6-shRNA2 and AAV2/6-shRNA2-GFP constructs in vivo (**Fig.25**).

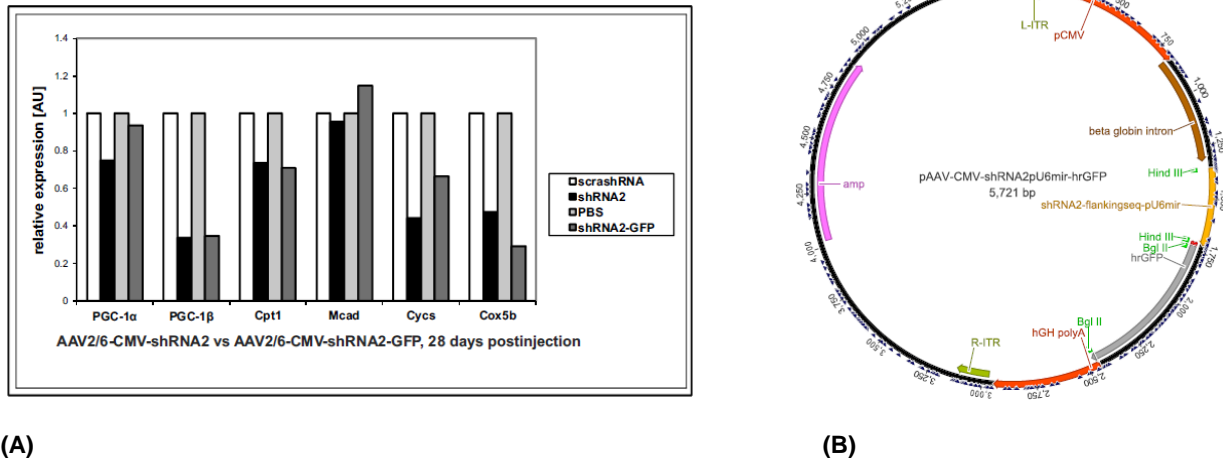


Fig.25. AAV2/6-CMV-shRNA2 vs AAV2/6-CMV-shRNA2-GFP

(A) AAV2/6 injections into mouse TA using 1×10^6 VG AAV2/6-CMV-shRNA2 and AAV2/6-CMV-shRNA2-GFP with AAV2/6-CMV-scrashRNA and PBS as control settings. Effect on gene expression levels of PGC-1 α , PGC-1 β and its target genes measured via semi-quantitative real time PCR. TA extraction was done 28 days postinjection. n=1. 18SrRNA was used as HKG. **(B)** cloning map of AAV2/6-CMV-shRNA2-GFP construct: Bgl II = Bgl II restriction sites

AAV2/6- knockdown of PGC-1 β - protein level

We then wanted to see if this downregulation on the mRNA level translated into diminished protein levels of PGC-1 β . Thus far, no commercially available antibody against PGC-1 β that worked in tissue had been characterized. We thus tested a range of PGC-1 antibodies:

The PGC-1 antibody from Chemicon (Millipore) was found to be the most reliable one in detecting overexpressed PGC-1 α and PGC-1 β in cell culture extracts (**Fig.26**).

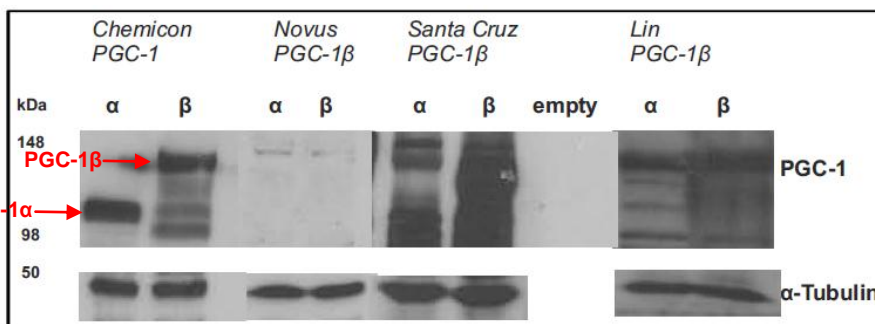


Fig.26: PGC-1/ PGC-1 β antibody test: *in vitro* samples

HEK293 cells were transfected with 5ug of PGC-1 α (α) or PGC-1 β (β) plasmids. 48hrs afterward, protein extract was prepared. 80ug of protein loaded on Western Blot. PGC-1 α : 90kDa, PGC1 β : 110kDa

We subsequently tried to ascertain how the PGC-1 antibody from Chemicon behaved when using samples from tissue: The samples that contained overexpressed PGC-1 α and PGC-1 β were detected at the right sizes; the PGC-1 antibody however did not detect either PGC-1 in skeletal muscle: TA, gastrocnemius, soleus and extensor digitorum longus (EDL) did not yield any band that seemed to be specific (**Fig.27**). For this reason, we did not try to further detect shRNA2 mediated knockdown of PGC-1 β via AAV2/6 on the protein level.

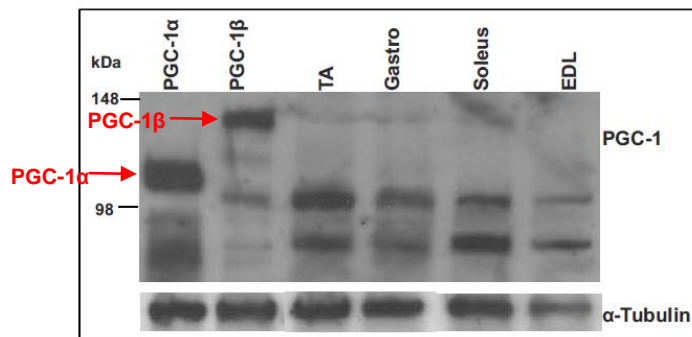


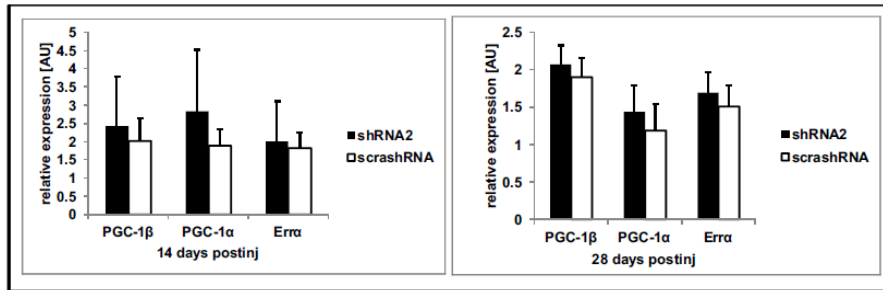
Fig.27: PGC-1/ PGC-1 β antibody test: *in vivo* samples

lanes 1-2: HEK293 cells were transfected with 5ug of PGC-1 α or PGC-1 β plasmids. 48hrs afterward, protein extract was prepared. Lanes 3-6: Skeletal muscle tissue from 5 month old C57 BL/6 WT mice: TA, gastrocnemius, soleus, EDL. 80ug of protein loaded on Western Blot.

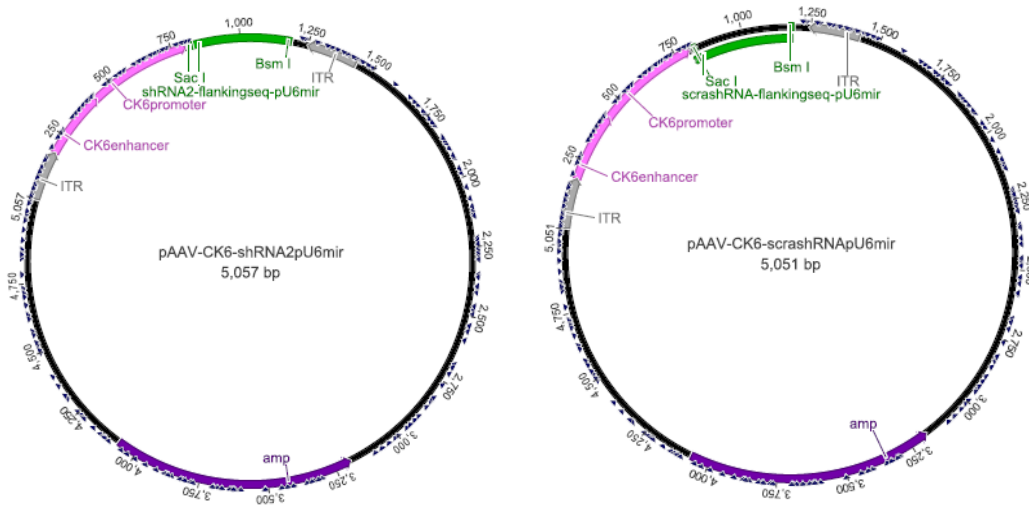
AAV2/6- skeletal muscle specific promoter

Thus far in this project, injection of shRNA to knock down PGC-1 β has only been done locally, in TA muscle. Systemic injection however allows for measurement of systemic parameters that change upon reduction of PGC-1 β : We therefore aimed at constructing a virus carrying a shRNA driven by a skeletal muscle specific promoter suitable for systemic injection.

We cloned the shRNA2/ scashRNA constructs plus flanking sequences into the pAAV plasmid containing the skeletal muscle specific creatine kinase6 (CK6) promoter, respectively and tested their potency directly *in vivo*: Prior to the planned systemic injection, we wanted to test promoter strength via local injection: TA was injected with AA2/6-shRNA2/ scashRNA- CK6 at 1×10^{10} VG: 14 and 28 days postinjection, TA was isolated and analyzed for PGC-1 α , PGC-1 β and its target gene Err α . Neither of them was changed significantly. This result implies that promoter strength of this tissue specific promoter may not be strong enough for driving shRNA expression (**Fig.28**).



(A)



(B)

Fig.28: AAV2/6-shRNA2 or scrashRNA-CK6 injection into mouse TA

(A) Gene expression levels of PGC-1α, PGC-1β and its target gene Erra were measured by semi quantitative real time PCR 14 and 28 days postinjection, respectively. 18SrRNA was used as HKG. n=3; +SEM. (B) cloning map of pAAV-CK6-shRNA2 and pAAV-CK6-scrashRNA. Sac I and Bsm I were the restriction enzymes used.

AAV2/6- effects of PGC-1β knockdown on fiber type distribution

With systemic injection being hampered by promoter properties, we still wanted to know if the decrease in PGC-1β expression levels seen after local TA injections using AAV2/6-CMV-shRNA2 has implications on fiber type composition: We thus looked at fiber type composition via expression levels: Given a significant reduction of PGC-1β levels, we would expect a decrease in IIX fibers.

There seemed to be a reduced expression in Mhcl, Ila, I Ib and I Ix fibers in the AAV2/6-CMV-shRNA2 injected TA. However, none of these reductions proved to be significant (Fig.29).

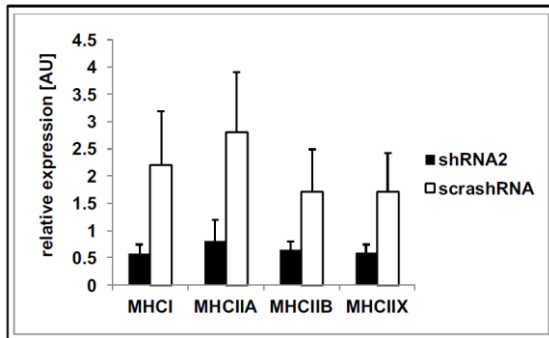


Fig.29: Fiber type expression pattern in TA of AAV2/6-CMV-shRNA2-CMV or AAV2/6-CMV-scrashRNA injected mice

Measurement of Mhcl, Ila; Iib and Iix by semi-quantitative real time PCR. 4 weeks postinjection. 18SrRNA was used as HKG. n=5; +SEM

5.5. Discussion

In this project, we used AAV to deliver an RNAi construct against the coactivator PGC-1 β into mouse skeletal muscle: We decided upon AAV2 pseudotyped with capsid 6 (AAV2/6) due to its low immunogenicity in the host and skeletal muscle specific expression of the construct.

Regarding the construct employed, we strived to develop different RNAi molecules: one conventional shRNA (pSuper backbone) and two pri-miRNAs (pU6mir and pMan backbones), the two latter of which integrate into the silencing pathway higher upstream to enhance knockdown potency and limit toxicity¹⁸⁵.

The AAV2/6 construct was then injected into mouse via systemic (intraperitoneal, intravenous) as well as local (intramuscular) injection. We also compared the use of two Polymerase II promoters, a ubiquitously expressed (CMV) and skeletal muscle specific (CK6) promoter to restrict shRNA expression to skeletal muscle.

Finally, we studied the effect of the knockdown on the morphological (H&E staining, inflammatory markers CD3 and CD68 staining) and gene expression level (semi-quantitative real time PCR of target genes).

Design of shRNAs against PGC-1 β

As mentioned above, there is a plethora of different shRNA design tools and strategies available the comparison of which would constitute a project of its own. In our design rationale, however, we had to respect *in vivo* requirements and applicability: It would have been tempting to use a wide array of different siRNA molecules to rapidly check knockdown efficiency prior to the more time consuming cloning steps. Yet, as our shRNAs and pri-miRNAs respect specific design criteria within the target sequence (exchange or removal of nucleotides), their effect cannot be compared to classical siRNA. We finally achieved a knockdown level of about 60% *in vitro* employing shRNA2 driven by the CMV promoter (**Fig.15**). Comparing the different shRNAs in their knockdown potency seemed all the more important as shRNA4 produced the strongest knockdown. If all constructs were driven by the same promoter, however, it fared as well as shRNA2 and much worse regarding the off target effects towards PGC-1 α .

Testing the efficiency and specificity of shRNAs against PGC-1 β

The testing of efficiency and specificity of the different shRNAs (1-4) against PGC-1 β was evaluated exclusively on the protein level (**Fig.14**): It would have been interesting, though, to prove the knockdown effects also on the gene expression level via semi-quantitative real time PCR. We thus designed specific primers to detect the knockdown of PGC-1 β ; however we did not see consistent decrease in the mRNA levels of PGC-1 β of shRNA treated cells (unpublished data). shRNAs lead to mRNA degradation as well as translational repression which may render the detection of decreased mRNA levels difficult¹⁵⁷. However, recent evidence indicates that the predominant way of shRNA action is via mRNA degradation¹⁸⁶.

AAV transduction

Although C2C12 myoblasts have already been successfully transduced with AAV2¹⁸⁷, our transduction approach was less successful (**Fig.19**): Other skeletal muscle cell culture models used like Sol8 or primary cells also could not be transduced. Only HEK293 cells took up the virus to a certain extent. Purification increased transduction efficiency for both C2C12 myoblasts and HEK293 cells; however it was still modest (**Fig.20**). A more potent transduction ratio would have necessitated upscaling of viral production and reliable titration of functional virus. We thus decided to have AAV2 produced with a company specialized in AAV production and purification (*INSERM U649, Institut de Recherche Thérapeutique, Nantes*). Among the three rounds of viral production that they did, one delivered rather low titers owing to increased cell lysis and degradation during AAV production: We thus concluded that shRNA toxicity may be responsible for these effects witnessed by two independent production processes.

shRNA and AAV toxicity

Among AV, LV and AAV, the latter is known for inciting least immunogenicity¹⁸⁸.

shRNA toxicity effects can emanate from three factors: first, the viral vector used, second, the hairpin used or third, the target sequence responsible for silencing:

Toxicity associated with hairpin structure may have been an issue, although embedding the shRNA into the pri-miRNA structure as well as the polymerase II promoter used should be able to mitigate this noxious effect^{159,185}. The fact that the increase in AAV293 producing cells for AAV production attenuated the toxic response may be indicative of a dose dependent effect of shRNA toxicity. Consequently, we were concerned that this *in vitro* phenomenon could recur *in vivo* and decided to use the lowest titer possible on a small number of animals for the first *in vivo* experiments.

AAV delivery

In vivo viral injections require optimization on a myriad of different levels: quantity, route of delivery, incubation time to identify time of peak expression and the therapeutic window when viral titer remains constant over a given time. The latter point is especially important if one considers doing systemic tests after viral delivery.

We soon realized that these variables not only interrelate and thus cannot be answered satisfactorily, but also that it would require much more virus to do serious time course studies to pinpoint maximum expression levels. With 1-3 animals injected per condition, no reliable statement about the knockdown level of PGC-1 β and its target genes could be made.

Systemic injection would have been the delivery route of choice. But owing to the insufficient titer levels for this procedure, we could not pursue this strategy further. Even companies specialized in AAV production

and purification do not seem to have solved this problem of concentrating AAV further (oral communication, Françoise Balter, *INSERM U649, Institut de Recherche Thérapeutique, Nantes*).

Promoter usage

Systemic injection can be considered if a tissue specific AAV serotype, as the AAV6 that was used for pseudotyping in our case is available. Another strategy would be to use a tissue specific promoter as the CK6 promoter in our case. Prior cell culture testing of such a promoter is a cost and time saving procedure. However, there is a major drawback regarding the testing of skeletal muscle specific promoters in cell culture models: Many growth factors, developmental and physiological stimuli cannot be mimicked in cell culture conditions. One study points out the difference in skeletal muscle promoter efficiency *in vitro* versus *in vivo* systems¹⁸⁹. We thus decided to test our CK6 driven construct immediately *in vivo*. Unfortunately, the CK6 promoter revealed to be less efficient than projected and we exclusively employed the CMV promoter for our studies.

PGC-1 β knockdown and PGC-1 α KO: global versus local

We initially strived for a model that would permit PGC-1 β knockdown in a skeletal muscle specific PGC-1 α deficiency mouse model. Unfortunately, due to breeding problems, we could not establish such a model during the course of this PhD project.

A project oriented towards a similar goal was conceived and published by Zechner et al recently¹⁵⁰: Ablation of both PGC-1 isoforms compared to the absence/ reduction of either PGC-1 α or PGC-1 β should shed light on the overlapping/ common targets of both isoforms as well as on the specific role of PGC-1 β in skeletal muscle: A skeletal muscle specific ablation of PGC-1 β was combined with a global ablation of PGC-1 α and described as a model of double skeletal muscle specific knockout: These animals show no signs of altered insulin sensitivity both on chow and HFD. This result should be viewed with caution though: PGC-1 α global knockout mice have different plasma glucose levels than skeletal muscle specific PGC-1 α knockout mice, which is probably due to organ cross talk between the pancreas and skeletal muscle¹³.

Regarding fiber type composition, Zechner's double KO animals display an increase in type I fibers; the number of IIX fibers that are typically induced by PGC-1 β though does not change. In this case, the global PGC-1 α KO mice also behave differently from the skeletal muscle specific PGC-1 α KO animals: The first do not undergo fiber type switch to type I fibers, whereas the latter do.

Consequently, for PGC-1 α and most likely also PGC-1 β , the global knockout model cannot substitute for a tissue specific knockout model¹²¹.

The importance of PGC-1 β in glucose homeostasis was underlined by another article that appeared recently: Wright et al overexpressed PGC-1 β in skeletal muscle: On HFD, the treated mice displayed ameliorated insulin sensitivity along with decreased levels of long-chain acyl-CoAs (LCACoAs) and increased antioxidant defenses¹⁴⁸.

Technical prospects

Despite construct design and delivery optimization efforts, we ultimately only achieved a knockdown of about 60% for PGC-1 β .

Optimizing vehicle (AAV) and construct (shRNA) structure may help increase KD efficiency:

Vehicle optimization

We could have increased the amount of functional virus delivered to 5x10E10 or 1x10E11 VG via repeated injections: Even though, this strategy should be avoided: A subset of the human population shares antibodies against AAV2 which may neutralize AAV2 that is subsequently injected¹⁹⁰. Although a similar phenomenon has not been described for mice, this possibility should not be discarded. As possible AAV antibodies are directed against the capsid, re-administration of a different serotype would help avoid this problem. However, capsid exchange also changes tissue tropism which would enhance uptake in tissues other than muscle.

The first AAV constructs that were developed exploited the single strand usage of the AAV genome. This single strand has to be replicated into a double strand DNA molecule prior to being transcribed by the host polymerase, explaining why the onset of transcript expression from AAV takes so long. A more recent development in AAV design circumvents this time lag: self- complementary AAV (scAAV) contains an ITR that links the sense target sequence to its complementary sequence. scAAVs have 10 to 100 fold higher transduction ratios and a faster onset of expression than the classical AAV¹⁹¹. We thus could have employed this strategy to increase shRNA expression.

Another avenue for enhancing expression of the transgene would be to coinfect TA muscle with the AAV2/6 carrying the shRNA together with an AAV containing enhancer elements for the CMV promoter used in AAV2/6. Through the interaction of enhancer and promoter, an increased transcription level can be achieved¹⁹².

These two approaches seem to be attractive strategies at first glance. Still, an increase in shRNA expression is associated with increased toxicity hazard. Improving the shRNA sequence itself may thus prove to be a better alternative.

Construct optimization

One approach to enhance RNAi efficiency is to express several miRNA hairpins¹⁹³ by stacking together several shRNA molecules on one single hairpin (extended shRNA= e-shRNA molecules with 43 BPs in length¹⁶²). Double long hairpin RNAs (dlhRNA) exploit a similar principle by which two e-shRNAs are combined with each other, yielding four siRNAs upon processing¹⁹⁴.

There are thus ample options for improvement on both the construct and the delivery level. Finding the best solution for our specific case would well have been more time consuming than generating a mouse harboring a tetracycline/ tamoxifen inducible PGC-1 β KO system. Furthermore, it is less cost intense to breed a sufficient amount of mice for experiments when using the PGC-1 β KO system.

It will still take some time until AAV and shRNA technology will have identified standard, hands-on and cost effective procedures for generating genetically modified animals.

5.6. Conclusions

Project2 demonstrated that skeletal muscle specific reduction of PGC-1 β leads to reduced expression of genes implicated in OXPHOS (e.g. Cox5b, Mcad, Cysc, Err α). Although the reduction in PGC-1 β did not change skeletal muscle myosin heavy chain fiber types, both PGC-1 α and PGC-1 β thus seem to be important for skeletal muscle energy homeostasis. It is thus also worth considering to not only modulate PGC-1 α levels for therapeutic purposes (prevention of atrophy), but also PGC-1 β levels.

6. Perspectives

The projects presented in this PhD thesis may seem at best remotely associated with each other via the studied coactivator PGC-1. However, they both converge in some regards:

Global vs local, ablation vs reduction

Project1 was based upon a global KO model, whereas in project2 a tissue specific KD should be generated:

Although the global PGC-1 α KO mice display a clear phenotype only in the challenged state^{125,112}, we already observed some deviations from the WT mice in the basal condition: We were faced with diminished survival rates of homozygous PGC-1 α KO mice offspring which may have been caused by an apparent dysregulation of body temperature. Also, among the surviving KO animals many mice failed to achieve WT bodyweight and size.

For this purpose, it would have been advantageous to generate retina specific PGC-1 α KO mice in project1. Owing to the great number of different retinal cell types, however, such an undertaking is hardly feasible.

In project2, however, ablation of PGC-1 β was localized to one single skeletal muscle, the TA: Unfortunately, the attempt to generate a skeletal muscle specific PGC-1 β KD mouse was unsuccessful as the CK6 promoter did not work in our hands *in vivo*. This is why we probably also did not witness any change in fiber type composition in knocking down PGC-1 β as can be seen with PGC-1 β overexpression¹⁴⁰.

Lipid metabolism

Elucidating the function of PGC-1 β in skeletal muscle was a main motivation in project2, as its role is best studied in liver to date. Lipid metabolism is also essential in retina: Poly – unsaturated fatty acids (PUFAs) are used for building up neurons' cell membranes and have anti apoptotic properties¹⁹⁵. Lipoprotein structures are responsible for taking up cholesterol into the retina¹⁹⁶. It would still be interesting to know if ablation of PGC-1 β in retina has effects on retinal health.

Compensatory effects

An interesting observation in both projects is the possible compensatory effect of either PGC-1 α or PGC-1 β in project2 or project1, respectively: It would not have been surprising if the global ablation of PGC-1 α

had led to increase in PGC-1 β in the light stress condition, which was not the case. Rather, both PGC-1s were downregulated in this setting.

In skeletal muscle, PGC-1 β reduction was quite small and thus compensatory increase of PGC-1 α rather unlikely: In fact, PGC-1 α was not changed significantly in this setting.

7. References

1. Puigserver, P. et al. A cold-inducible coactivator of nuclear receptors linked to adaptive thermogenesis. *Cell* **92**, 829-39(1998).
2. Lin, J. et al. Peroxisome proliferator-activated receptor gamma coactivator 1beta (PGC-1beta), a novel PGC-1-related transcription coactivator associated with host cell factor. *The Journal of biological chemistry* **277**, 1645-8(2002).
3. Andersson, U. & Scarpulla, R.C. PGC-1-Related Coactivator , a Novel , Serum-Inducible Coactivator of Nuclear Respiratory Factor 1-Dependent Transcription in Mammalian Cells. *Molecular and cellular biology* **21**, 3738-3749(2001).
4. Wu, Z. et al. Mechanisms controlling mitochondrial biogenesis and respiration through the thermogenic coactivator PGC-1. *Cell* **98**, 115-24(1999).
5. Michael, L.F. et al. Restoration of insulin-sensitive glucose transporter (GLUT4) gene expression in muscle cells by the transcriptional coactivator PGC-1. *Proceedings of the National Academy of Sciences of the United States of America* **98**, 3820-5(2001).
6. Yoon, J.C. et al. Control of hepatic gluconeogenesis through the transcriptional coactivator PGC-1. *Nature* **413**, 131-8(2001).
7. Mootha, V.K. et al. PGC-1alpha-responsive genes involved in oxidative phosphorylation are coordinately downregulated in human diabetes. *Nature genetics* **34**, 267-73(2003).
8. Mootha, V.K. et al. Err alpha and Gabpa/b specify PGC-1 alpha -dependent oxidative phosphorylation gene expression that is altered in diabetic muscle. *PNAS* **101**, 1-6(2004).
9. Vega, R.B., Huss, J.M. & Kelly, D.P. The coactivator PGC-1 cooperates with peroxisome proliferator-activated receptor alpha in transcriptional control of nuclear genes encoding mitochondrial fatty acid oxidation enzymes. *Molecular and cellular biology* **20**, 1868-76(2000).
10. Baar, K. et al. Adaptations of skeletal muscle to exercise: rapid increase in the transcriptional coactivator PGC-1. *The FASEB journal : official publication of the Federation of American Societies for Experimental Biology* **16**, 1879-86(2002).
11. Herzig, S. et al. CREB regulates hepatic gluconeogenesis through the coactivator PGC-1. *Nature* **413**, 179-83(2001).
12. Lehman, J.J. et al. Peroxisome proliferator-activated receptor gamma coactivator-1 promotes cardiac mitochondrial biogenesis. *The Journal of clinical investigation* **106**, 847-56(2000).

13. Handschin, C. et al. Abnormal glucose homeostasis in skeletal muscle – specific PGC-1 α knockout mice reveals skeletal muscle – pancreatic β cell crosstalk. **117**, 3463-3474(2007).
14. Lamb, T.D. & Pugh, E.N. Phototransduction, dark adaptation, and rhodopsin regeneration the proctor lecture. *Investigative ophthalmology & visual science* **47**, 5137-52(2006).
15. Jones, K.A. & Kadonaga, J.T. Exploring the transcription – chromatin interface. *Genes & Development* **14**, 1992-1996(2000).
16. Glass, C.K. & Rosenfeld, M.G. The coregulator exchange in transcriptional functions of nuclear receptors. *Genes & Development* **14**, 121-141(2000).
17. McKenna, N.J. & Malley, B.W.O. Combinatorial Control of Gene Expression by Nuclear Receptors and Coregulators. *Cell* **108**, 465-474(2002).
18. Handschin, C. & Spiegelman, B.M. Peroxisome proliferator-activated receptor gamma coactivator 1 coactivators, energy homeostasis, and metabolism. *Endocrine reviews* **27**, 728-35(2006).
19. Lin, J., Handschin, C. & Spiegelman, B.M. Metabolic control through the PGC-1 family of transcription coactivators. *Cell metabolism* **1**, 361-70(2005).
20. Puigserver, P. Activation of PPAR Coactivator-1 Through Transcription Factor Docking. *Science* **286**, 1368-1371(1999).
21. Wallberg, A.E. et al. Coordination of p300-mediated chromatin remodeling and TRAP/mediator function through coactivator PGC-1alpha. *Molecular cell* **12**, 1137-49(2003).
22. Li, S. et al. Genome-wide Coactivation Analysis of PGC-1alpha Identifies BAF60a as a Regulator of Hepatic Lipid Metabolism. *Cell Metabolism* **8**, 105-117(2009).
23. Monsalve, M. et al. Direct coupling of transcription and mRNA processing through the thermogenic coactivator PGC-1. *Molecular cell* **6**, 307-16(2000).
24. Soyak, S. et al. PGC-1alpha: a potent transcriptional cofactor involved in the pathogenesis of type 2 diabetes. *Diabetologia* **49**, 1477-88(2006).
25. Borgius, L.J. et al. Glucocorticoid signaling is perturbed by the atypical orphan receptor and corepressor SHP. *The Journal of biological chemistry* **277**, 49761-6(2002).
26. Tiefenböck, S.K. et al. The Drosophila PGC-1 homologue Spargel coordinates mitochondrial activity to insulin signalling. *The EMBO journal* **29**, 171-83(2010).
27. LeMoine, C.M.R., Loughheed, S.C. & Moyes, C.D. Modular evolution of PGC-1alpha in vertebrates. *Journal of molecular evolution* **70**, 492-505(2010).

28. Tiraby, C. et al. Acquirement of brown fat cell features by human white adipocytes. *The Journal of biological chemistry* **278**, 33370-6(2003).
29. Esterbauer, H. et al. Human peroxisome proliferator activated receptor gamma coactivator 1 (PPARGC1) gene: cDNA sequence, genomic organization, chromosomal localization, and tissue expression. *Genomics* **62**, 98-102(1999).
30. Knutti, D., Kaul, A. & Kralli, A. A tissue-specific coactivator of steroid receptors, identified in a functional genetic screen. *Molecular and cellular biology* **20**, 2411-22(2000).
31. Schreiber, S.N. et al. The estrogen-related receptor alpha (ERR alpha) functions in PPAR gamma coactivator 1 alpha (PGC-1 alpha)- induced mitochondrial biogenesis. *PNAS* **101**, (2004).
32. Wang, Y.-X. et al. Peroxisome-proliferator-activated receptor delta activates fat metabolism to prevent obesity. *Cell* **113**, 159-70(2003).
33. Oberkofler, H. Peroxisome Proliferator-Activated Receptor-gamma Coactivator-1 Gene Locus: Associations with Hypertension in Middle-Aged Men. *Hypertension* **41**, 368-372(2003).
34. Nervina, J.M. et al. PGC-1alpha is induced by parathyroid hormone and coactivates Nurr1-mediated promoter activity in osteoblasts. *Bone* **39**, 1018-25(2006).
35. Delerive, P. et al. PGC-1 functions as a transcriptional coactivator for the retinoid X receptors. *The Journal of biological chemistry* **277**, 3913-7(2002).
36. Kallen, J. et al. Evidence for ligand-independent transcriptional activation of the human estrogen-related receptor alpha (ERRalpha): crystal structure of ERRalpha ligand binding domain in complex with peroxisome proliferator-activated receptor coactivator-1alpha. *The Journal of biological chemistry* **279**, 49330-7(2004).
37. Rhee, J. et al. Regulation of hepatic fasting response by PPAR gamma coactivator-1 alpha (PGC-1): Requirement for hepatocyte nuclear factor 4 alpha in gluconeogenesis. *PNAS* **100**, 4012-7(2003).
38. Zhang, Y. et al. Peroxisome proliferator-activated regulates triglyceride metabolism by activation of the nuclear receptor FXR. *Genes & Development* **18**, 157-169(2004).
39. Lin, J. et al. Peroxisome proliferator-activated receptor gamma coactivator 1beta (PGC-1beta), a novel PGC-1-related transcription coactivator associated with host cell factor. *The Journal of biological chemistry* **277**, 1645-8(2002).
40. Lin, J. et al. Transcriptional co-activator PGC-1 α drives the formation of slow-twitch muscle fibres. *Nature* **418**, 797-801(2002).

41. Handschin, C. Regulation of skeletal muscle cell plasticity by the peroxisome proliferator-activated receptor γ coactivator 1 α . *Journal of receptor and signal transduction research* **30**, 376-84(2010).
42. Puigserver, P. et al. Insulin-regulated hepatic gluconeogenesis through FOXO1 – PGC-1 α interaction. *Nature* **423**, (2003).
43. St-Pierre, J. et al. Suppression of reactive oxygen species and neurodegeneration by the PGC-1 transcriptional coactivators. *Cell* **127**, 397-408(2006).
44. Portilla, D. et al. Alterations of PPAR α and its coactivator PGC-1 in cisplatin-induced acute renal failure. *Kidney international* **62**, 1208-18(2002).
45. Fernandez-Marcos, P.J. & Auwerx, J. Regulation of PGC-1 α , a nodal regulator of mitochondrial biogenesis. *American Journal of Clinical Nutrition* **93**, 884-890(2011).
46. Handschin, C. et al. An autoregulatory loop controls peroxisome expression in muscle. *Cancer* **100**, (2003).
47. Petersen, A.M.W. & Pedersen, B.K. The anti-inflammatory effect of exercise. *Journal of applied physiology (Bethesda, Md. : 1985)* **98**, 1154-62(2005).
48. Akimoto, T. et al. Exercise stimulates PGC-1 α transcription in skeletal muscle through activation of the p38 MAPK pathway. *The Journal of biological chemistry* **280**, 19587-93(2005).
49. Zong, H. et al. AMP kinase is required for mitochondrial biogenesis in skeletal muscle in response to chronic energy deprivation. *Proceedings of the National Academy of Sciences of the United States of America* **99**, 15983-7(2002).
50. Leick, L. et al. PGC-1 α is required for AICAR induced expression of GLUT4 and mitochondrial proteins in mouse skeletal muscle. *American journal of physiology. Endocrinology and metabolism* **299**, 456-65(2010).
51. Boss, O. et al. Role of the beta(3)-adrenergic receptor and/or a putative beta(4)-adrenergic receptor on the expression of uncoupling proteins and peroxisome proliferator-activated receptor-gamma coactivator-1. *Biochemical and biophysical research communications* **261**, 870-6(1999).
52. Cao, W. et al. p38 Mitogen-Activated Protein Kinase Is the Central Regulator of Cyclic AMP-Dependent Transcription of the Brown Fat Uncoupling Protein 1 Gene. *Molecular and Cellular Biology* **24**, 3057-3067(2004).
53. Southgate, R.J. et al. PGC-1 α gene expression is down-regulated by Akt-mediated phosphorylation and nuclear exclusion of FoxO1 in insulin-stimulated skeletal muscle. *The FASEB Journal* **24**, 1-24(2005).

54. Jäger, S. et al. AMP-activated protein kinase (AMPK) action in skeletal muscle via direct phosphorylation of PGC-1alpha. *Proceedings of the National Academy of Sciences of the United States of America* **104**, 12017-22(2007).
55. Puigserver, P. et al. Cytokine Stimulation of Energy Expenditure through p38 MAP Kinase Activation of PPAR γ Coactivator-1. *Molecular Cell* **8**, 971-982(2001).
56. Li, X. et al. Akt/PKB regulates hepatic metabolism by directly inhibiting PGC-1alpha transcription coactivator. *Nature* **447**, 1012-6(2007).
57. Cantó, C. et al. AMPK regulates energy expenditure by modulating NAD⁺ metabolism and SIRT1 activity. *Nature* **458**, 1056-60(2009).
58. Anderson, R.M. et al. Dynamic regulation of PGC-1alpha localization and turnover implicates mitochondrial adaptation in calorie restriction and the stress response. *Aging cell* **7**, 101-11(2008).
59. Rytinki, M.M. & Palvimo, J.J. SUMOylation attenuates the function of PGC-1alpha. *The Journal of biological chemistry* **284**, 26184-93(2009).
60. Teyssier, C. et al. Activation of nuclear receptor coactivator PGC-1 alpha by arginine methylation. *Genes & Development* **19**, 1466-1473(2005).
61. Fan, M. et al. Suppression of mitochondrial respiration through recruitment of p160 myb binding protein to PGC-1 alpha : modulation by p38 MAPK. *Genes & Development* **18**, 278-289(2004).
62. Kakuma, T. et al. Role of leptin in peroxisome proliferator-activated receptor gamma coactivator-1 expression. *Endocrinology* **141**, 4576-82(2000).
63. Miura, S. et al. Isoform-specific increases in murine skeletal muscle peroxisome proliferator-activated receptor-gamma coactivator-1alpha (PGC-1alpha) mRNA in response to beta2-adrenergic receptor activation and exercise. *Endocrinology* **149**, 4527-33(2008).
64. Yoshioka, T. et al. Identification and characterization of an alternative promoter of the human PGC-1alpha gene. *Biochemical and biophysical research communications* **381**, 537-43(2009).
65. Chang, J.S. et al. Regulation of NT-PGC-1alpha subcellular localization and function by protein kinase A-dependent modulation of nuclear export by CRM1. *The Journal of biological chemistry* **285**, 18039-50(2010).
66. Palmer, J., Tandler, B. & Hoppel, C. Biochemical Properties of Subsarcolemmal and Interfibrillar Mitochondria Isolated from Rat Cardiac Muscle. *The Journal of Biological Chemistry* **252**, 8731-8739(1977).

67. Calvo, J. a et al. Muscle-specific expression of PPARgamma coactivator-1alpha improves exercise performance and increases peak oxygen uptake. *Journal of applied physiology (Bethesda, Md. : 1985)* **104**, 1304-12(2008).
68. Summermatter, S. et al. Peroxisome proliferator-activated receptor gamma coactivator 1alpha (PGC-1alpha) promotes skeletal muscle lipid refueling in vivo by activating de-novo lipogenesis and the pentose phosphate pathway. *The Journal of biological chemistry* **285**, 32793-32800(2010).
69. Wende, A.R. et al. A role for the transcriptional coactivator PGC-1alpha in muscle refueling. *The Journal of biological chemistry* **282**, 36642-51(2007).
70. Arany, Z. et al. HIF-independent regulation of VEGF and angiogenesis by the transcriptional coactivator PGC-1alpha. *Nature* **451**, 1008-12(2008).
71. Handschin, C. et al. Nutritional regulation of hepatic heme biosynthesis and porphyria through PGC-1alpha. *Cell* **122**, 505-15(2005).
72. Wenz, T. et al. Increased muscle PGC-1alpha expression protects from sarcopenia and metabolic disease during aging. *Proceedings of the National Academy of Sciences of the United States of America* **106**, 20405-10(2009).
73. St-Pierre, J. et al. Bioenergetic analysis of peroxisome proliferator-activated receptor gamma coactivators 1alpha and 1beta (PGC-1alpha and PGC-1beta) in muscle cells. *The Journal of biological chemistry* **278**, 26597-603(2003).
74. Norrbom, J. et al. PGC-1alpha mRNA expression is influenced by metabolic perturbation in exercising human skeletal muscle. *Journal of applied physiology* **96**, 189-94(2004).
75. Pette, D. The adaptive potential of skeletal muscle fibers. *Can J Appl Physiol.* **27**, 423-48(2002).
76. Sandri, M. et al. PGC-1alpha protects skeletal muscle from atrophy by suppressing FoxO3 action and atrophy-specific gene transcription. *Proceedings of the National Academy of Sciences of the United States of America* **103**, 16260-5(2006).
77. Handschin, C. et al. PGC-1 alpha regulates the neuromuscular junction program and ameliorates Duchenne muscular dystrophy. *Genes & Development* **21**, 770-783(2007).doi:10.1101/gad.1525107.etal
78. Kandel, E., Schwartz, J. & Jessel, T. *Principles of Neural Science*. 1414(McGraw-Hill, New York., 2000).
79. Liu, C. & Lin, J.D. PGC-1 coactivators in the control of energy metabolism. *Acta Biochimica et Biophysica Sinica* **43**, 248 - 257(2011).

80. Nathans, J. Molecular biology of visual pigments. *Ann.Rev.Neuroscie.* **10**, 2897-908(1987).
81. Liu, C. et al. Transcriptional coactivator PGC-1alpha integrates the mammalian clock and energy metabolism. *Nature* **447**, 477-81(2007).
82. Lin, J.D. Minireview: the PGC-1 coactivator networks: chromatin-remodeling and mitochondrial energy metabolism. *Molecular endocrinology* **23**, 2-10(2009).
83. Storch, K.-F. et al. Intrinsic circadian clock of the mammalian retina: importance for retinal processing of visual information. *Cell* **130**, 730-41(2007).
84. Patti, M.E. et al. Coordinated reduction of genes of oxidative metabolism in humans with insulin resistance and diabetes: Potential role of PGC1 and NRF1. *Proceedings of the National Academy of Sciences of the United States of America* **100**, 8466-71(2003).
85. Zheng, Z. et al. Improvements of retinal vascular injury in diabetic rats by statins is associated with the inhibition of mitochondrial reactive oxygen species pathway mediated by peroxisome-proliferator- activated receptor gamma coactivator 1 alpha. *Diabetes* **59**, 2315-25(2010).
86. Herzlich, A.A. et al. Peroxisome proliferator-activated receptor and age-related macular degeneration. *Open Biol J.* **2**, 141-148(2009).
87. Ershov, A.V. & Bazan, N.G. Photoreceptor phagocytosis selectively activates PPARgamma expression in retinal pigment epithelial cells. *J Neurosci Res.* **60**, 328 - 337(2000).
88. Wenzel, A. et al. Molecular mechanisms of light-induced photoreceptor apoptosis and neuroprotection for retinal degeneration. *Progress in retinal and eye research* **24**, 275-306(2005).
89. Remé, C. et al. Apoptotic cell death in retinal degenerations. *Progress in retinal and eye research* **17**, 443-64(1998).
90. Wyllie, A.H. "Where, O Death, Is Thy Sting?" A Brief Review of Apoptosis Biology. *Molecular neurobiology* 4-9(2010).doi:10.1007/s12035-010-8125-5
91. Saraste, A. & Pulkki, K. Morphologic and biochemical hallmarks of apoptosis. *Cardiovascular research* **45**, 528-37(2000).
92. Kerr, J., Wyllie, A. & Currie, A. Apoptosis: a basic biological phenomenon with wide-ranging implications in tissue kinetics. *Br.J.Cancer* **26**, 239-257(1972).
93. Ashkenazi, A. Targeting death and decoy receptors of the tumour-necrosis factor superfamily. *Nature reviews. Cancer* **2**, 420-30(2002).

94. Riedl, S.J. & Salvesen, G.S. The apoptosome: signalling platform of cell death. *Nature reviews. Molecular cell biology* **8**, 405-13(2007).
95. Wajant, H. Death receptors. *Essays Biochem.* **39**, 53-71(2003).
96. Hengartner, M.O. The biochemistry of apoptosis. *Nature* **407**, 770-6(2000).
97. Yuan, J. & Kroemer, G. Alternative cell death mechanisms in development and beyond. *Genes & Development* **24**, 2592-2602(2010).
98. Hamann, S., Schorderet, D.F. & Cottet, S. Bax-induced apoptosis in Leber's congenital amaurosis: a dual role in rod and cone degeneration. *PloS one* **4**, e6616(2009).
99. Sahel, J., Bonnel, S., Mrejen, S., Paques, M. Retinitis pigmentosa and other dystrophies. *Dev Ophthalmol.* **47**, 160-7.(2010).
100. Crisanti-Iassiaz, P., Martin, E. & Torriglia, A. *Apoptosis in the retina- Molecular pathways of retinal apoptosis. Apoptosis in the retina* **661**, 43-62(Kerala, 2006).
101. Grimm, C. et al. Protection of Rpe65-deficient mice identifies rhodopsin as a mediator of light-induced retinal degeneration. *Nature genetics* **25**, 63-6(2000).
102. Saari, J.C. et al. Visual Cycle Impairment in Cellular Retinaldehyde Binding Protein (CRALBP) Knockout Mice Results in Delayed Dark Adaptation. *Neuron* **29**, 739-748(2001).
103. Grimm, C. et al. Blue Light ' s Effects on Rhodopsin : Photoreversal of Bleaching in Living Rat Eyes. *Investigative ophthalmology & visual science* **41**, 3984-3990(2000).
104. Chen, C.K. et al. Abnormal photoresponses and light-induced apoptosis in rods lacking rhodopsin kinase. *Proceedings of the National Academy of Sciences of the United States of America* **96**, 3718-22(1999).
105. Hao, W. et al. Evidence for two apoptotic pathways in light-induced retinal degeneration. *Nature genetics* **32**, 254-60(2002).
106. Hafezi, F. et al. The absence of c-fos prevents light-induced apoptotic cell death of photoreceptors in retinal degeneration in vivo. *Nature Medicine* **3**, 346-349(1997).
107. Marti, A. et al. Light-Induced Cell Death of Retinal Photoreceptors in the Absence of p53. *Invest Ophthalmol Vis Sci.* **39**, 846-849(1998).
108. Donovan, M., Carmody, R.J. & Cotter, T.G. Light-induced photoreceptor apoptosis in vivo requires neuronal nitric-oxide synthase and guanylate cyclase activity and is caspase-3-independent. *The Journal of biological chemistry* **276**, 23000-8(2001).

109. Grimm, C. et al. HIF-1-induced erythropoietin in the hypoxic retina protects against light-induced retinal degeneration. *Nature medicine* **8**, 718-24(2002).
110. Samardzija, M. et al. Differential role of Jak-STAT signaling in retinal degenerations. *FASEB* **20**, 2411-3(2006).
111. Joly, S. et al. Leukemia inhibitory factor extends the lifespan of injured photoreceptors in vivo. *The Journal of neuroscience* **28**, 13765-74(2008).
112. Leone, T.C. et al. PGC-1alpha deficiency causes multi-system energy metabolic derangements: muscle dysfunction, abnormal weight control and hepatic steatosis. *PLoS biology* **3**, e101(2005).
113. Adhihetty, P.J. et al. The role of PGC-1alpha on mitochondrial function and apoptotic susceptibility in muscle. *American journal of physiology. Cell physiology* **297**, C217-25(2009).
114. Saleem, A., Adhihetty, P.J. & Hood, D. a Role of p53 in mitochondrial biogenesis and apoptosis in skeletal muscle. *Physiological genomics* **37**, 58-66(2009).
115. Liang, J. et al. Down-expression of PGC-1alpha partially mediated by JNK/c-Jun through binding to CRE site during apoptotic procedure in cerebellar granule neurons. *Journal of neuroscience research* **88**, 1918-25(2010).
116. Finck, B.N. & Kelly, D.P. Review series PGC-1 coactivators : inducible regulators of energy metabolism in health and disease. **116**, 615-622(2006).
117. Handschin, C. The biology of PGC-1alpha and its therapeutic potential. *Trends in pharmacological sciences* **30**, 322-9(2009).
118. Ames, A., Li, Y.Y., Heher, E.C., Kimble, C.R. Energy metabolism of rabbit retina as related to function: high cost of Na⁺ transport. *The Journal of neuroscience* **12**, 840-53(1992).
119. Okawa, H., Sampath, A.P., Laughlin, S.B., Fain, G.F. ATP Consumption by Mammalian Rod Photoreceptors in Darkness and Light. *Curr.Biol.* **18**, 1917-1921(2008).
120. Wu, J. et al. The unfolded protein response mediates adaptation to exercise in skeletal muscle through a PGC-1 α /ATF6 α complex. *Cell metabolism* **13**, 160-9(2011).
121. Handschin, C. et al. Skeletal muscle fiber-type switching, exercise intolerance, and myopathy in PGC-1alpha muscle-specific knock-out animals. *The Journal of biological chemistry* **282**, 30014-21(2007).
122. Handschin, C. & Spiegelman, B.M. The role of exercise and PGC-1alpha in inflammation and chronic disease. *Nature* **454**, 463-469(2008).

123. Mears, A.J. et al. Nrl is required for rod photoreceptor development. *Nature genetics* **29**, 447-52(2001).
124. Chang, B. et al. Two mouse retinal degenerations caused by missense mutations in the beta-subunit of rod cGMP phosphodiesterase gene. *Vision Res.* **47**, 624-633(2007).
125. Lin, J. et al. Defects in adaptive energy metabolism with CNS-linked hyperactivity in PGC-1alpha null mice. *Cell* **119**, 121-35(2004).
126. Organisciak, D.T. & Vaughan, D.K. Retinal Light Damage: Mechanisms and Protection. *Prog Retin Eye Res.* **29**, 113-134(2010).
127. Naash, M.I. et al. Simulation of human autosomal dominant retinitis pigmentosa in transgenic mice expressing a mutated murine opsin gene. *Proceedings of the National Academy of Sciences of the United States of America* **90**, 5499-503(1993).
128. Daniele, L.L. et al. Cone-like morphological, molecular, and electrophysiological features of the photoreceptors of the Nrl knockout mouse. *Investigative ophthalmology & visual science* **46**, 2156-67(2005).
129. Samardzija, M. et al. Caspase-1 ablation protects photoreceptors in a model of autosomal dominant retinitis pigmentosa. *Investigative ophthalmology & visual science* **47**, 5181-90(2006).
130. Kim, H., Jee, H.J. & Yun, J. DNA damage induces down-regulation of PEPCK and G6P gene expression through degradation of PGC-1a. *Acta Biochim Biophys Sin (Shanghai)*. **43**, 589 - 594(2011).
131. Handschin, C. & Spiegelman, B.M. PGC-1 coactivators and the regulation of skeletal muscle fiber-type determination. *Cell metabolism* **13**, 351; author reply 352(2011).
132. Arany, Z. et al. Transcriptional coactivator PGC-1 alpha controls the energy state and contractile function of cardiac muscle. *Cell metabolism* **1**, 259-71(2005).
133. Yu, L. & Yang, S.J. AMP-activated protein kinase mediates activity-dependent regulation of peroxisome proliferator-activated receptor gamma coactivator-1alpha and nuclear respiratory factor 1 expression in rat visual cortical neurons. *Neuroscience* **169**, 23-38(2010).
134. Won, J.C. et al. Peroxisome proliferator-activated receptor-gamma coactivator 1-alpha overexpression prevents endothelial apoptosis by increasing ATP/ADP translocase activity. *Arteriosclerosis, thrombosis, and vascular biology* **30**, 290-7(2010).
135. D'Errico, I. et al. Peroxisome proliferator-activated receptor-gamma coactivator 1-alpha (PGC1alpha) is a metabolic regulator of intestinal epithelial cell fate. *Proceedings of the National Academy of Sciences of the United States of America* **108**, 6603-8(2011).

136. Tanimoto, N. et al. Vision tests in the mouse: Functional phenotyping with electroretinography. *Frontiers in Bioscience* **14**, 2730-2737(2009).
137. Fischer, M.D. et al. Noninvasive, in vivo assessment of mouse retinal structure using optical coherence tomography. *PloS one* **4**, e7507(2009).
138. Sonoda, J. et al. Nuclear receptor ERR alpha and coactivator PGC-1 beta are effectors of IFN- gamma -induced host defense. *Genes & Development* **21**, 1909-1920(2007).
139. Sonoda, J. et al. PGC-1beta controls mitochondrial metabolism to modulate circadian activity, adaptive thermogenesis, and hepatic steatosis. *Proceedings of the National Academy of Sciences of the United States of America* **104**, 5223-8(2007).
140. Arany, Z. et al. The transcriptional coactivator PGC-1beta drives the formation of oxidative type IIX fibers in skeletal muscle. *Cell metabolism* **5**, 35-46(2007).
141. Lin, J. et al. Hyperlipidemic effects of dietary saturated fats mediated through PGC-1beta coactivation of SREBP. *Cell* **120**, 261-73(2005).
142. Oberkofler, H. et al. Transcriptional co-activator peroxisome proliferator-activated receptor (PPAR)gamma co-activator-1beta is involved in the regulation of glucose-stimulated insulin secretion in INS-1E cells. *Journal of molecular medicine (Berlin, Germany)* **87**, 299-306(2009).
143. Wolfrum, C. & Stoffel, M. Coactivation of Foxa2 through Pgc-1beta promotes liver fatty acid oxidation and triglyceride/VLDL secretion. *Cell metabolism* **3**, 99-110(2006).
144. Nagai, Y. et al. The role of peroxisome proliferator-activated receptor gamma coactivator-1 beta in the pathogenesis of fructose-induced insulin resistance. *Cell metabolism* **9**, 252-64(2009).
145. Lelliott, C.J. et al. Ablation of PGC-1beta results in defective mitochondrial activity, thermogenesis, hepatic function, and cardiac performance. *PLoS biology* **4**, e369(2006).
146. Vianna, C.R. et al. Hypomorphic Mutation in PGC-1beta causes mitochondrial dysfunction and liver insulin resistance. *Cell Metabolism* **4**, 453-464(2007).
147. Rowe, G.C. et al. PGC-1beta regulates angiogenesis in skeletal muscle. *American journal of physiology Endocrinology and metabolism* **301**, E155-63(2011).
148. Wright, L.E. et al. Amelioration of lipid-induced insulin resistance in rat skeletal muscle by overexpression of Pgc-1 β involves reductions in long-chain acyl-CoA levels and oxidative stress. *Diabetologia* **54**, 1417-26(2011).
149. Lelliott, C.J. et al. Hepatic PGC-1beta overexpression induces combined hyperlipidemia and modulates the response to PPARalpha activation. *Arteriosclerosis, thrombosis, and vascular biology* **27**, 2707-13(2007).

150. Zechner, C. et al. Total skeletal muscle PGC-1 deficiency uncouples mitochondrial derangements from fiber type determination and insulin sensitivity. *Cell metabolism* **12**, 633-42(2010).
151. Jacobs-El, J., Ashley, W. & Russell, B. Iix and slow myosin expression follow mitochondrial increases in transforming muscle fibers. *The American journal of physiology* **265**, C79-84(1993).
152. Larsson, L. et al. MHC composition and enzyme-histochemical and physiological properties of a novel fast-twitch motor unit type. *The American journal of physiology* **261**, C93-101(1991).
153. Mortensen, O.H. et al. PGC-1beta is downregulated by training in human skeletal muscle: no effect of training twice every second day vs. once daily on expression of the PGC-1 family. *Journal of applied physiology* **103**, 1536-42(2007).
154. Meirhaeghe, A. et al. Characterization of the human , mouse and rat PGC1 β (peroxisome-proliferator-activated receptor- γ co-activator 1 β) gene in vitro and in vivo. *Biochim.J.* **373**, 155-165(2003).
155. Ling, C. et al. Multiple environmental and genetic factors influence skeletal muscle PGC-1 α and PGC-1 β gene expression in twins. *Journal of Clinical Investigation* **114**, (2004).
156. Fire, A, Montgomery, MK, Kostas, SA, Driver, SE, Mello, C. Potent and specific genetic interference by double-stranded RNA in *Caenorhabditis elegans*. *Nature* **391**, 806-11(1998).
157. Djuranovic, S., Nahvi, a & Green, R. A Parsimonious Model for Gene Regulation by miRNAs. *Science* **331**, 550-553(2011).
158. Hamilton, a J. A Species of Small Antisense RNA in Posttranscriptional Gene Silencing in Plants. *Science* **286**, 950-952(1999).
159. Kim, D.H. & Rossi, J.J. Strategies for silencing human disease using RNA interference. *Nature reviews. Genetics* **8**, 173-84(2007).
160. Liu, Y.P. & Berkhout, B. miRNA cassettes in viral vectors: Problems and solutions. *Biochimica et biophysica acta* (2011).doi:10.1016/j.bbagr.2011.05.014
161. Grimm, D. et al. Fatality in mice due to oversaturation of cellular microRNA/short hairpin RNA pathways. *Nature* **441**, 537-41(2006).
162. Liu, Y.P., Haasnoot, J. & Berkhout, B. Design of extended short hairpin RNAs for HIV-1 inhibition. *Nucleic acids research* **35**, 5683-93(2007).

163. Duxbury, M.S. et al. RNA interference targeting focal adhesion kinase enhances pancreatic adenocarcinoma gemcitabine chemosensitivity☆. *Biochemical and Biophysical Research Communications* **311**, 786-792(2003).
164. Lewandoski, M. Conditional control of gene expression in the mouse. *Nature reviews. Genetics* **2**, 743-55(2001).
165. Gao, X. & Zhang, P. Transgenic RNA interference in mice. *Physiology* **22**, 161-6(2007).
166. Dickins, R.A. et al. Tissue-specific and reversible RNA interference in transgenic mice. *Nature Genetics* **39**, 914-921(2007).
167. Mingozzi, F. & High, K. a Therapeutic in vivo gene transfer for genetic disease using AAV: progress and challenges. *Nature reviews. Genetics* **12**, 341-55(2011).
168. Gaudet, D. et al. Review of the clinical development of alipogene tiparvovec gene therapy for lipoprotein lipase deficiency. *Atherosclerosis. Supplements* **11**, 55-60(2010).
169. Srivastava, a, Lusby, E.W. & Berns, K.I. Nucleotide sequence and organization of the adeno-associated virus 2 genome. *Journal of virology* **45**, 555-64(1983).
170. Fisher, K.J. et al. Transduction with recombinant adeno-associated virus for gene therapy is limited by leading-strand synthesis. *Journal of virology* **70**, 520-32(1996).
171. Wu, Z., Asokan, A. & Samulski, R.J. Adeno-associated virus serotypes: vector toolkit for human gene therapy. *Molecular therapy : the journal of the American Society of Gene Therapy* **14**, 316-27(2006).
172. Gao, G.-P. et al. Novel adeno-associated viruses from rhesus monkeys as vectors for human gene therapy. *Proceedings of the National Academy of Sciences of the United States of America* **99**, 11854-9(2002).
173. Pan, R.Y. et al. Disease-inducible transgene expression from a recombinant adeno-associated virus vector in a rat arthritis model. *Journal of virology* **73**, 3410-7(1999).
174. Zincarelli, C. et al. Analysis of AAV serotypes 1-9 mediated gene expression and tropism in mice after systemic injection. *Molecular therapy : the journal of the American Society of Gene Therapy* **16**, 1073-80(2008).
175. Gregorevic, P. et al. Systemic delivery of genes to striated muscles using adeno-associated viral vectors. *Nature medicine* **10**, 828-34(2004).
176. Chirmule, N. et al. Humoral immunity to adeno-associated virus type 2 vectors following administration to murine and nonhuman primate muscle. *Journal of virology* **74**, 2420-5(2000).

177. Kotin, R.M. Large-scale recombinant adeno-associated virus production. *Human molecular genetics* **20**, R2-6(2011).
178. Silva, J.M. et al. Second-generation shRNA libraries covering the mouse and human genomes. *Nature genetics* **37**, 1281-8(2005).
179. Rao, M.K. & Wilkinson, M.F. Tissue-specific and cell type-specific RNA interference in vivo. *Nature protocols* **1**, 1494-501(2006).
180. Brummelkamp, T.R., Bernards, R. & Agami, R. A system for stable expression of short interfering RNAs in mammalian cells. *Science* **296**, 550-3(2002).
181. Shimpo, M. et al. AAV-mediated VEGF gene transfer into skeletal muscle stimulates angiogenesis and improves blood flow in a rat hindlimb ischemia model. *Cardiovascular Research* **53**, 993-1001(2002).
182. Yang, L. et al. A myocardium tropic adeno-associated virus (AAV) evolved by DNA shuffling and in vivo selection. *Proceedings of the National Academy of Sciences of the United States of America* **106**, 3946-51(2009).
183. Monteilhet, V. et al. Prevalence of Serum IgG and Neutralizing Factors and 9 in the Healthy Population : Implications for Gene Therapy Using AAV Vectors. *Human Gene Therapy* **712**, 704-712(2010).
184. Moulay, G. et al. Soluble TNF- α receptor secretion from healthy or dystrophic mice after AAV6-mediated muscle gene transfer. *Gene therapy* **17**, 1400-10(2010).
185. Boudreau, R.L., Martins, I. & Davidson, B.L. Artificial microRNAs as siRNA shuttles: improved safety as compared to shRNAs in vitro and in vivo. *Molecular therapy : the journal of the American Society of Gene Therapy* **17**, 169-75(2009).
186. Guo, H. et al. Mammalian microRNAs predominantly act to decrease target mRNA levels. *Nature* **466**, 835-840(2011).
187. Yang, M. et al. Adeno-associated virus-mediated bone morphogenetic protein-7 gene transfer induces C2C12 cell differentiation into osteoblast lineage cells. *Acta pharmacologica Sinica* **26**, 963-8(2005).
188. Grimm, D. Small silencing RNAs: state-of-the-art. *Advanced drug delivery reviews* **61**, 672-703(2009).
189. Barnhart, K.M. et al. Enhancer and Promoter Chimeras in Plasmids Designed for Intramuscular Injection: A Comparative In Vivo and In Vitro Study. *Human Gene Therapy* **9**, 2545-2553(1998).

190. Moskalenko, M. et al. Epitope mapping of human anti-adenovirus type 2 neutralizing antibodies: implications for gene therapy and virus structure. *Journal of virology* **74**, 1761-6(2000).
191. McCarty, D.M., Monahan, P.E. & Samulski, R.J. Self-complementary recombinant adenovirus (scAAV) vectors promote efficient transduction independently of DNA synthesis. *Gene therapy* **8**, 1248-54(2001).
192. Dongsheng, D. et al. NEW TECHNOLOGY A new dual-vector approach to enhance recombinant adenovirus-mediated gene expression through intermolecular cis activation. *Nature Medicine* **6**, 595-598(2000).
193. Sun, D. et al. Multi-miRNA hairpin method that improves gene knockdown efficiency and provides linked multi-gene knockdown. *BioTechniques* **41**, 59-63(2006).
194. Saayman, S., Arbuthnot, P. & Weinberg, M.S. Deriving four functional anti-HIV siRNAs from a single Pol III-generated transcript comprising two adjacent long hairpin RNA precursors. *Nucleic acids research* **38**, 6652-63(2010).
195. Fernstrom, J. Effects of dietary polyunsaturated fatty acids on neuronal function. *Lipids* **2**, (1999).
196. Fliesler, S. & Bretillon, L. The ins and outs of cholesterol in the vertebrate retina. *Journal of Lipid Research* **12**, 3399-413(2010).

8. Curriculum vitae

Personal

Full name Anna Franziska Egger
Day and place of birth December 21, 1979, Innsbruck, Austria
Nationality Austrian

Key competence 1

Molecular biology

- 01.2010 - 02.2010 **Joint research project in gene therapy**
Baker IDI Heart and Diabetes Institute, Melbourne (AUS)
Cloning, production and purification of Adeno - Associated Virus (AAV)
in Dr. Paul Gregorevic's lab
- 02.2009 - 10.2011 **Lab relocation and completion of PhD thesis (Dr.sc.nat.)**
Institute of Pharmacology, Biozentrum Basel, University of Basel (CH)
in Prof. Christoph Handschin's lab
- 07.2007 - 01.2009 **PhD thesis in biomedical research**
Institute of Physiology, University of Zurich (CH)
- PhD thesis and lab foundation with Prof. Christoph Handschin
 - Involvement of the coactivator PGC-1 α in retinal health (Prof. Christian Grimm)
 - Role of PGC-1 β in skeletal muscle (Dr. Paul Gregorevic)
- 10.2002 - 12.2006 **Bachelor and Master (MSc) in molecular biology**
University of Innsbruck and Innsbruck Medical University (AUT)
- Master thesis with Prof. Alexandra Lusser
 - Molecular characterization of the histone chaperone Asf1
 - Graduation with distinction

Key competence 2

Translating and interpreting

- 2005 - 2007 **Manuscript editor**
Institute of Analytical Chemistry and Radiochemistry, University of Innsbruck
- 2002 - 2003 **Simultaneous conference interpreter**
General Assembly of SOS Children's Villages International, Innsbruck
Schweizerische Kadervereinigung, Chur (CH)
Martell & Co, Cognac (F)
- 09.1999 - 01.2000 **ERASMUS university exchange program**
Université François-Rabelais, Tours (F)
- 10.1998 - 07.2002 **Master's degree in interpreting (French, English) (MPhil)**
University of Innsbruck

Training during the PhD

03. 2011	Clinical investigator course: basics of clinical trials and ICH-GCP University Hospital, Basel
03.2010 - 06.2010	Venture lab 2010: How to establish and manage a start-up Swiss Commission for Technology and Innovation (KTI), Basel
2009	WIN 2009 (Women into Industry) Competitive promotion program for female PhDs and postdocs Novartis AG, Basel

Methodological skills in molecular biology

<i>In vivo</i>	Viral injections into mouse <i>tibialis anterior</i> muscle Retina isolation and explant cultivation
<i>In vitro</i>	Cultivation, transfection and transduction of several skeletal muscle cell lines, production and purification of AAV, microarray and quantitative real- time PCR, FACS

Languages

German	Mother tongue
English	Proficient, oral and written
French	Proficient, oral and written
Italian	Basic knowledge, oral and written
Portuguese	Basic knowledge, oral and written

IT skills

General Molecular Biology	MS Office (Word, Excel, Powerpoint), SPSS, Adobe Acrobat X Pro, Corel Draw Partek, Geneious, Vector NTI
------------------------------	--

Teaching and voluntary activities

Teaching	Trainer in French and English during high school Tutor for medical students during PhD in Zurich
Voluntary	Member of the Mentee Steering Committee of WIN 2009: organization of meetings, moderator in discussion panel with Novartis opinion leaders

Publication record

- Manuscript: PGC-1alpha determines light-damage susceptibility of the retina**
Egger A, Sothilingam V, Tanimoto N, Lange C, Okoniewski ML, Fang L, Salatino S, Garcia-Garrido M, Beck S, Neutzner A, Seeliger MS, Grimm C & Handschin C
- PGC-1 α and myokines in the aging muscle – a mini - review** Arnold AS, Egger A, Handschin C, Gerontology. 2011;57(1):37-43. Epub 2010 Feb 4. Review.

9. Acknowledgements

I would like to thank

my Doktorvater Prof. Dr. Christoph Handschin for giving me the opportunity to do my doctorate thesis in his lab, where he provided an encouraging environment characterized by complete scientific freedom without having to think of money as a limiting issue, treating all lab members with great respect, always finding time for discussion.

Prof. Dr. Christian Grimm for being an outstanding mentor, providing continuous support, prompt and valuable feedback and expertise, displaying a lot of patience for his coworkers.

Prof. Dr. Mathias Seeliger and his team for carrying out the ERG measurements

Dr. Paul Gregorevic and his lab members for hosting me in his Melbourne lab

the Handschin and Rüegg group members for support

my family and friends for their encouragement, patience, support and simply for listening.